

Extracellular Matrix Proteomics Reveals Interplay of Aggrecan and Aggrecanases in Vascular Remodeling of Stented Coronary Arteries

Running Title: *Suna et al, Extracellular Matrix Remodeling after Stenting*

Gonca Suna, MD, PhD, et al.

The full author list is available on page 21.

Address for Correspondence:

Manuel Mayr, MD, PhD
King's British Heart Foundation Centre
King's College London
125 Coldharbour Lane
London SE5 8NU, UK
Tel: +44 (0) 207848 5446
Fax: +44 (0) 20 7848 5298
Email: manuel.mayr@kcl.ac.uk



Abstract

Background—Extracellular matrix (ECM) remodeling contributes to in-stent restenosis and thrombosis. Despite its important clinical implications little is known about ECM changes post-stent implantation.

Methods—Bare-metal (BMS) and drug-eluting stents (DES) were implanted in pig coronary arteries with an overstretch under optical coherence tomography guidance. Stented segments were harvested 1, 3, 7, 14 and 28 days post-stenting for proteomics analysis of the media and neointima.

Results—A total of 151 ECM and ECM-associated proteins were identified by mass spectrometry. After stent implantation, proteins involved in regulating calcification were upregulated in the neointima of DES. The earliest changes in the media were proteins involved in inflammation and thrombosis, followed by changes in regulatory ECM proteins. By day 28, basement membrane proteins were reduced in DES compared with BMS. In contrast, the large aggregating proteoglycan aggrecan was increased. Aggrecanases of the ADAMTS (a disintegrin and metalloproteinase with thrombospondin motifs) family contribute to the catabolism of vascular proteoglycans. An increase in ADAMTS-specific aggrecan fragments was accompanied by a notable shift from *ADAMTS1* and *ADAMTS5* to *ADAMTS4* gene expression after stent implantation. Immunostaining in human stented coronary arteries confirmed the presence of aggrecan and aggrecan fragments, in particular at the contacts of the stent struts with the artery. Further investigation of aggrecan presence in the human vasculature revealed that aggrecan and aggrecan cleavage were more abundant in human arteries compared to veins. Also, aggrecan synthesis was induced upon grafting a vein into the arterial circulation, suggesting an important role for aggrecan in vascular plasticity. Finally, lack of ADAMTS-5 activity in mice resulted in an accumulation of aggrecan and a dilation of the thoracic aorta, confirming that aggrecanase activity regulates aggrecan abundance in the arterial wall and contributes to vascular remodeling.

Conclusions—Significant differences were identified by proteomics in the ECM of coronary arteries after BMS and DES implantation, most notably an upregulation of aggrecan, a major ECM component of cartilaginous tissues that confers resistance to compression. The accumulation of aggrecan coincided with a shift in *ADAMTS* gene expression. This study provides the first evidence implicating aggrecan and aggrecanases in the vascular injury response after stenting.

Key Words: extracellular matrix; mass spectrometry; stent; neointima; coronary artery disease

Clinical Perspective

What is new?

- Despite continuous development in stent technology, in-stent restenosis and neoatherosclerosis remains a considerable cause of stent failure.
- A proteomics approach to identify extracellular matrix protein changes in response to bare-metal stent and drug-eluting stent insertion revealed differential expression of aggrecan, a proteoglycan that is usually associated with articular cartilage.
- Aggrecanase activity is part of the vascular injury response post-stenting.

What are the clinical implications?

- Aggrecan cleavage is the hallmark of cartilage degeneration in a number of degenerative diseases including rheumatoid arthritis and osteoarthritis.
- Aggrecanase activity might offer new drug targets to alter extracellular matrix remodeling in the vasculature.



Circulation


Percutaneous coronary intervention with stent implantation has become the most widely used treatment for coronary artery disease. Use of stents reduced the impact of acute elastic recoil and occlusive dissection on restenosis observed with balloon angioplasty.^{1,2} However, stent implantation induced an excessive healing process, which in case of bare-metal stents (BMS) led to neointimal hyperplasia and in-stent restenosis. The introduction of drug-eluting stents (DES) reduced the burden of in-stent restenosis and repeat revascularization.^{3,4} On the other hand, DES implantation delays vessel re-endothelialization due to the non-selective nature of these drugs, resulting in an increased risk of late and very late stent thrombosis requiring prolonged dual antiplatelet therapy.⁵ Late stent thrombosis has also been associated with the inflammation and hypersensitivity reactions to the non-biocompatible polymer coatings on DES.⁶ Moreover, in the long term neoatherosclerosis is likely to occur earlier in DES than in BMS.⁷ Second-generation DES with durable biocompatible polymers are current standard of care because of their excellent efficacy and safety. A further development in stent technology uses biodegradable polymers as well as fully biodegradable non-metallic scaffolds.^{8,9}

However, despite continuous development in technology, in-stent restenosis remains a considerable cause of stent failure.¹⁰ Neointimal hyperplasia involves the interaction between inflammatory cells, platelets, smooth muscle cells (SMC) and endothelial cells (EC) leading to progressive obliteration of the vascular lumen.¹¹ Platelet activation and inflammation as an early response to stent deployment result in increased SMC migration, proliferation and extracellular matrix (ECM) production. Yet, little is known about changes in ECM composition upon vascular stent injury, even though more than 50% of the neointimal hyperplasia consists of ECM proteins.¹² Our current knowledge of ECM remodeling after stent injury and during neointima formation is mainly based on histopathological analysis investigating the role of only few

selected ECM proteins.^{12, 13} In comparison, proteomics is a powerful underpinning technology to profile not just individual ECM proteins by antibody staining but characterize the different stages of ECM remodeling by liquid chromatography tandem mass spectrometry (LC-MS/MS).

Therefore, the aim of the present study was to use proteomics to characterize ECM remodeling in porcine coronary arteries stented with BMS and DES. Pigs are well suited for these studies, since the stages of the healing process closely resemble the human disease, but the time course of neointimal hyperplasia formation is notably shorter.^{14, 15}

Methods

An expanded methods section is available in the online-only Data Supplement at  <http://circ.ahajournals.org/>. The data, analytic methods, and study materials will not be made available to other researchers for purposes of reproducing the results or replicating the procedure due to the limited amount of tissues. The proteomics data, however, are deposited in PRIDE (<https://www.ebi.ac.uk/pride/archive/>) with the dataset identifier PXD005726 and 10.6019/PXD005726.

Porcine Model of Stent Injury

All porcine animal procedures were approved by the local ethical committee for animal experiments, Institute of Pharmacology Polish Academy of Science, Cracow, Poland. 12 healthy male and female domestic pigs (3-4 months old, 28-48kg) underwent percutaneous coronary intervention through transfemoral access. To prevent the risk of in-stent thrombosis pigs received a loading dose of aspirin and clopidogrel orally 24h before intervention and remained on this dual antiplatelet therapy until termination. The coronary arteries of each animal (LAD, LCX and RCA) were either stented with a BMS (MULTI-LINK cobalt-chromium stent, Abbott Vascular,

US) or DES based on the same cobalt-chromium platform (XIENCE PRO everolimus-eluting stent with durable fluoropolymer, Abbott Vascular, US) or had balloon angioplasty alone (BA). Full strut expansion was achieved for each deployed stent. Quantitative coronary angiography and optical coherence tomography (OCT) were performed 1, 3, 7, 14 or 28 days post-stent implantation, followed by harvesting of the coronary arteries. The neointima lesions that had developed in stented arteries at day 28 were dissected from the media and analyzed separately. In total, 31 samples were analyzed by LC-MS/MS for the media (n=3 BMS and n=3 DES at each time-point 1, 3, 7 and 28 days; n=4 BA early [day1-day3] and n=3 BA late [day 14 - day28]). For the neointima, a total of 14 samples were analyzed (n=7 BMS, n=7 DES at 28 days). Six coronary arteries of 4.5 months old healthy pigs were harvested as unstented controls.



ECM Extraction

The ECM proteins for the media were extracted in a three-step manner with a method previously developed in our laboratory for the enrichment of ECM proteins.¹⁶ In brief, newly synthesized, loosely bound ECM proteins were extracted in 0.5M NaCl (1.5h), followed by decellularization of the tissue in 0.08% SDS (1.5h) to remove intracellular material. Eventually the tissue pieces were incubated in 4M guanidine HCl buffer (GuHCl, 48h) by vigorous shaking at room temperature to extract the strongly bound ECM components. The buffers contained protease inhibitors and EDTA to prevent ECM protein degradation by proteases. Proteins of the thinner neointimal tissues were extracted only in GuHCl buffer for 48h.

Proteomics Analysis in Porcine Tissue

After deglycosylation, proteins were subjected to in-solution digestion and analyzed by liquid chromatography tandem-mass spectrometry (LC-MS/MS). 15µg of deglycosylated proteins of the GuHCl extracts were denatured with 6M urea and 2M thiourea, reduced with 10mM DDT

and alkylated with 50mM iodoacetamide, followed by acetone precipitation of the proteins and tryptic digestion overnight. Subsequently, peptides were cleaned up using C18 spin plates and separated on a nanoflow high-performance LC column (Acclaim, ThermoFisher) using an UltiMate 3000 RSLCnano LC system (ThermoFisher) interfaced to a Q Exactive Plus Orbitrap mass spectrometer (ThermoFisher). MS/MS analysis was performed on the 15 most abundant ions in each full MS scan with dynamic exclusion enabled.¹⁷ Raw files were searched using Proteome Discoverer 1.4 against a custom-made database, containing porcine ECM proteins with a human proteome background (UniProtKB/Swiss-Prot Release 2014_06, 20220 protein entries) using Mascot. All data were exported to mzIdentML format using Scaffold and deposited to the ProteomeXchange Consortium via the PRIDE partner repository.



Immunohistochemistry in Human Specimen

Human samples were collected under the Bristol Coronary Biobank ethical approval 08/H0107/48. The artery including stent was fixed in 10% formalin, then the stent was removed and the tissues were paraffin embedded and sectioned at 3µm thickness using a microtome. For immunostaining deparaffinised and rehydrated samples were incubated in 0.3% H₂O₂ for 10min to block endogenous peroxidases, then incubated in boiling water bath in preheated 10mM sodium citrate buffer (pH6.0) for antigen retrieval. Sections were blocked with either 20% goat (for rabbit primary) or rabbit serum (for goat primary) in PBS for 1h and subsequently incubated with primary antibody or matched rabbit IgG control (5µg/ml) in 1% goat or rabbit serum and incubated at 4°C overnight. Primary antibodies were used to aggrecan (1:400; Abcam, ab36861), the NITEGE neoepitope of aggrecan (1:400; Thermo, AF-PA11746), HPLN1 (1:200; Abcam, ab103455), the DPEAAE neoepitope of versican (1:400; Abcam, ab19345), MGP (1:100; Abcam, ab86233) and SPP24 (1:50; sc-169408, Santa Cruz). Biotinylated goat anti-rabbit

(1:250; Sigma, B7389) or rabbit anti-goat (1:250; Dako, E0466) secondary antibodies were applied for 1 h, followed by wash steps and Extravidin-HRP (1:250; Sigma, E2886) incubation. DAB solution (Vector) for 10min was used for detection. Sections were washed in dH₂O, counterstained for 15 sec in modified Harris Haematoxylin, dehydrated and mounted in DPX. Histological slides were digitally scanned using a digital scanning system (LEICA SCN400F) to provide a high resolution digital image.

Statistical Analysis

Data are shown as average (Av) \pm standard error of the mean (SEM). MS data were quantified using ion intensities (total ion current, TIC). IBM® SPSS® statistics software (version 22) and Microsoft® Excel® (version 15.20) were used for statistical calculations, GraphPad Prism® (version 6.0e) and Microsoft® Excel® (version 15.20) for data illustration. For optical coherence tomography (OCT) analysis, 2-way analysis of variance (ANOVA) was applied to assess neointimal volume, minimal lumen area and strut coverage between BMS and DES at different time points. 1-way ANOVA was applied for changes in protein abundance and gene expression in BMS and DES at different time-points. Unpaired Student's *t*-test with unequal variance was applied for proteomics differences between neointimal BMS and DES, BA early and late, for differences between BMS and DES at each time point (visualized as a volcano plot for changes at day 28) as well as the comparison between BMS or DES day 28 vs. BA late. Unpaired, two-tailed Student's *t*-test with unequal variance was also used for the proteomics data in mice, as well as comparisons on murine aortic diameter, blood pressure and cardiac output. MultiExperiment Viewer software (MeV, version v4.9) was applied using Pearson correlation for protein clustering. For gene expression analysis of porcine tissue *t*-tests were applied for differences between BMS and DES and regression analysis for changes at different time-points

(*P* value for trend). Student's *t*-test with unequal variance was used for densitometry quantification of immunoblots. Correction for multiple comparisons was performed using the Benjamini-Hochberg procedure¹⁸, controlling the false discovery rate (FDR). Uncorrected *P* values and FDR are presented in the tables. *P* values < 0.05 were considered significant. A FDR threshold of 10% was applied.

Results

Proteomics Analysis of a Porcine Model of Stent Injury

BMS or DES were implanted in porcine coronary arteries. Coronary arteries subjected to balloon angioplasty alone without stent deployment served as controls (**Figure 1A**). At five time points 1, 3, 7, 14 and 28 days post-stent implantation OCT was performed (**Figure 1B**). The OCT analysis revealed that at 14 days post-stent implantation neointimal volume was higher in BMS compared to DES (*P*=0.025) with no significant difference at day 28. The minimal lumen area and the stent strut coverage were not different for BMS and DES during the 28 days follow-up. Time points without significant differences were chosen for proteomic analysis to identify differences in the ECM composition. In total, 45 samples were analyzed by proteomics (Supplemental Figure 1). Characteristics of all samples are summarized in Supplemental Table 1.

A three-step extraction method as previously described was used to sequentially extract the ECM proteins of the vascular media.¹⁶ 28 days post-stent implantation, a neointima had evolved on top of the stent struts regardless of the stent-type. The neointima was separated from the media before proteomics analyses. Following deglycosylation and tryptic digestion, proteomics analysis was performed of the neointima and the media by LC-MS/MS (**Figure 1C**). Duplicate measurements performed on the neointima samples showed good reproducibility for

spectral counts and sequence coverage as well as number of identified peptides (Supplemental Figure 2).

To improve the identification of ECM proteins upon MS, a custom-made pig ECM protein database was generated for database search containing a comprehensive porcine sequence list of previously published ECM proteins (Supplemental Figure 3). A total of 151 unique ECM proteins were identified overall in the neointima and the media with a minimum of 2 high-confidence peptides (Supplemental Figure 4, Supplemental Table 2-4). Proteins only identified in the media (n=11) or neointima (n=26) are marked with an asterisk.

Comparison of the neointima of DES and BMS

Compared to BMS, the neointima of arteries with DES implantation contained less structural constituents of the ECM like collagen type I, III, V as well as regulatory ECM proteins such as biglycan, lumican, fibromodulin or periostin (**Figure 2A**); in contrast, proteins involved in the regulation of calcification such as matrix Gla protein (MGP), secreted phosphoprotein 24 (SPP24) and bone morphogenetic protein 1 (BMP1) were increased (**Figure 2B**). Interestingly, proteomics also uncovered the presence of chondroadherin in coronary arteries with DES (**Figure 2B**). This small leucine-rich proteoglycan (SLRP) has not been previously reported in the vasculature. Next, we tested whether everolimus treatment had an effect on calcification of human aortic SMCs in culture using the o-Cresolphthalein assay (**Figure 2C**). Everolimus was coated on the DES used in porcine coronary arteries. Indeed, an inhibition of calcification was observed upon everolimus treatment. Immunohistochemistry localised both MGP and SPP24 in human coronary arteries with atherosclerotic plaques with and without stent implantation (**Figure 2D**).

ECM Changes in the Media Post-stenting

ECM remodelling in response to stent implantation was compared at four different time points (**Figure 3A-B**). Coronary arteries subject to balloon angioplasty without stent implantation served as controls (**Figure 3C**). At an early stage, proteins regulating hemostasis (e.g. plasminogen, fibrinogen, antithrombin-III) and inflammation (e.g. pentraxin-related protein PTX3, prophenin and tritrypticin precursor) were increased, alongside apolipoproteins found on VLDL particles, including apoC-III, apoE, and apoR.¹⁹ Proteins with a late response included large aggregating proteoglycans (aggrecan, versican), fibrillar collagens (e.g. type I, III and V), SLRPs (decorin, biglycan, fibromodulin, podocan, asporin) and matricellular proteins (e.g. periostin, tenascin, SPARC). Generally, fewer proteins changed in the BA group than in stented arteries and more pronounced changes were seen in DES compared to BMS (**Figure 3D**; Supplemental Table 5). Differences in the ECM between DES and BMS became most obvious at day 28 (**Figure 3E**) and were not revealed by OCT imaging. Thus, DES not only affect cell proliferation but also the composition of the ECM.

Comparison of the Media of DES and BMS

At day 28, the anti-proliferative effects of DES compared to BMS were reflected in a lower abundance of basement membrane proteins such as collagen alpha-2 IV (CO4A2), collagen alpha-1 XVIII (COIA1), as well as laminin beta-1 (LAMB1), laminin beta-2 (LAMB2) and laminin gamma-1 (LAMC1) (**Figure 4A**; Supplemental Table 6). In contrast, the large aggregating proteoglycan aggrecan (PGCA) was upregulated after stenting, particularly in DES (**Figure 4B**). Aggrecan is the major proteoglycan in the articular cartilage and interacts with hyaluronic acid. Its rise mirrored the increase of versican, the major large aggregating proteoglycan in the vasculature (**Figure 4B**). Aggregates of aggrecan and versican with

hyaluronic acid are stabilized by hyaluronan and proteoglycan link protein 1 (HPLN1). HPLN1 was reduced in the media of DES compared to BMS (**Figure 4B**).

Stent-induced Changes in Aggrecan and Aggrecanase Expression

Due to its unknown function in the vasculature, aggrecan was selected for further validation. For comparison, we used versican as a structurally and functionally related large proteoglycan. A rise of aggrecan and versican expression after stenting was confirmed at the transcript level (**Figure 4C**). Consistent with the proteomics findings, there was no equivalent increase in the gene expression of hyaluronan and proteoglycan link protein 1 (*HAPLN1*).

Besides gene expression, protein degradation determines the abundance of ECM proteins in the vessel wall. Aggrecanases are members of the ADAMTS (a disintegrin and metalloprotease with thrombospondin motifs) family that can cleave aggrecan and other large aggregating proteoglycans like versican. Thus, we used neoepitope antibodies that only recognize aggrecan and versican upon cleavage by members of the ADAMTS family, but not by other proteases like matrix metalloproteinases. For aggrecan, we probed for the signature cleavage at NITEGE³⁷³-ARGTV in the interglobular domain at the N-terminus, whereas versican fragments were detected by the DPEAAE neoepitope (**Figure 5A**). The rise in aggrecan was accompanied by increased detectability of the NITEGE neoepitope in DES (**Figure 5B**, Supplemental Figure 5). After an initial loss at day 3, a similar increase of the ADAMTS-generated DPEAAE containing versican fragments was observed (**Figure 5B**, Supplemental Figure 5). At day 28, both were more pronounced in DES compared to BMS (**Figure 5C**, Supplemental Figure 6). These findings demonstrate, for the first time, the contribution of aggrecanases to vascular remodeling upon stent implantation.

As the neopeptide antibodies do not distinguish between the activities of the different aggrecanases and may reflect differences in substrate availability rather than changes in aggrecanolytic activity, we investigated the gene expression of the three main ADAMTS enzymes that cleave large aggregating proteoglycans: ADAMTS-1, -4 and -5. Upon stenting, there was a notable reduction in *ADAMTS1* and *5* gene expression, followed by an increase in *ADAMTS4* (**Figure 5D**). *ADAMTS1* showed the highest expression levels in porcine coronary arteries (**Figure 5E**).

Aggrecan and Aggrecanase Expression in Human Vascular Cells

To relate the findings in the porcine model of stent injury to human vascular cells, we investigated the gene expression of *ADAMTS1*, *4* and *5* in endothelial cells (EC) and in SMCs from human coronary arteries (**Figure 5F**). Human coronary artery ECs express *ADAMTS1* and *ADAMTS4* but neither *ADAMTS5*, aggrecan nor *HAPLN1*. In contrast, human coronary artery SMCs express all aggrecanases, including *ADAMTS5*, as well as aggrecan, versican and *HAPLN1*. Thus, resident vascular cells can contribute to the aggrecanase activity and aggrecan expression in the arterial wall, with ECs expressing aggrecanases but not aggrecan.

Aggrecan in the Human Vasculature

To further validate our findings in human tissue, we used immunohistochemistry to localize aggrecan and aggrecan cleavage in stented human coronary arteries (**Figure 6A**). Coronary arteries with atherosclerotic plaques but without stents served as a reference control. Aggrecan and HPLN1 co-localized in the media of control arteries. In stented coronary arteries, staining for the aggrecan NITEGE neopeptide was observed predominantly below the periluminal cellular layer and at the contacts of the stent struts with the coronary artery (**Figure 6B**, Supplemental Figure 7). This was also supported by the finding that human coronary artery ECs express

ADAMTS1 and *ADAMTS4* (**Figure 5F**). To further investigate aggrecan in the human vasculature, we compared specimens of human saphenous veins and human thoracic aorta. Targeted proteomics revealed that similar to versican, aggrecan was more abundant in the aorta than in veins (**Figure 6C**, Supplemental Table 7). The SLRP decorin served as a control. Likewise, the ADAMTS-specific aggrecan NITEGE neopeptide was detectable in the aorta (**Figure 6D**, Supplemental Figure 8). Aggrecan and ADAMTS-induced aggrecan cleavage was seen throughout the media of the human aorta as confirmed by immunofluorescence staining (**Figure 6E**).

Aggrecan and Aggrecanases in Mice

ADAMTS-5 is the main aggrecan degrading enzyme in mice.²⁰ To examine the effects of ADAMTS-5 on the vasculature, we used proteomics to compare the ECM of aortas from mice lacking the catalytic domain of ADAMTS-5²⁰ with aortas from littermate controls (Supplemental Table 8). Loss of ADAMTS-5 activity resulted in an accumulation of aggrecan (**Figure 7A**) confirming the importance of aggrecanases in regulating the abundance of aggrecan in the vessel wall. These structural changes in the aortic wall were accompanied by an increase in the diameter of the thoracic, but not of the abdominal aorta (**Figure 7B**). Notably, cardiac output as measured by cardiac MRI and blood pressure were not significantly different from wildtype controls (Supplemental Figure 9 and Supplemental Figure 10). This genetic mouse model confirms the importance of aggrecanases in regulating the abundance of aggrecan in the vessel wall and suggests a link between aggrecanase activity and aortic diameter.

The higher abundance of aggrecan in stented porcine coronary arteries and human aortas compared to veins is suggestive of mechanical stretch inducing aggrecan expression in the vasculature. In order to explore this potential mechanism, veins were grafted into carotid arteries

of mice.²¹ After grafting, mice were fed a diet of stable isotope labelled amino acids for 28 days to label newly synthesized proteins (**Figure 8A**). Using targeted LC-MS/MS analysis (Supplemental Table 9), the incorporation of the stable isotope labelled amino acids was compared between ECM proteins in veins, vein grafts and arteries. 60% of aggrecan peptides were found to be labelled in the murine aorta, demonstrating active synthesis of this proteoglycan in the arterial wall. In contrast, labelled aggrecan peptides were undetectable in veins. The incorporation ratio in vein grafts, however, was comparable with the aorta. Thus, aggrecan synthesis was inducible in veins by exposure to arterial blood pressure. Representative histological sections are shown in **Figure 8B**, where aggrecan was markedly elevated after grafting. The upregulation coincided with cleavage of the versican core as indicated by staining for the ADAMTS-specific DPEAAE neoepitope. Thus, besides their established role in cartilage, aggrecan and aggrecanases are important contributors to ECM remodeling in the vasculature upon stenting and mechanical stretch (**Figure 8C**).

Discussion

This is the first proteomics analysis to profile the ECM remodeling of stented coronary arteries and to compare the effects of DES versus BMS on the vascular ECM. Diverging from the traditional focus on collagens and matrix metalloproteinases, this study highlights the contribution of aggrecan and aggrecanases to ECM remodeling after stent implantation. Findings in the large animal model were validated in human specimen and followed-up in two small animal models. Thus far, little is known about the role of aggrecan in the vasculature and stimuli that induce its expression.²² We demonstrate that aggrecan is more abundant in arteries than in

veins, that the synthesis of aggrecan is inducible by grafting veins to arteries and that aggrecan abundance is influenced by aggrecanase activity in the arterial wall.

ECM Changes in the Neointima

The vascular ECM plays a critical role in providing structural support to the vessel wall and influences cell behavior and signaling. Our proteomics comparison of the neointima revealed the following findings: First, a more organized and structured ECM assembly in the neointima forming over BMS compared to DES. Presumably ECM organization occurs at an earlier stage in arteries treated with BMS compared to DES; Secondly, an upregulation of proteins associated with the regulation of calcification in neointimal lesions of arteries treated with DES. The upregulation of these proteins may be a protective response as demonstrated by the presence of MGP and SPP24 in human control arteries. MGP is thought to act as an inhibitor of calcification.²³ Similarly, SPP24 is not osteogenic but binds to and affects the activity of BMP-2.²⁴ Indeed, calcification assays in human arterial SCMs demonstrated an inhibition of calcification under everolimus treatment. Everolimus is an inhibitor of the mechanistic target of rapamycin (mTOR). Further studies will need to clarify whether this observation is directly related to the observed ECM protein changes upon drug treatment or other drug effects. Drug effects could induce a phenotypic change of SMCs. This may also explain why MGP and SPP24 appear increased in normal vessels versus stented human vessels. Finally, we observed chondroadherin in DES stented arteries. This SLRP is mainly expressed in cartilaginous tissue²⁵ and has been previously associated with disc degeneration²⁶, but its expression in the vasculature has never been reported at the protein level. Yet, there is evidence for an association of chondroadherin with vascular pathology, since its transcription was found to be specifically induced in atherosclerotic plaques of femoral arteries.²⁷ It remains to be elucidated, if these

proteins might provide a link to the increased incidence or accelerated course of *de novo* atherosclerosis within DES-stented vessels.²⁸

Early Changes upon Vascular Injury

Our discovery-based proteomics comparison allowed an analysis of ECM proteins during early and late stages of vascular healing in response to stents. The early response to injury was independent of the applied stent type. Some changes were also observed after BA alone without stent insertion, indicating a response to vascular injury rather than stenting. Three different functional classes were increased: First, proteins involved in thrombosis such as fibrinogen, plasminogen, antithrombin III and thrombospondin, which is in line with findings in histopathological studies of platelet activation and thrombosis formation during the early stage of vascular healing.²⁹ Secondly, inflammatory proteins associated with innate immunity, such as PTX3 and prophenin and tritrtpticin, implicating the recruitment of inflammatory cells to the site of vascular injury. Lactadherin, for example, contributes to phagocytic removal of apoptotic cells³⁰ and showed a peak expression at 7 days post-stent insertion in the DES group. Finally, various apolipoproteins, such as apolipoproteins E, C-III, and R and also lipoprotein lipase were retained. It is noteworthy that these are VLDL-associated apolipoproteins.¹⁹ We have recently observed that plasma levels of VLDL-associated apolipoproteins predict cardiovascular events³¹ and that they are also present in human atherosclerotic plaques.³²

ECM Changes in the Media

ECM changes were observed predominantly after 28 days, which is likely explained by the time it takes for SMCs to lay down enough new ECM. A significant increase at day 28 was seen in fibrillar collagens, such as type I, III and V, as well as matricellular proteins (periostin, tenascin, SPARC) and SLRPs like decorin, biglycan, fibromodulin, podocan and asporin. These are

important regulatory proteins and involved in a variety of cellular functions such as collagen fibril assembly, inflammation, cell proliferation, adhesion and migration as well as fibrosis.³³ Generally more proteins showed a significant change in the DES compared to BMS group, with the differences being more pronounced at later stages. In DES, a uniform down-regulation of basement membrane proteins, indicative of the reduced cellularity, was accompanied by an increase in aggrecan, also known as cartilage-specific proteoglycan core protein.

Aggrecan in the Vasculature

Aggrecan is well studied in cartilage but its expression and function in the vasculature has only recently begun to be appreciated. It is the major proteoglycan in cartilage^{34, 35} and characterized by its ability to bind hyaluronan, a large carbohydrate polymer, to form even larger aggregates.³⁶ Between its G2 and G3 domain aggrecan carries numerous glycosaminoglycans (GAGs), namely keratan sulfate and chondroitin sulfate chains, giving the protein an enormous amount of fixed negative charges (**Figure 5A**). These highly negatively charged GAGs provide the basis for the viscoelastic properties of cartilage.

Due to its water-attracting property that confers resistance to compression, aggrecan may be part of an adaptive response of the vasculature to absorb mechanical forces. Additionally, proteoglycans present growth factors and cytokines to the surrounding tissue³⁷ and their interactions with other ECM components modulate a wide range of cellular responses, including inflammation.³⁸ It has been suggested that the lipoprotein binding to negatively charged GAG side chains might contribute to atherosclerosis.^{22, 39} Aggrecan expression was demonstrated in advanced lesions of atherosclerotic aortas of ApoE/LDLr deficient mice by immunohistochemistry, further supporting that cartilage-associated ECM proteins may be involved in the pathogenesis of atherosclerosis.⁴⁰ Similarly, we observed staining for aggrecan in

the atherosclerotic lesion of the human control coronary artery (**Figure 6A**, *indicates plaque location). Notably, a previous proteomics analysis discovered aggrecan in vascular intimal hyperplasia.⁴¹ Our proteomics study provides the first evidence for an upregulation of aggrecan after stenting and upon grafting veins from a low- to a high-pressure environment. Future studies are needed to investigate whether aggrecan or its cleavage products may contribute to the more frequent and accelerated onset of neoatherosclerosis in DES.⁴² Kumar *et al.* have recently reported that reduced aggrecan cleavage was associated with decreased macrophage numbers and less atherosclerosis in *Adamts4*^{-/-} *ApoE*^{-/-} mice.⁴³

Aggrecanases in the Vasculature

Besides aggrecan, the aggrecan NITEGE neopeptide was detected in porcine coronary arteries upon stenting. This aggrecan neopeptide is generated upon digestion by aggrecanases, but not by other proteases. As aggrecan is not abundant in uninjured vessels (**Figure 4B**), the NITEGE neopeptide predominantly reflects differences in substrate availability (**Figure 5B**). Instead, the versican DPEAAE neopeptide reflects the loss of aggrecanolytic activity at day 3 post stenting (**Figure 5B**). The neopeptide antibodies do not distinguish between the cleavage products of ADAMTS-1, ADAMTS-4 and -5 activity. *ADAMTS1*, *ADAMTS4* and *ADAMTS5*, however, showed a notable shift in gene expression in stented porcine coronary arteries. Expression of *ADAMTS1* and *ADAMTS5* was markedly reduced upon stent implantation. Instead, *ADAMTS4* was induced, in particular in BMS. Human coronary artery ECs only express *ADAMTS1* and *ADAMTS4*, while human coronary artery SMCs express *ADAMTS1*, *ADAMTS4* and *ADAMTS5* as well as aggrecan. Thus, loss of arterial ECs upon stenting could contribute to the initial loss of aggrecanase expression in the vessel wall.⁴⁴ Moreover, the effects of DES might facilitate the accumulation of large aggregating proteoglycans in the vessel wall. Treatment of human

coronary artery SMC with everolimus reduced gene expression of *ADAMTS4*, while expression levels of *ADAMTS1* remained unchanged (data not shown). Upon vascular injury, however, inflammatory cells are likely to contribute to the ADAMTS-4 activity in the vessel wall.⁴³

Aggrecan and its ADAMTS-cleaved fragments were also co-localized in the media of the human thoracic aorta. Aggrecanase activity regulates the abundance of aggrecan in the vessel wall as evidenced by the build-up of aggrecan in the aorta of mice lacking the catalytic domain of ADAMTS-5. Their vascular phenotype closely resembled recent observations in *Adamts-1* heterozygous mice.⁴⁵ In *Adamts-1*^{+/-} mice, thoracic aortic aneurysm formation and dissection were induced by an increase in inducible nitric oxide synthase and medial degeneration. In our analysis, loss of ADAMTS-5 activity resulted in thoracic aortic dilation with a build-up of aggrecan. This finding extends our previous report on the catabolic properties of ADAMTS-5 on vascular proteoglycans and its ability to alter proteoglycan-mediated lipoprotein retention in a mouse model of atherosclerosis.²²

Strengths and Limitations

A particular strength of our study is the combination of proteomics with a clinically relevant large animal model of human disease.¹⁵ In the porcine model, peak neointima growth is observed at 28 days after stent deployment corresponding to 6 months in human. Few changes occur beyond this time point, with the exception of slight neointima thinning later on.¹⁴ The pigs, however, are young and free of atherosclerosis. A caveat of working with porcine tissue is the limited availability of antibodies, and proteomics was key for a comprehensive protein analysis without constraints imposed by antibodies.

Conclusions

The effects of DES go beyond inhibition of smooth muscle cell proliferation, but have a wider impact on vascular remodeling by altering the composition of the ECM. The antiproliferative effect of DES was evident by a reduction in basement membrane proteins. Moreover, the decreased cellularity was accompanied by increased production of large proteoglycans like aggrecan and versican. Aggrecan and aggrecanases are integral components during ECM remodeling after stenting. A summary of our findings is provided in **Figure 8C**.

Authors

Gonca Suna, MD, PhD¹; Wojciech Wojakowski, MD²; Marc Lynch, MSc¹; Javier Barallobre-Barreiro, PhD¹; Xiaoke Yin, PhD¹; Ursula Mayr, MD¹; Ferheen Baig, MSc¹; Ruifang Lu, PhD¹; Marika Fava, PhD¹; Robert Hayward, BSc¹; Chris Molenaar, PhD¹; Stephen J. White, PhD³; Tomasz Roleder, MD²; Krzysztof P. Milewski, MD⁴; Pawel Gasior, MD²; Piotr P. Buszman, MD⁴; Pawel Buszman, MD⁴; Marjan Jahangiri, MD⁵; Cathy Shanahan, PhD¹; Jonathan Hill, MD⁶; Manuel Mayr, MD, PhD¹



Affiliations

¹King's British Heart Foundation Centre, King's College London, London, UK; ²3rd Division of Cardiology, Medical University of Silesia, Katowice, Poland; ³Healthcare Science Research Centre, Manchester Metropolitan University, Manchester, UK; ⁴Centre for Cardiovascular Research and Development, American Heart of Poland, Katowice, Poland; ⁵St. George's Vascular Institute, St George's Healthcare NHS Trust, London, UK; ⁶King's College Hospital and King's Health Partners Academic Health Sciences, London, UK

Acknowledgments

Stents were supplied free of charge by Abbott Vascular. Fluorescent microscopic images were acquired at the Nikon Imaging Centre at King's College London. We acknowledge the technical contribution of Norman Catibog and Mei Chong. We thank Dr. Raimund Pechlaner for his advice on the statistical analysis.

Sources of Funding

Dr. Suna was supported by a PhD studentship from the British Heart Foundation (BHF). Prof. Wojakowski received funding from RMT foundation. Dr. White is supported by BHF CH95/001 and the National Institute for Health Research (NIHR) Bristol Biomedical Research Unit in Cardiovascular Medicine. Prof. Mayr is a BHF Chair Holder (CH/16/3/32406) with BHF programme grant support (RG/16/14/32397) and supported by the NIHR Biomedical Research Centre based at Guy's and St Thomas' National Health Service Foundation Trust and King's College London in partnership with King's College Hospital.

Disclosures

Dr. Hill is part of the Consultant Advisory Board at St Jude Medical.

References

1. Fischman DL, Leon MB, Baim DS, Schatz RA, Savage MP, Penn I, Detre K, Veltri L, Ricci D, Nobuyoshi M, Cleman M, Heuser R, Almond D, Teirstein PS, Fish RD, Colombo A, Brinker J, Moses J, Shakhovich A, Hirshfeld J, Bailey S, Ellis S, Rake R, Goldberg S, for the Stent Restenosis Study Investigators. A randomized comparison of coronary-stent placement and balloon angioplasty in the treatment of coronary artery disease. *N Engl J Med*. 1994;331:496-501. doi: 10.1056/NEJM199408253310802.
2. Serruys PW, de Jaegere P, Kiemeneij F, Macaya C, Rutsch W, Heyndrickx G, Emanuelsson H, Marco J, Legrand V, Materne P, Belardi J, Sigwart U, Colombo A, Goy JJ, van den Heuvel P,

- Delcan J, Morel M, for the Benestent Study Group. A comparison of balloon-expandable-stent implantation with balloon angioplasty in patients with coronary artery disease. *N Engl J Med*. 1994;331:489-495. doi: 10.1056/NEJM19940825331080.
3. Morice MC, Serruys PW, Sousa JE, Fajadet J, Ban Hayashi E, Perin M, Colombo A, Schuler G, Barragan P, Guagliumi G, Molnar F, Falotico R, for the RAVEL Study Group. A randomized comparison of a sirolimus-eluting stent with a standard stent for coronary revascularization. *N Engl J Med*. 2002;346:1773-1780. doi: 10.1056/NEJMoa012843.
4. Stone GW, Ellis SG, Cox DA, Hermiller J, O'Shaughnessy C, Mann JT, Turco M, Caputo R, Bergin P, Greenberg J, Popma JJ, Russell ME, for the TAXUS-IV Investigators. A polymer-based, paclitaxel-eluting stent in patients with coronary artery disease. *N Engl J Med*. 2004;350:221-231. doi: 10.1056/NEJMoa032441.
5. Stettler C, Wandel S, Allemann S, Kastrati A, Morice MC, Schomig A, Pfisterer ME, Stone GW, Leon MB, de Lezo JS, Goy JJ, Park SJ, Sabate M, Sirtop MJ, Kelbaek H, Spaulding C, Menichelli M, Vermeersch P, Dirksen MT, Cervinka P, Petronio AS, Nordmann AJ, Diem P, Meier B, Zwahlen M, Reichenbach S, Trelle S, Windecker S, Juni P. Outcomes associated with drug-eluting and bare-metal stents: a collaborative network meta-analysis. *Lancet*. 2007;370:937-948. doi: 10.1016/S0140-6736(07)61444-5.
6. Nakazawa G, Finn AV, Vorpahl M, Ladich ER, Kolodgie FD, Virmani R. Coronary responses and differential mechanisms of late stent thrombosis attributed to first-generation sirolimus- and paclitaxel-eluting stents. *J Am Coll Cardiol*. 2011;57:390-398. doi: 10.1016/j.jacc.2010.05.066.
7. Nakazawa G, Otsuka F, Nakano M, Vorpahl M, Yazdani SK, Ladich E, Kolodgie FD, Finn AV, Virmani R. The pathology of neoatherosclerosis in human coronary implants bare-metal and drug-eluting stents. *J Am Coll Cardiol*. 2011;57:1314-1322. doi: 10.1016/j.jacc.2011.01.011.
8. Erbel R, Di Mario C, Bartunek J, Bonnier J, de Bruyne B, Eberli FR, Erne P, Haude M, Heublein B, Horrigan M, Ilesley C, Bose D, Koolen J, Luscher TF, Weissman N, Waksman R, for the PROGRESS-AMS Investigators. Temporary scaffolding of coronary arteries with bioabsorbable magnesium stents: a prospective, non-randomised multicentre trial. *Lancet*. 2007;369:1869-1875. doi: 10.1016/S0140-6736(07)60853-8.
9. Pilgrim T, Heg D, Roffi M, Tuller D, Muller O, Vuilliminet A, Cook S, Weilenmann D, Kaiser C, Jamshidi P, Fahrni T, Moschovitis A, Noble S, Eberli FR, Wenaweser P, Juni P, Windecker S. Ultrathin strut biodegradable polymer sirolimus-eluting stent versus durable polymer everolimus-eluting stent for percutaneous coronary revascularisation (BIOSCIENCE): a randomised, single-blind, non-inferiority trial. *Lancet*. 2014;384:2111-2122. doi: 10.1016/S0140-6736(14)61038-2.
10. Alfonso F, Byrne RA, Rivero F, Kastrati A. Current treatment of in-stent restenosis. *J Am Coll Cardiol*. 2014;63:2659-2673. doi: 10.1016/j.jacc.2014.02.545.
11. Inoue T, Croce K, Morooka T, Sakuma M, Node K, Simon DI. Vascular inflammation and repair: implications for re-endothelialization, restenosis, and stent thrombosis. *JACC Cardiovasc Interv*. 2011;4:1057-1066. doi: 10.1016/j.jcin.2011.05.025.
12. Farb A, Kolodgie FD, Hwang JY, Burke AP, Tefera K, Weber DK, Wight TN, Virmani R. Extracellular matrix changes in stented human coronary arteries. *Circulation*. 2004;110:940-947. doi: 10.1161/01.CIR.0000139337.56084.30.
13. Chung IM, Gold HK, Schwartz SM, Ikari Y, Reidy MA, Wight TN. Enhanced extracellular matrix accumulation in restenosis of coronary arteries after stent deployment. *J Am Coll Cardiol*. 2002;40:2072-2081. doi: 10.1016/S0735-1097(02)02598-6.

14. Schwartz RS, Chronos NA, Virmani R. Preclinical restenosis models and drug-eluting stents: still important, still much to learn. *J Am Coll Cardiol*. 2004;44:1373-1385. doi: 10.1016/j.jacc.2004.04.060.
15. Virmani R, Kolodgie FD, Farb A, Lafont A. Drug eluting stents: are human and animal studies comparable? *Heart*. 2003;89:133-138. doi:10.1136/heart.89.2.133
16. Didangelos A, Yin X, Mandal K, Baumert M, Jahangiri M, Mayr M. Proteomics characterization of extracellular space components in the human aorta. *Mol Cell Proteomics*. 2010;9:2048-2062. doi: 10.1074/mcp.M110.001693.
17. Yin X, Bern M, Xing Q, Ho J, Viner R, Mayr M. Glycoproteomic analysis of the secretome of human endothelial cells. *Mol Cell Proteomics*. 2013;12:956-978. doi: 10.1074/mcp.M112.024018.
18. Benjamini Y, Hochberg Y. Controlling the false discovery rate: a practical and powerful approach to multiple testing. *J R Stat Soc Series B Stat Methodol*. 1995;57:289-300. doi: 10.2307/2346101
19. Cooper ST, Attie AD. Pig apolipoprotein R: a new member of the short consensus repeat family of proteins. *Biochemistry*. 1992;31:12328-12336. doi: 10.1021/bi00164a006.
20. Stanton H, Rogerson FM, East CJ, Golub SB, Lawlor KE, Meeker CT, Little CB, Last K, Farmer PJ, Campbell IK, Fourie AM, Fosang AJ. ADAMTS5 is the major aggrecanase in mouse cartilage in vivo and in vitro. *Nature*. 2005;434:648-652. doi: 10.1038/nature03417.
21. Mayr M, Li C, Zou Y, Huemer U, Hu Y, Xu Q. Biomechanical stress-induced apoptosis in vein grafts involves p38 mitogen-activated protein kinases. *Faseb J*. 2000;14:261-270. doi: 10.1096/fj.1530-6860.
22. Didangelos A, Mayr U, Monaco C, Mayr M. Novel role of ADAMTS-5 protein in proteoglycan turnover and lipoprotein retention in atherosclerosis. *J Biol Chem*. 2012;287:19341-19345. doi: 10.1074/jbc.C112.350785.
23. Schurgers LJ, Cranenburg EC, Vermeer C. Matrix Gla-protein: the calcification inhibitor in need of vitamin K. *Thromb Haemost*. 2008;100:593-603. doi: 10.1160/TH08-02-0087.
24. Tian H, Li CS, Zhao KW, Wang JC, Duarte ME, David CL, Phan K, Atti E, Brochmann EJ, Murray SS. A carboxy terminal BMP/TGF-beta binding site in secreted phosphoprotein 24 kD independently affects BMP-2 activity. *J Cell Biochem*. 2015;116:667-676. doi: 10.1002/jcb.25023.
25. Haglund L, Tillgren V, Onnerfjord P, Heinegard D. The C-terminal peptide of chondroadherin modulates cellular activity by selectively binding to heparan sulfate chains. *J Biol Chem*. 2013;288:995-1008. doi: 10.1074/jbc.M112.430512.
26. Akhatib B, Onnerfjord P, Gawri R, Ouellet J, Jarzem P, Heinegard D, Mort J, Roughley P, Haglund L. Chondroadherin fragmentation mediated by the protease HTRA1 distinguishes human intervertebral disc degeneration from normal aging. *J Biol Chem*. 2013;288:19280-19287. doi: 10.1074/jbc.M112.443010.
27. Levula M, Oksala N, Airla N, Zeitlin R, Salenius JP, Jarvinen O, Venermo M, Partio T, Saarinen J, Somppi T, Suominen V, Virkkunen J, Hautalahti J, Laaksonen R, Kahonen M, Mennander A, Kytomaki L, Soini JT, Parkkinen J, Peltto-Huikko M, Lehtimäki T. Genes involved in systemic and arterial bed dependent atherosclerosis -Tampere Vascular study. *PLoS One*. 2012;7:e33787. doi: 10.1371/journal.pone.0033787.
28. Romero ME, Yahagi K, Kolodgie FD, Virmani R. Neoatherosclerosis from a pathologist's point of view. *Arterioscler Thromb Vasc Biol*. 2015;35:e43-49. doi: 10.1161/ATVBAHA.115.306251.

29. Grewe PH, Deneke T, Machraoui A, Barmeyer J, Muller KM. Acute and chronic tissue response to coronary stent implantation: pathologic findings in human specimen. *J Am Coll Cardiol*. 2000;35:157-163. doi: 10.1016/S0735-1097(99)00486-6.
30. Ait-Oufella H, Kinugawa K, Zoll J, Simon T, Boddaert J, Heeneman S, Blanc-Brude O, Barateau V, Potteaux S, Merval R, Esposito B, Teissier E, Daemen MJ, Leseche G, Boulanger C, Tedgui A, Mallat Z. Lactadherin deficiency leads to apoptotic cell accumulation and accelerated atherosclerosis in mice. *Circulation*. 2007;115:2168-21177. doi: 10.1161/CIRCULATIONAHA.106.662080
31. Pechlaner R, Tsimikas S, Yin X, Willeit P, Baig F, Santer P, Oberhollenzer F, Egger G, Witztum JL, Alexander VJ, Willeit J, Kiechl S, Mayr M. Very-low density lipoprotein-associated apolipoproteins predict cardiovascular events are lowered by inhibition of apoC-III. *J Am Coll Cardiol*. 2017; 69: 789-800. doi: 10.1016/j.jacc.2016.11.065
32. Langley SR, Willeit K, Didangelos A, Matic LP, Skroblin P, Barallobre-Barreiro J, Lengquist M, Rungger G, Kapustin A, Kedenko L, Molenaar C, Lu R, Barwari T, Suna G, Yin X, Iglseider B, Paulweber B, Willeit P, Shalhoub J, Pasterkamp G, Davies AH, Monaco C, Hedin U, Shanahan CM, Willeit J, Kiechl S, Mayr M. Extracellular matrix proteomics identifies molecular signature of symptomatic carotid plaques. *J Clin Invest*. 2017;127:1546-1560. doi: 10.1172/JCI86924
33. Merline R, Schaefer RM, Schaefer L. The matricellular functions of small leucine-rich proteoglycans (SLRPs). *J Cell Commun Signal*. 2009;3:323-35. doi: 10.1007/s12079-009-0066-2.
34. Danielson BT, Knudson CB, Knudson W. Extracellular processing of the cartilage proteoglycan aggregate and its effect on CD44-mediated internalization of hyaluronan. *J Biol Chem*. 2015;290:9555-9570. doi: 10.1074/jbc.M115.643171.
35. Huang K, Wu LD. Aggrecanase and aggrecan degradation in osteoarthritis: a review. *J Int Med Res*. 2008;36:1149-1160.
36. Morawski M, Bruckner G, Arendt T, Matthews RT. Aggrecan: Beyond cartilage and into the brain. *Int J Biochem Cell Biol*. 2012;44:690-693. doi: 10.1016/j.biocel.2012.01.010.
37. Rienks M, Papageorgiou AP, Frangogiannis NG, Heymans S. Myocardial extracellular matrix: an ever-changing and diverse entity. *Circ Res*. 2014;114:872-888. doi: 10.1161/CIRCRESAHA.114.302533.
38. Wu YJ, La Pierre DP, Wu J, Yee AJ, Yang BB. The interaction of versican with its binding partners. *Cell Res*. 2005;15:483-494. doi: 10.1038/sj.cr.7290318.
39. Skalen K, Gustafsson M, Rydberg EK, Hulten LM, Wiklund O, Innerarity TL, Boren J. Subendothelial retention of atherogenic lipoproteins in early atherosclerosis. *Nature*. 2002;417:750-754. doi: 10.1038/nature00804.
40. Strom A, Ahlqvist E, Franzen A, Heinegard D, Hultgardh-Nilsson A. Extracellular matrix components in atherosclerotic arteries of Apo E/LDL receptor deficient mice: an immunohistochemical study. *Histol Histopathol*. 2004;19:337-347.
41. Talusan P, Bedri S, Yang S, Kattapuram T, Silva N, Roughley PJ, Stone JR. Analysis of intimal proteoglycans in atherosclerosis-prone and atherosclerosis-resistant human arteries by mass spectrometry. *Mol Cell Proteomics*. 2005;4:1350-1357. doi: 10.1074/mcp.M500088-MCP200.
42. Otsuka F, Byrne RA, Yahagi K, Mori H, Ladich E, Fowler DR, Kutys R, Xhepa E, Kastrati A, Virmani R, Joner M. Neoatherosclerosis: overview of histopathologic findings and

implications for intravascular imaging assessment. *Eur Heart J*. 2015;36:2147-2159. doi: 10.1093/eurheartj/ehv205.

43. Kumar S, Chen M, Li Y, Wong FH, Thiam CW, Hossain MZ, Poh KK, Hirohata S, Ogawa H, Angeli V, Ge R. Loss of ADAMTS4 reduces high fat diet-induced atherosclerosis and enhances plaque stability in ApoE(-/-) mice. *Sci Rep*. 2016;6:31130. doi: 10.1038/srep31130.

44. Joner M, Nakazawa G, Finn AV, Quee SC, Coleman L, Acampado E, Wilson PS, Skorija K, Cheng Q, Xu X, Gold HK, Kolodgie FD, Virmani R. Endothelial cell recovery between comparator polymer-based drug-eluting stents. *J Am Coll Cardiol*. 2008;52:333-342. doi: 10.1016/j.jacc.2008.04.030.

45. Oller J, Mendez-Barbero N, Ruiz EJ, Villahoz S, Renard M, Canelas LI, Briones AM, Alberca R, Lozano-Vidal N, Hurle MA, Milewicz D, Evangelista A, Salaices M, Nistal JF, Jimenez-Borreguero LJ, De Backer J, Campanero MR and Redondo JM. Nitric oxide mediates aortic disease in mice deficient in the metalloprotease Adamts1 and in a mouse model of Marfan syndrome. *Nat Med*. 2017;23:200-212. doi: 10.1038/nm.4266



Circulation

Figure Legends

Figure 1. Porcine Model of Stent Injury. (A) Pigs underwent PCI with BMS/DES/BA treatment. Coronary arteries were retrieved for proteomics at 1, 3, 7, 14 and 28 days after stent deployment. The evolved neointimal lesions at day 28 were analyzed separately. In total, 45 samples were analyzed by LC-MS/MS. (B) Quantitative analysis of the neointima was performed by OCT. The neointimal structure was classified into homogenous with peristrut attenuation/ring, heterogeneous or layered. At 14 days post-stent implantation neointimal volume was higher in BMS compared to DES ($*P=0.025$) with no significant difference at day 28. $P=0.89$ (2-way ANOVA). (C) ECM proteins were obtained using our previously published extraction procedure, followed by LC-MS/MS analysis of the deglycosylated tryptic peptides.

Figure 2. ECM Remodeling in the Neointima. (A) Heat map of proteins with differential abundance. $n=7$ per group (t -test with unequal variance) (B) Proteins involved in the regulation of calcification (SPP24, MGP, BMP1) and chondroadherin were predominantly found in the DES group. $*P<0.05$. TIC=total ion current. BMP 1, chondroadherin and SPP24 were undetectable in the control group, thus a t -test was not performed. (C) Everolimus treatment reduced SMC calcification as revealed by Alizarin Red staining and o-Cresolphthalein Complexone assay. n =triplicates of 4 independent experiments. $***P<0.001$ (t -test with unequal variance). (D) MGP and SPP24 in human stented and control coronary arteries. Scale bars=1 mm.

Figure 3. ECM Remodeling in the Media. (A-C) Heat maps of ECM proteins with differential abundance at different time points. BMS/DES: $n=3$ per time point. $P<0.05$ (1-way ANOVA).

BA: n=3-4 per group. $P < 0.05$ (t -test with unequal variance). **(D)** Number of significant protein changes in BA late compared to BMS and DES at day 28. **(E)** Number of proteins with differential abundance between DES versus BMS at day 1, 3, 7 and 28 post stent implantation. Abbreviations: ITI heavy chain H2, inter-alpha-trypsin inhibitor heavy chain H2; PTX3, pentraxin-related protein PTX3; sFRP-1, secreted frizzled-related protein 1; IGF, insulin-like growth factor; SD, superoxide dismutase; LTBP, latent-transforming growth factor beta-binding protein; AE, adipocyte enhancer.

Figure 4. ECM Composition in DES and BMS in the Media. **(A)** Volcano plot of differentially expressed proteins between DES and BMS at day 28. n=3 per group (t -test with unequal variance). PGCA, aggrecan; HPLN1, hyaluronan and proteoglycan link protein 1 **(B)** Changes in aggrecan, versican and HPLN1 protein abundance at day 1, 3, 7 and 28 post stent implantation. n=3 per group. $*P < 0.05$ (t -test with unequal variance). TIC, total ion current. **(C)** Corresponding gene expression in stented (n=3 per time point) and control unstented coronary arteries (n=6); Gene expression values were normalized to unstented control arteries. Linear regression analysis for P value for trend. *HAPLN1*, gene name for hyaluronan and proteoglycan link protein 1.

Figure 5. Aggrecanase Expression in the Porcine Model of Stent Injury and Comparison to Human Vascular Cells. **(A)** The aggrecan neopeptide NITEGE and the versican neopeptide DPEAAE are generated by ADAMTS cleavage. **(B)** Aggrecan NITEGE and versican DPEAAE neopeptides in DES at day 1, 3, 7 and 28 post stent implantation. n=3 per time point. **(C)** Differences between BMS and DES at day 28. n=4 per group. **(D)** Gene expression of

ADAMTS1, 4 and 5 in porcine tissue. n=3 per time point for BMS/DES; n=6 for control coronary arteries. Gene expression values were normalized to unstented control arteries. Linear regression analysis for *P* value for trend. **(E)** Basal *ADAMTS* expression levels in porcine coronary arteries. Cycle threshold (CT) values by qPCR are given as 40-CT (higher values indicate higher abundance). n=6 per group. **(F)** Gene expression of *ADAMTS1*, 4 and 5 as well as versican, aggrecan and *HAPLN1* in ECs and SMCs of human coronary arteries. Cycle threshold (CT) values by qPCR are given as 40-CT (higher values indicate higher abundance). HCAEC, human coronary artery endothelial cells; HCASMC, human coronary artery SMCs; n=triplicates of 3 independent cell passages. ****P*<0.001 (*t*-test with unequal variance).

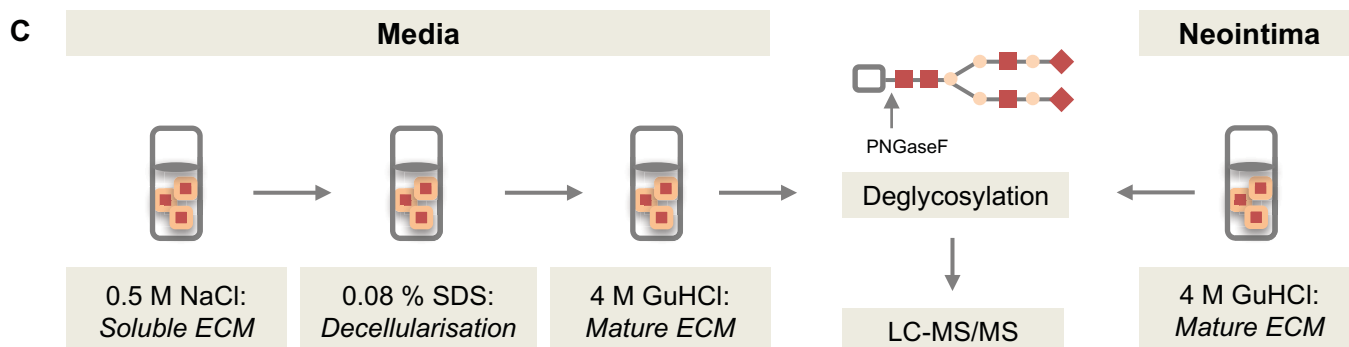
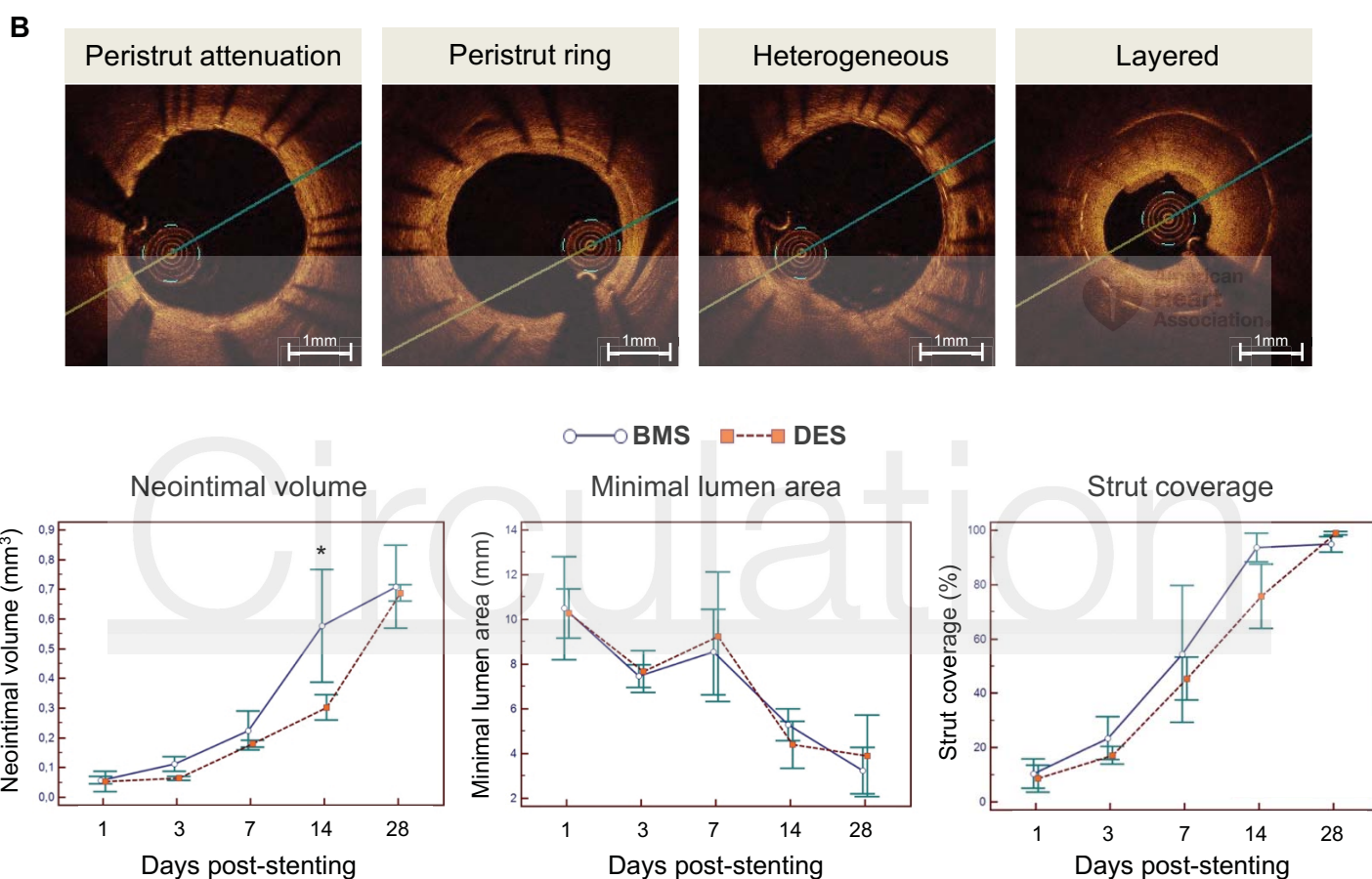
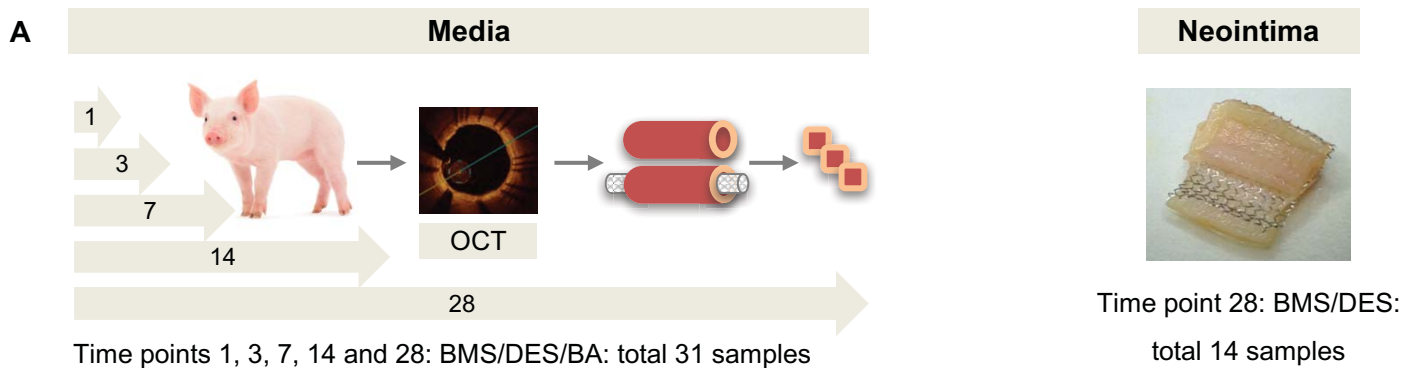


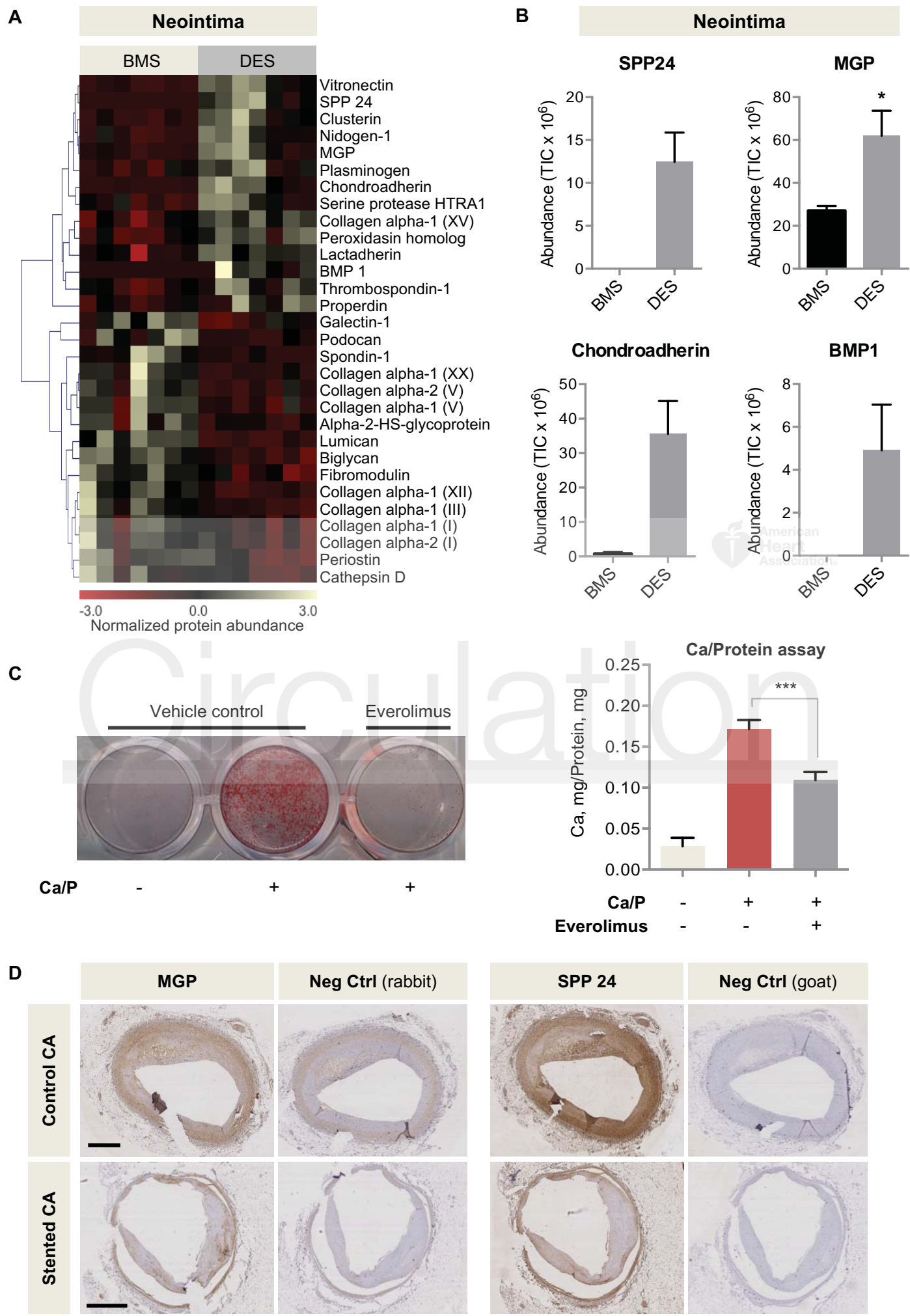
Figure 6. Aggrecan in the Human Vasculature. **(A)** Localization of aggrecan, the aggrecan NITEGE and versican DPEAAE neoepitopes (neo), and HPLN1 in stented and control human coronary arteries with presence of atherosclerosis (*). Arrows mark the contacts of the stent struts with coronary artery. Scale bars=1 mm. **(B)** Co-localization of aggrecan (Alexa 633, displayed in green) and aggrecan NITEGE neoepitope (Alexa 568, displayed in red) in human stented coronary arteries by immunofluorescence. Note the presence of aggrecan fragments at the contacts of the stent struts with the artery and in the subendothelial layer (zoomed-in areas). Overview image 20x, scale bar=500 μ m; Zoomed-in areas 60x, scale bar=25 μ m. **(C)** Adjusted peak area for aggrecan, versican and decorin in the human thoracic aorta and saphenous veins as determined by targeted proteomics. n=7 per group. **P*<0.05, ***P*<0.01 (*t*-test with unequal variance). **(D)** Immunoblots for the aggrecan NITEGE neoepitope and versican in the human thoracic aorta and saphenous veins. The SLRP decorin served as a loading control. n=4 per group. **(E)** Co-localization of aggrecan (Alexa 633, displayed in green) and aggrecan NITEGE

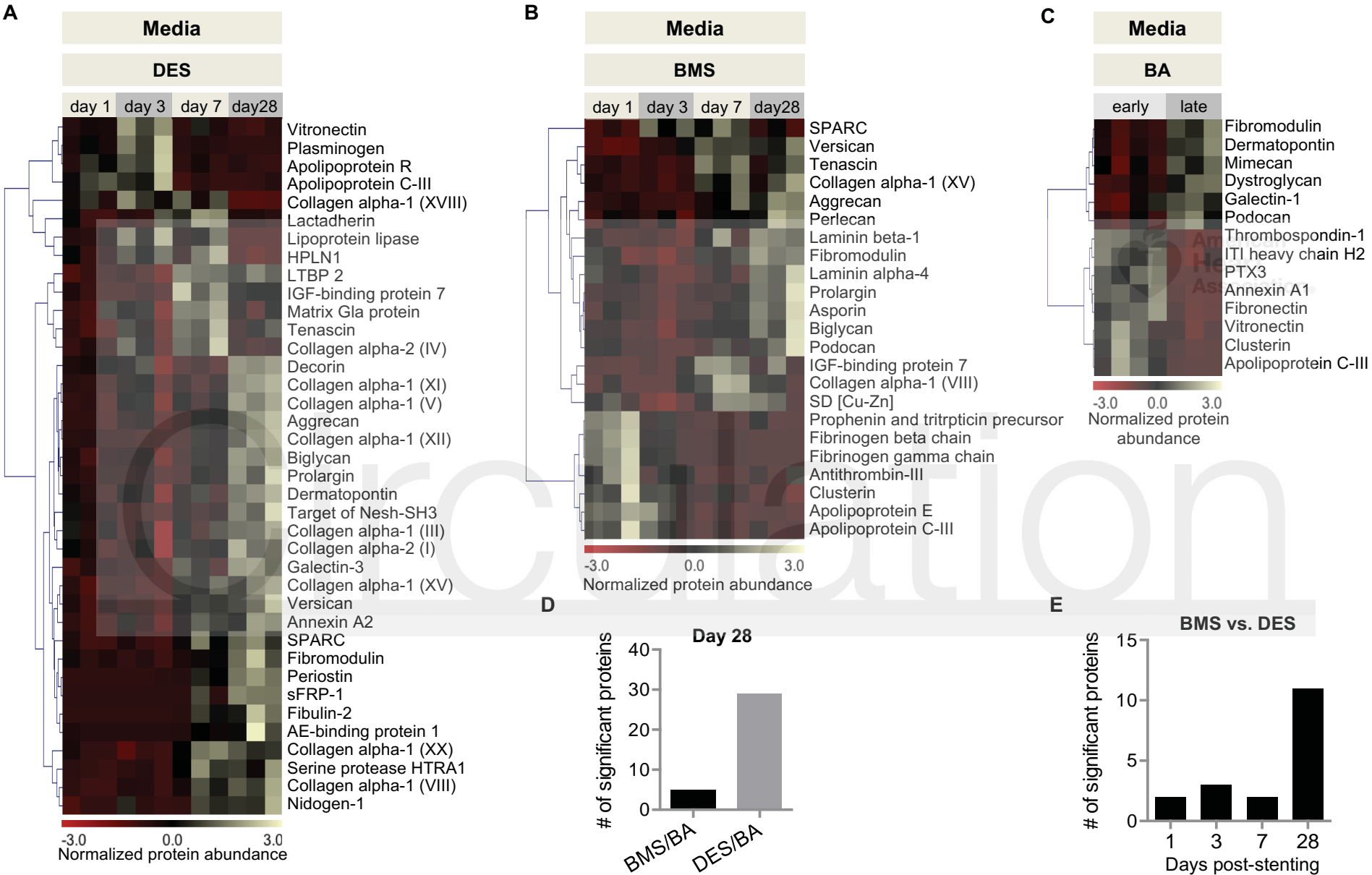
neoepitope (Alexa 568, displayed in red) in human aorta visualized by immunofluorescence. Elastin fibers in white (autofluorescence with 488nm laser excitation captured in the green emission channel). Control sections stained with isotype IgGs. Magnification 60x, scale bars=20 μm .

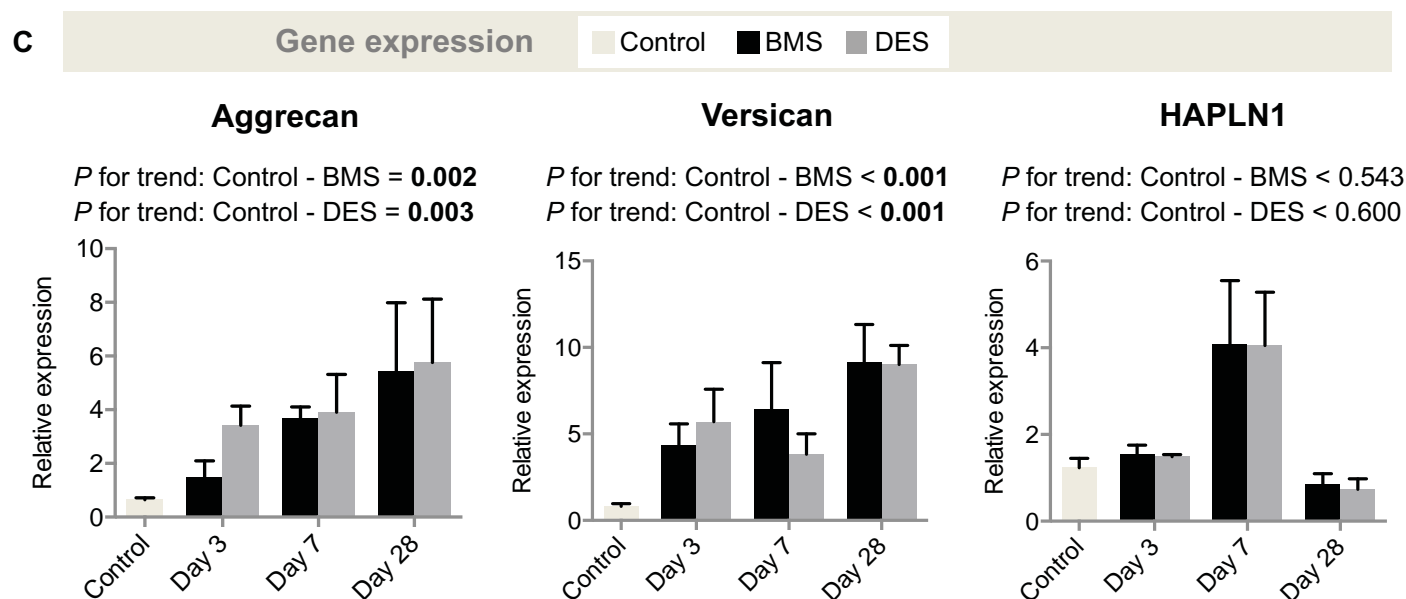
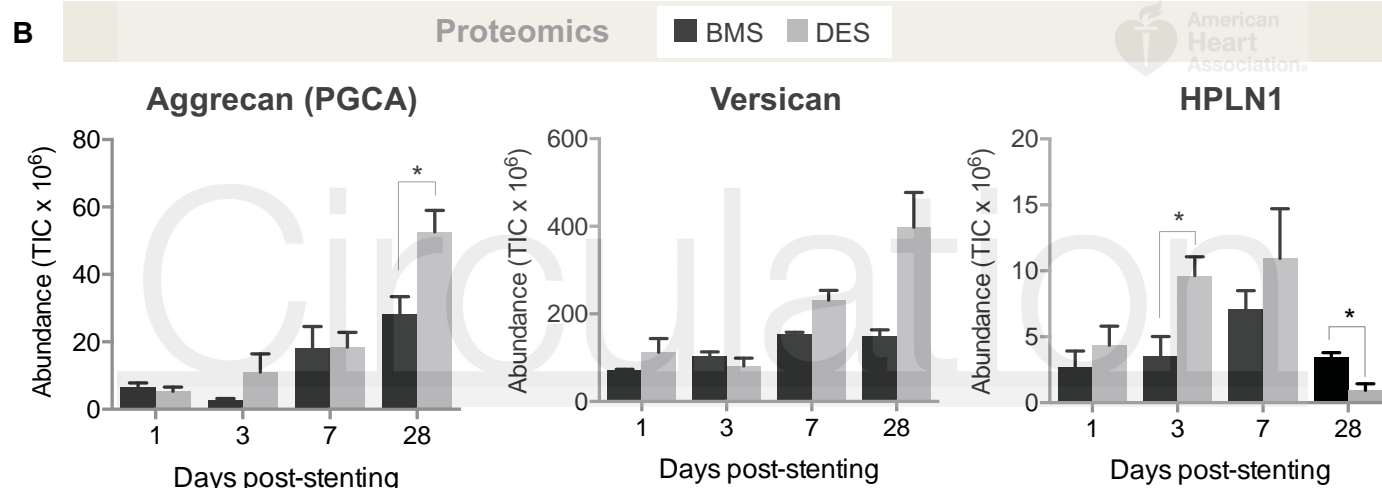
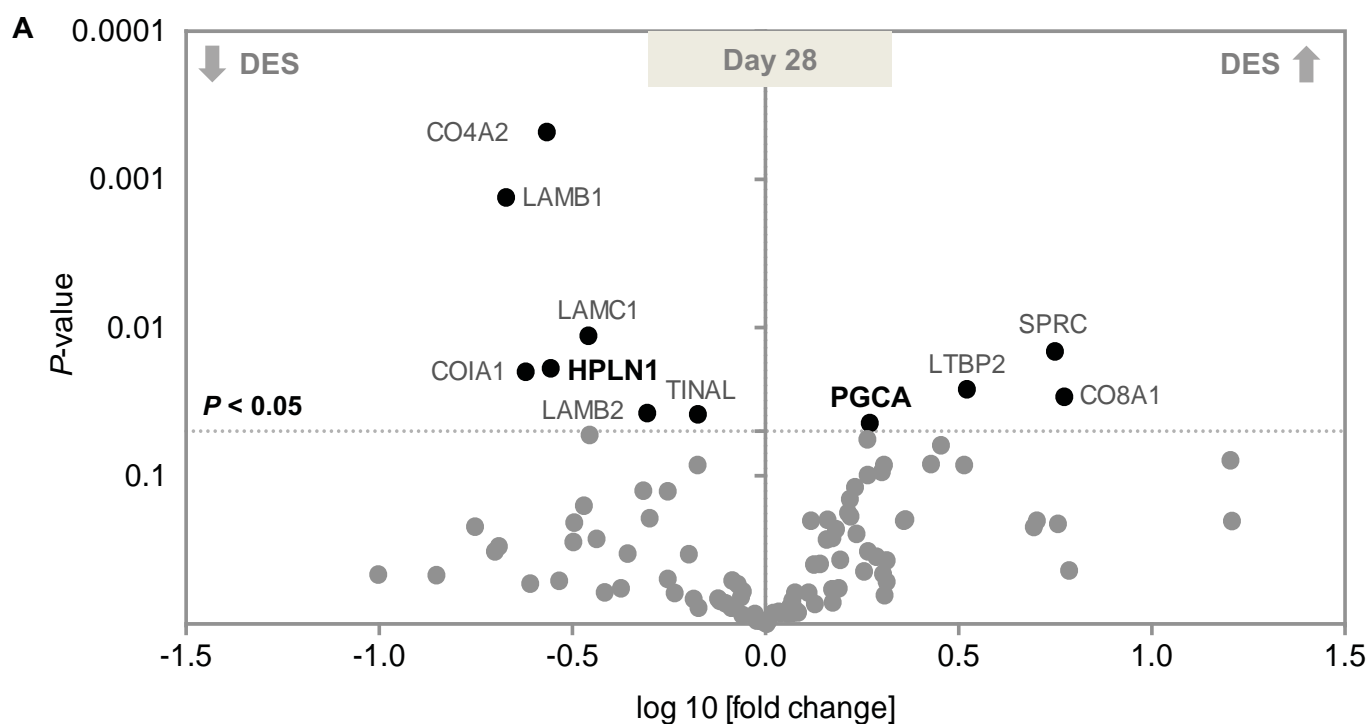
Figure 7. Aggrecan and Aggrecanases in the Murine Aorta (A) Volcano plot of differentially expressed proteins between the aorta of wild-type littermate controls (WT) and mice lacking the catalytic domain of ADAMTS-5 (*Adamts5* Δcat). n=6 (WT), n=5 (*Adamts5* Δcat), *t*-test with unequal variance. PGCA, aggrecan; MIME, mimecan; VTNC, vitronectin. (B) Aortic diameters of aortic ring (AoR), ascending aorta (AsAo) and abdominal aorta (AbAo) as measured by ultrasonography. Representative ultrasound images are shown, values are represented as box-and-whisker plots. n=5 per group **P*<0.05 (*t*-test with unequal variance).

Figure 8. Aggrecan in Vascular Remodeling. (A) The isogenic *venae cavae* were grafted to carotid arteries of mice fed a diet with stable isotope labelled amino acids. Incorporation ratios for aggrecan, versican and decorin in interposition grafts, vena cava inferior and aortas. n=8-9 per group. N.D.=not detectable. (B) Immunostaining for aggrecan, the versican DPEAAE neoepitope and decorin. Magnification 10x, scale bars=200 μm . (C) Summary. Changes in ADAMTS expression accompany the increase of the large aggregating proteoglycans aggrecan and versican post-stenting.

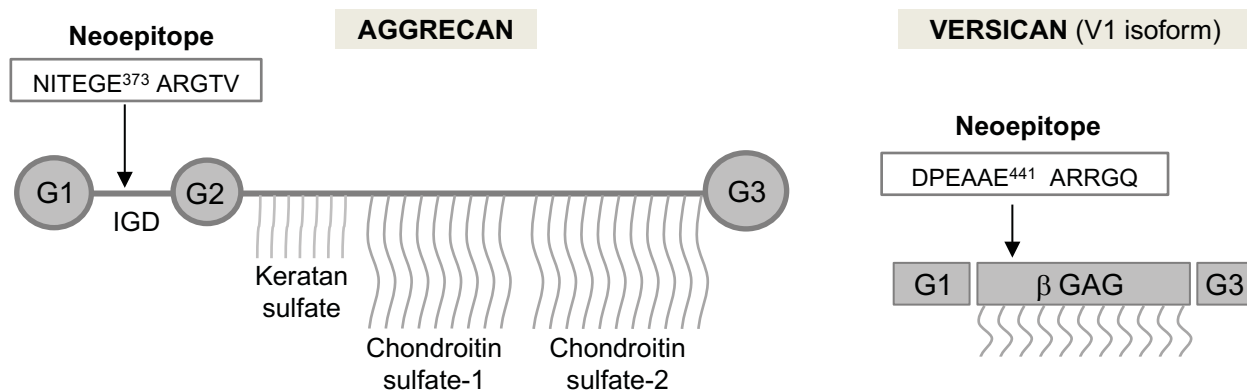




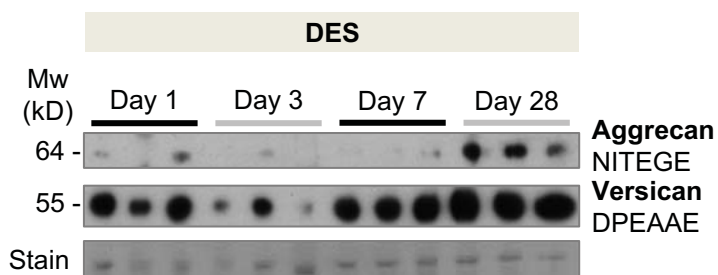




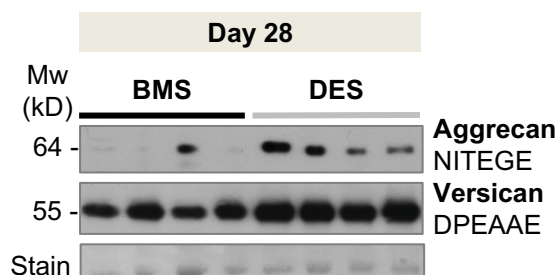
A



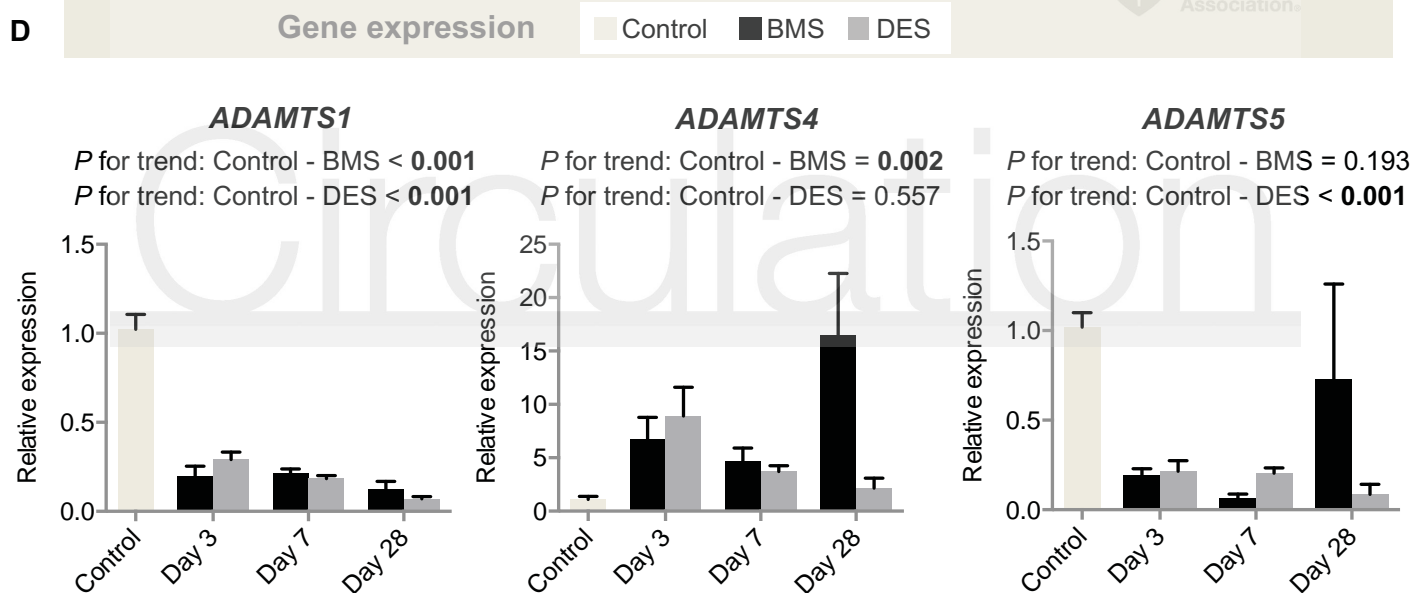
B



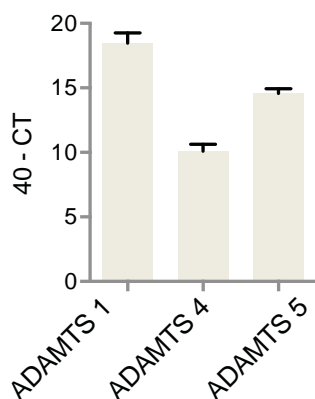
C



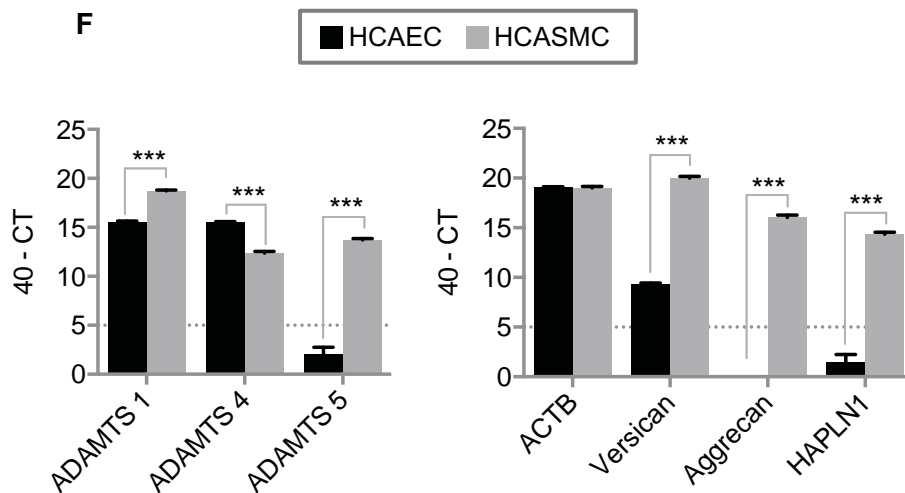
D

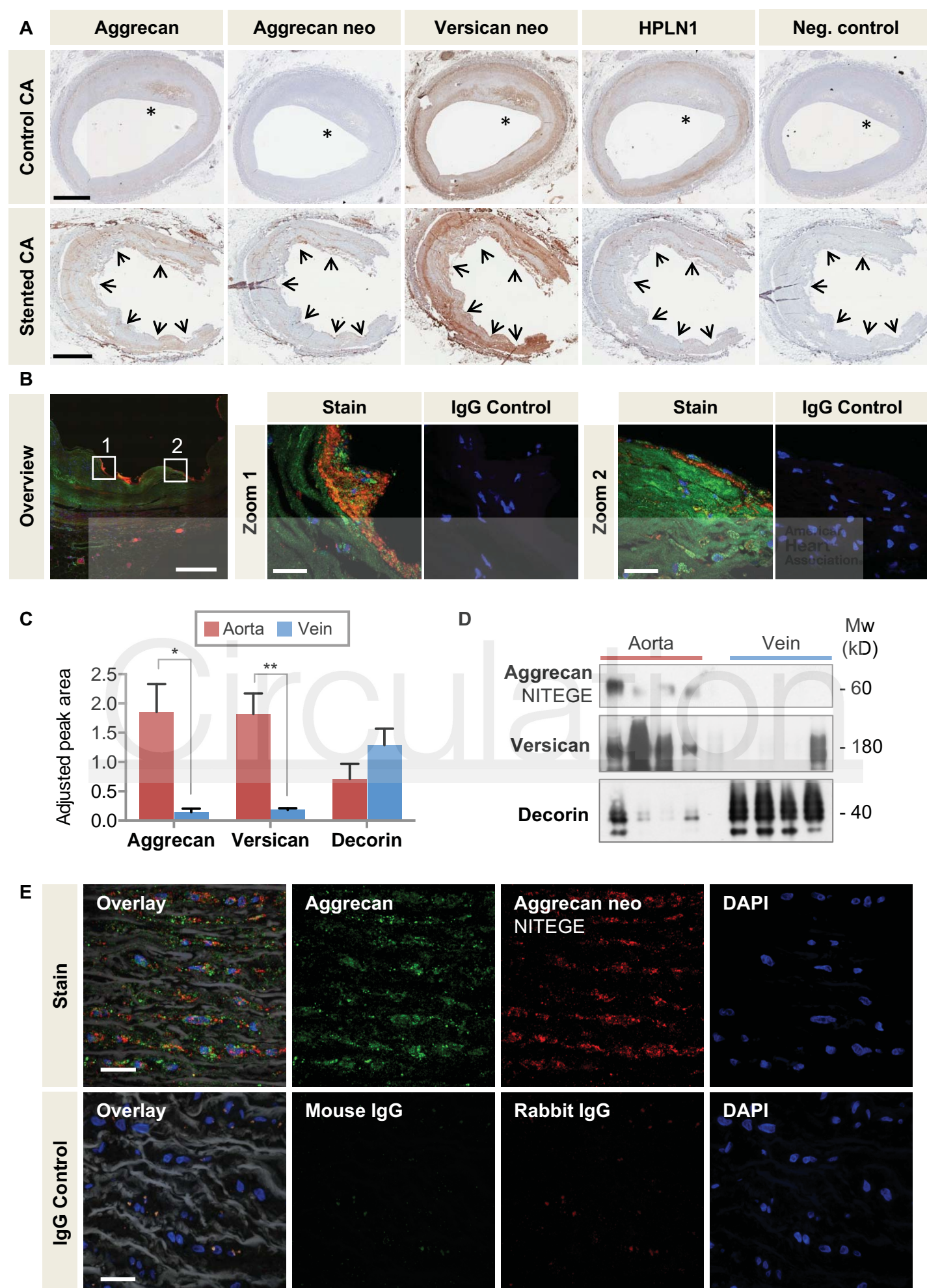


E Basal ADAMTS expression in porcine coronary arteries

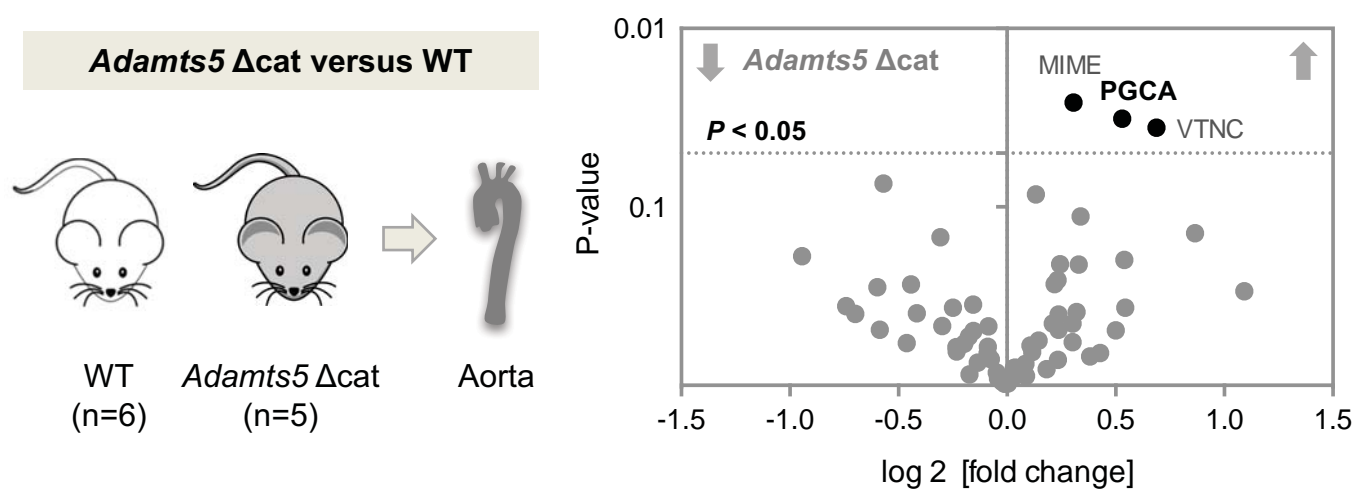


F

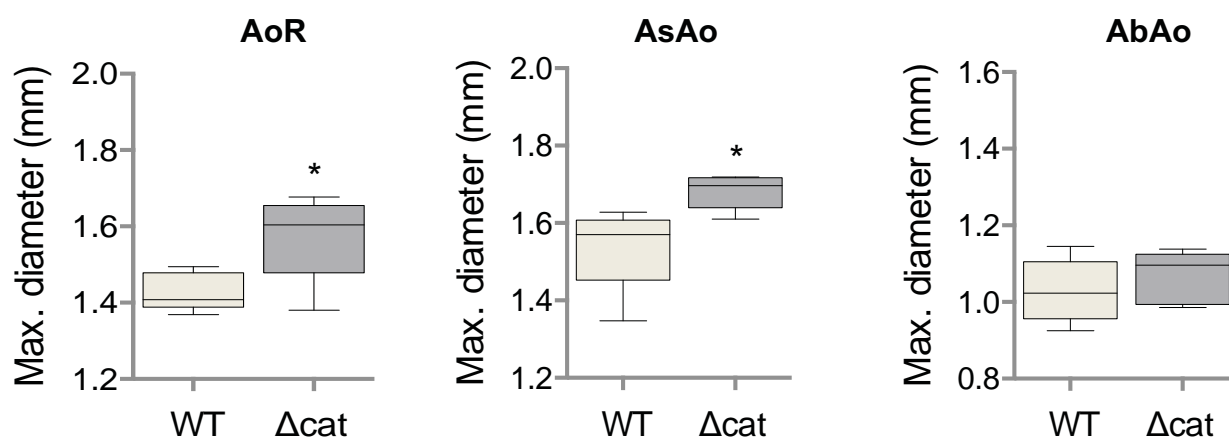
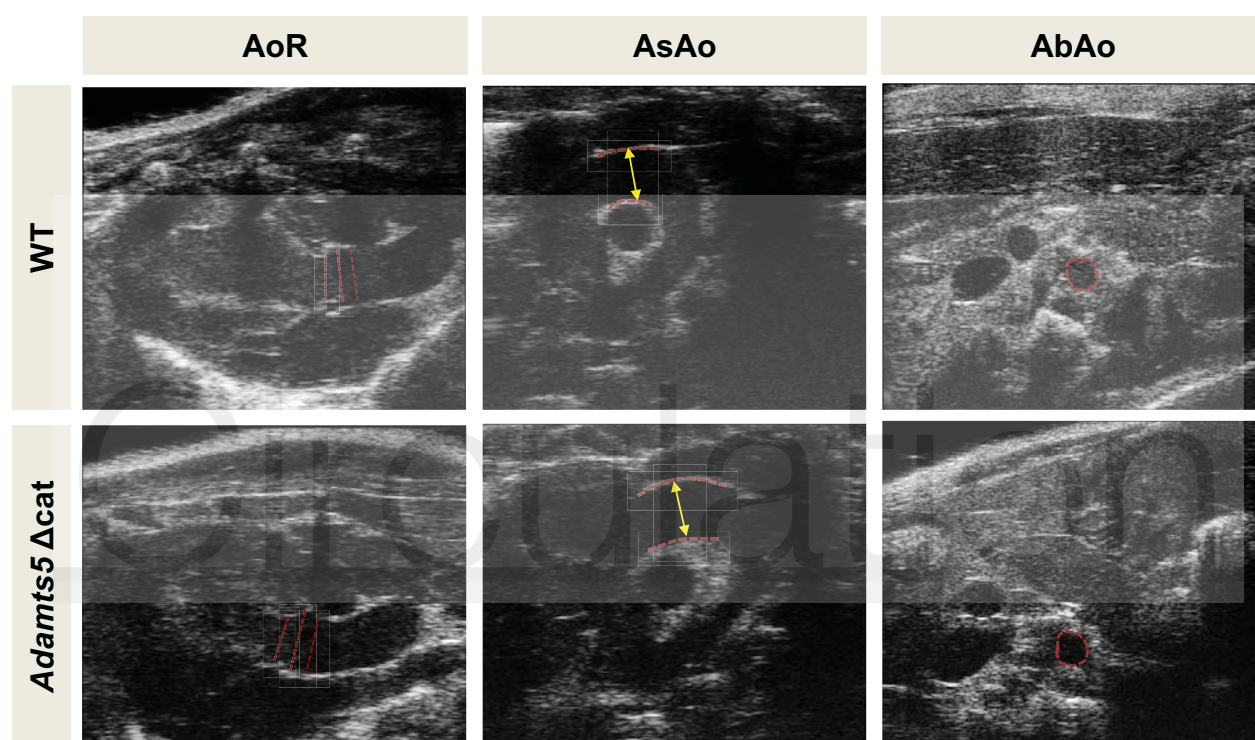




A



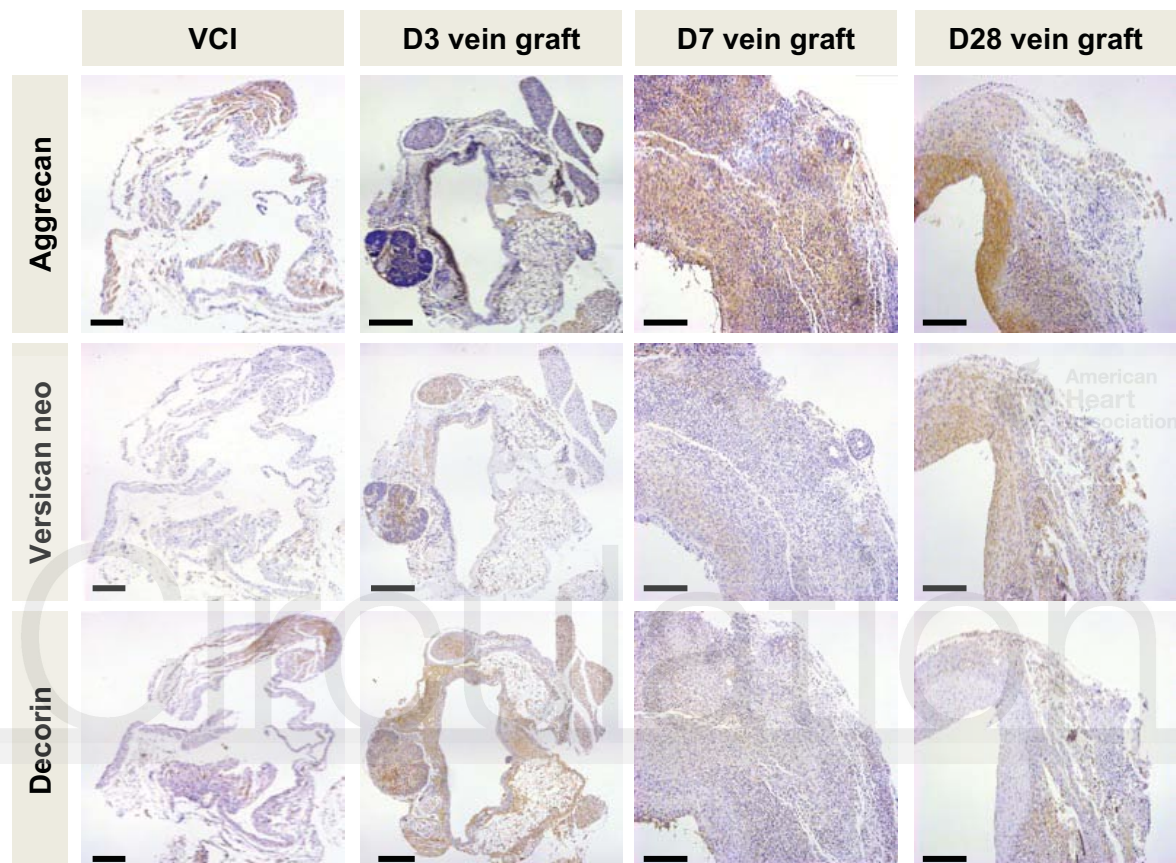
B



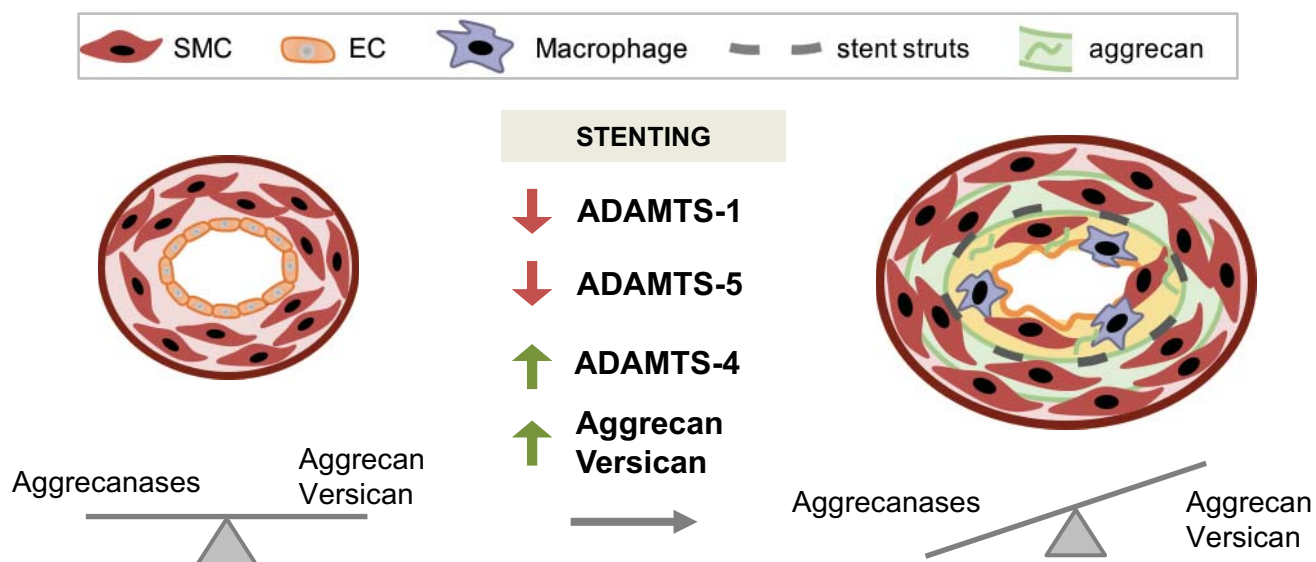
A



B



C



Extracellular Matrix Proteomics Reveals Interplay of Aggrecan and Aggrecanases in Vascular Remodeling of Stented Coronary Arteries

Gonca Suna, Wojciech Wojakowski, Marc Lynch, Javier Barallobre-Barreiro, Xiaoke Yin, Ursula Mayr, Ferheen Baig, Ruifang Lu, Marika Fava, Robert Hayward, Chris Molenaar, Stephen J. White, Tomasz Roleder, Krzysztof Milewski, Pawel Gasior, Piotr P. Buszman, Pawel E. Buszman, Marjan Jahangiri, Cathy Shanahan, Jonathan M Hill and Manuel Mayr

Circulation. published online October 13, 2017;

Circulation is published by the American Heart Association, 7272 Greenville Avenue, Dallas, TX 75231

Copyright © 2017 American Heart Association, Inc. All rights reserved.

Print ISSN: 0009-7322. Online ISSN: 1524-4539

The online version of this article, along with updated information and services, is located on the World Wide Web at:

<http://circ.ahajournals.org/content/early/2017/10/12/CIRCULATIONAHA.116.023381>

Free via Open Access

Data Supplement (unedited) at:

<http://circ.ahajournals.org/content/suppl/2017/10/12/CIRCULATIONAHA.116.023381.DC1>

Permissions: Requests for permissions to reproduce figures, tables, or portions of articles originally published in *Circulation* can be obtained via RightsLink, a service of the Copyright Clearance Center, not the Editorial Office. Once the online version of the published article for which permission is being requested is located, click Request Permissions in the middle column of the Web page under Services. Further information about this process is available in the [Permissions and Rights Question and Answer](#) document.

Reprints: Information about reprints can be found online at:

<http://www.lww.com/reprints>

Subscriptions: Information about subscribing to *Circulation* is online at:

<http://circ.ahajournals.org/subscriptions/>

SUPPLEMENTAL MATERIAL

EXTRACELLULAR MATRIX PROTEOMICS

REVEALS INTERPLAY OF AGGREGAN AND AGGREGANASES IN VASCULAR

REMODELING OF STENTED CORONARY ARTERIES

Gonca Suna, MD, PhD¹; Wojciech Wojakowski, MD²; Marc Lynch, MSc¹; Javier Barallobre-Barreiro, PhD¹; Xiaoke Yin, PhD¹; Ursula Mayr, MD¹; Ferheen Baig, MSc¹; Ruifang Lu, PhD¹; Marika Fava, PhD¹; Robert Hayward, BSc¹; Chris Molenaar, PhD¹; Stephen J. White, PhD³; Tomasz Roleder, MD²; Krzysztof P. Milewski, MD⁴; Pawel Gasior, MD²; Piotr P. Buszman, MD⁴; Pawel Buszman, MD⁴; Marjan Jahangiri, MD⁵; Cathy Shanahan, PhD¹; Jonathan Hill, MD⁶; Manuel Mayr, MD, PhD¹

¹King's British Heart Foundation Centre, King's College London, London, UK

²³rd Division of Cardiology, Medical University of Silesia, Katowice, Poland

³Healthcare Science Research Centre, Manchester Metropolitan University, Manchester, UK

⁴Centre for Cardiovascular Research and Development, American Heart of Poland, Katowice, Poland

⁵St. George's Vascular Institute, St George's Healthcare NHS Trust, London, United Kingdom

⁶King's College Hospital and King's Health Partners Academic Health Sciences, London, United Kingdom.

Address for Correspondence:

Prof. Manuel Mayr, MD, PhD, King's British Heart Foundation Centre, King's College London, 125 Coldharbour Lane, London SE5 NU, UK, Phone: +44 (0) 207848 5446

Fax: +44 (0) 20 7848 5298, Email: manuel.mayr@kcl.ac.uk

Twitter: https://twitter.com/Vascular_Prot

SUPPLEMENTAL METHODS

OCT Image Analysis in Pigs. OCT imaging was performed at stent implantation and at follow-up using the ILUMIEN OPTIS imaging system (St. Jude Medical, US). The OCT probe (mid marker of the OCT Dragonfly catheter) was positioned 5 mm distally to the analysed stent. All OCT imaging was performed using automated pullback triggered by hand injection of contrast. Every 1 mm of the stent was scrutinized by OCT to assess minimal lumen area, stent struts apposition, stent struts coverage and neointimal volume. Qualitative analysis of neointima was performed classifying the neointimal structure into heterogeneous, layered or homogenous with peristrut attenuation or ring.¹ If peristrut attenuation was visible in the whole circumference of the stent at the single OCT cross-sectional frame, the peristrut ring was recognized. The data was analysed using the OCT image analysing system, CAAS IntraVascular (version 1.1, Pie Medical Imaging).

Deglycosylation of ECM Extracts. GuHCl was removed by ethanol precipitation and the proteins were deglycosylated using deglycosylation enzymes. The deglycosylation enzymes included: chondroitinase ABC (1:100), keratanase (1:500) and heparinase II (1:500) (all from Sigma-Aldrich) for the removal of GAG side chains; 2 different debranching enzymes including α 2-3,6,8,9-Neuraminidase (1:200) and β -N-acetylglucosaminidase (1:200) as well as O-glycosidase for the removal of the remaining O-linked sugars (1:200) (all from Millipore). After 24 h incubation samples were speed-vac dried. PNGase F (1:200, from Millipore) was added together with ¹⁸O labelled water (Sigma-Aldrich) for another 48 h of incubation.

Generation of Custom-made Porcine ECM Protein Database. To achieve the best peptide sequence coverage by LC-MS/MS, and identify as many proteins as possible, a search database containing a comprehensive list of porcine ECM proteins was generated. Previously reported cardiovascular ECM proteins identified in human, porcine and murine cardiovascular tissues²⁻⁴ were searched for their porcine sequences in the Uniprot protein database. Porcine sequences of many of these proteins were found and retrieved from Uniprot either as annotated proteins or after blasting the human sequence against non-annotated,

uncharacterized porcine proteins. The remaining ECM proteins with no matching sequences in Uniprot were deduced from public nucleotide databases (including mRNA annotated sequences and expressed sequence tags [EST]) using tBLASTn. Exclusively the best matches ($\geq 90\%$ identity) were assigned to a protein sequence and retrieved for the database. The final database contained a total of 270 manually included porcine ECM protein sequences. All canonical human sequences were used as background in order to obtain a database suitable for search algorithms (i.e. Mascot). To avoid redundancies all human ECM proteins were manually removed and replaced by their porcine counterparts.

Human Tissue. All procedures involving use of human tissues were approved by a local Research Ethics Committee (London, United Kingdom, Wandsworth research ethics committee approval REC number 08/H0803/257). Normal saphenous vein specimens were obtained by surgical resection in consented patients undergoing coronary artery bypass surgeries; the segment of the saphenous vein near the knee level was collected for analysis from each patient. Control aortic samples from consented patients without connective tissue disorder were obtained upon aortotomy performed during routine aortic valve replacement from positions of the ascending aorta that were free of macroscopically evident vascular pathology. All samples were snap frozen following surgical removal. There were no known potential confounders during sampling of clinical specimens and tissues.

Immunoblot Analysis. Porcine samples: 10 μ g of deglycosylated GuHCl extracts of stented porcine coronary arteries (n=3 first cohort; n=4 second cohort day 28) were denatured at 95 °C for 5 min and reduced with sample buffer (0.1 mol/l Tris, pH 6.8, 40% glycerol, 2% SDS, 2% beta-mercaptoethanol and 0.02% bromophenol blue) and separated by SDS-PAGE. Subsequently proteins were blotted to a nitrocellulose membrane, which was blocked in 5% milk and incubated with primary antibodies to the aggrecan NITEGE neoepitope (Thermo, AF-PA1-1746) and the versican DPEAAE neoepitope (Abcam, ab19345) over night. After 3 washes (15 min each) with PBS-Tween, the membranes were treated with appropriate HRP-conjugated light chain-specific detection antibody (1:5000, Jackson ImmunoResearch) for 1 h. The membranes were washed again 3 times and developed using enhanced

chemiluminescence (ECL, GE Healthcare) on a Xograph processor in 30 sec increments. ImageJ software was used for densitometric quantification. Human samples: Same protocol was applied. 7 µg of GuHCl extracts of human thoracic aorta and saphenous vein were loaded per lane. Antibodies against the aggrecan NITEGE neoepitope (Thermo, AF-PA1-1746), versican (Santa Cruz, sc-25831) and decorin (Thermo Fisher PA5-19151) were used.

Cell Culture. Endothelial cells: Human coronary artery endothelial cells were obtained from PromoCell (C-12222) and cultured on 0.04% gelatine in appropriate Endothelial Cell Growth Medium (PromoCell C-22020) at 37 °C in a humidified atmosphere of 95% air/5% CO₂. Cells were washed with cold PBS twice and scraped off the surface with Qiazol. RNA was extracted as described below and reversely transcribed using SuperScript® VILO MasterMix (Life Technologies). The experiments were carried out with cells at passage 4-9. Smooth muscle cells: Human coronary artery smooth muscle cells (HCASMCs) were obtained from PromoCell (C-12511) and grown in M199 medium (Gibco™) on 0.04% gelatine. For experiments cell passages 7-11 were used.

Calcification Assay. Human aortic SMCs were cultured in M199 supplemented with 5% fetal bovine serum and treated with everolimus 20 nM or equivalent concentration of DMSO as vector control. Everolimus was a kind gift from Novartis, Switzerland and was shipped under a material transfer agreement with King's College London. To induce mineralization the medium was supplemented with calcium (2.7 mM) and phosphate (2.5 mM).⁵ Calcification was visualized after fixation with 4% formaldehyde using Alizarin red (2% weight/volume, pH 4.2) and quantified spectrophotometrically using the o-Cresolphthalein complexone assay after 8 days of Ca/P treatment +/- everolimus. Calcium concentrations were normalized to protein concentrations determined by the Biorad DC protein assay. Each experiment was carried out in triplicates and cells were used at passages between 10-12.

Real-time Polymerase Chain Reaction (qPCR). RNA from the porcine tissue was extracted using the miRNeasy Mini kit (Qiagen) according to the manufacturer's instructions. For gene expression analysis, porcine RNA was reversely transcribed using SuperScript® VILO MasterMix (Life Technologies). Taqman® assays were used to assess the expression

of individual target genes. Diluted reverse transcription products were combined with TaqMan® expression (Applied Biosystems) and TaqMan® Universal PCR Master Mix No AmpErase® UNG (2x) to a final volume of 5µl. For ADAMTS-1, -4 and -5 expression analysis in porcine tissue samples, SYBRgreen primers were designed and the reaction volume was set up with SYBR Select Master Mix (2x):

ADAMTS1: fwd CGTGAACAAGACCGACAAGA/ rev AACTCCTCCACCACACGTTC;

ADAMTS4: fwd CCCCATGTGCAACGTCAAG/ rev AGTCTCCACAAATCTGCTCAGTGA;

ADAMTS5: fwd TCACGAAATTGGACATCTGC/ rev CTGGTCAGGATGGAGGACAT.

ACTB: fwd TCTGGCACCACACCTTCT/ rev GATCTGGGTCATCTTCTCAC).

The qPCR reaction was performed in a ViiA7 qPCR instrument (ThermoFisher Scientific) under following conditions: 95 °C for 10 min, followed by 40 cycles of 95 °C for 15sec and 60 °C for 1 min. Samples were normalized to the expression of β-actin (ACTB) for gene expression targets. Target relative amounts were quantified using the $2^{-\Delta\Delta CT}$ method.⁶

Vein Graft Surgery in Mice. An established mouse model of venous bypass graft was used by grafting *isogeneic venae cavae* to common carotid arteries of female C57BL/6J mice (Jackson laboratories), as described previously.⁷ Briefly, mice were anaesthetised by intraperitoneal injection of ketamine (75 mg/kg) and medetomidine HCL (1 mg/kg). A segment (approx. 1 cm) of vena cava from a donor animal was grafted end-to-end to carotid arteries using a cuff technique. Grafts and vena cava were harvested at time point 3, 7 and 28 days post-surgery for histological characterization. Other mice were fed a SILAC (stable isotope labeling with amino acids in cell culture) diet containing heavy lysine *ad libitum* and had access to water. Stable isotope-labelled mouse feed was obtained from Silantes (Munich, Germany). Mice were euthanized by anesthetic overdose 28 days postoperatively. The vein grafts were harvested by cutting the implanted segments from the native vessels at the cuff end together with the vena cava and the aorta. The vessels were processed using the ECM extraction method as described above. GuHCl extracts were subject to tryptic digests and used for targeted proteomics analysis as described in the following paragraph.

Targeted Proteomic Analysis.

SILAC-fed mice tissue: Proteotypic peptides were scheduled using the retention time obtained from untargeted experiments with same HPLC configuration and eluting gradient. All proteotypic peptides were lysine (K)-terminated to allow quantification of SILAC incorporation. Skyline software (MacCoss Lab, University of Washington, Seattle) was used first to predict collision energies and optimize retention times, and second to quantify peak areas for MS2 ions after Parallel Reaction Monitoring (PRM). The identity of a specific peptide was confirmed by the presence of multiple transitions at the same retention time. Retention time windows were set +/- 4 min. All peaks were manually reviewed and integrated. A mass tolerance of 5ppm was used as a minimum requirement for fragment ions. SILAC incorporation rates were derived from the proportion between ions derived from peptides containing either heavy or light lysines (i.e. Lys152 and Lys146) using the following formula: $\text{Incorporation rate} = [\text{Heavy}] / [\text{Heavy} + \text{Light}]$. The intensities of heavy and light peptides were calculated using the peak areas after MS2. The following peptides were used for targeted proteomics in mice tissue: aggrecan GDPETSVSGVGDDFSGLPSPGK (G1172 – K1192), TVYLYPN[+3]QTGLPDPLSK (T661 – K677); versican VSVPTHPDDVGDAASLTMTVK (V101 – K119); decorin DLHTLILVNNK (D101 – K111), NSGIENGAFQGLK (N183 – K195), and VVQC[+57]SDLGLDK (V59 – K69).

Human vascular tissue: For targeted proteomics in human aorta and veins same methodology was applied except the SILAC labeling. Following peptides were used: aggrecan C[+57]GGNLLGVR (C318 - R326), versican LATVGELQAAWR (L277 - R288), decorin NLHALILVNNK (N106 - K116).

Immunofluorescence Staining in Human Vessels. Vessels were processed as described for immunohistochemistry. Sections of 5 µm (aorta) or 3 µm (coronary artery) were incubated with 0.5 unit/ml chondroitinase ABC (Sigma C3667) for 1 h at 37 °C. After blocking with 10% donkey serum in PBS for 1 h, sections were co-incubated with primary antibodies to aggrecan (1:10; Abcam, ab3778) and the aggrecan NITEGE neoepitope (1:200; Thermo, AF-PA11746) as well as matched isotope IgGs for negative controls. Secondary antibodies (Life Technology) were applied as indicated. Cell nuclei were stained with DAPI (Life Technology).

Sections were visualized with a 20x CFI S Plan Fluor ELWD ADM objective or 60x Plan Apo VC NA 1.40 Nikon using an inverted Nikon NI-E microscope equipped with a Yokogawa CSU-X1 Spinning disk confocal unit and an Andor iXon 3 EM-CCD camera. Images were acquired using NIS-elements 4.0 software, and represent a maximum projection image of a Z-stack of 0.5 μm steps compassing 9 μm .

Immunohistochemistry in Murine Vein Grafts. For histological analysis, mice tissues were fixed overnight with 10% formalin before being dehydrated in graded ethanol baths, cleared in xylene and embedded in paraffin. Histological sectioning began at the centre of the graft to avoid the effects of the cuff. 3 μm -thick cross-sections were made throughout the dissected tissue. Immunohistochemical analysis was performed using antibodies to aggrecan (1:100; Abcam, ab36861), the DPEAAE neoepitope of versican (1:100; Abcam, ab19345) and decorin (1:100; Sigma-Aldrich, SAB2100539). Negative controls were generated with 10% solution of normal goat serum (Vector labs). Slides were incubated with the primary antibody overnight at 4 °C. After washing, a secondary antibody (1:400, biotin conjugated goat anti-rabbit IgG; Vector labs) was applied for 30 min at room temperature. Specific immunohistochemical staining was detected by thoroughly washing slides and subsequently incubating with horseradish peroxidase (HRP) labelled avidin D (Vector labs) for 2 h at room temperature. The final detection step was carried out using a DAB (diaminobenzidine) peroxidase kit according to the manufactures instructions (Vector Labs). Sections were counterstained with haematoxylin and mounted. Images were taken by a Leica DM 2000 microscope interfaced to LAS software (version 4.3.0; Leica microsystems).

Adamts5 Δcat Mice. Animal experiments were approved by the U.K. authorities (licensed to Q. Xu, PPL70/7266). 10 to 12-week-old wild-type mice (WT) or mice lacking the catalytic domain of Adamts5 (*Adamts5 Δcat*)⁸ were utilized for the following experiments. For each of the experiments between 5 - 7 mice per group were utilized. Aortas were dissected from WT or *Adamts5 Δcat* mice from the aortic root to the iliac bifurcation. Periaortic fat and lymph nodes were removed under a dissecting microscope. Cleaned aortas were washed, diced and subjected to a three-step extraction method in order to enrich the ECM proteins as

described under 'ECM extraction'. 15 µg of deglycosylated proteins of the GuHCl fraction were subjected to in-solution digestion and analysed by LC-MS/MS as described in the manuscript under 'proteomics analysis in porcine tissue'. The raw files were searched against the UniProt mouse database (UniProtKB/Swiss-Prot Release 2016_02, 16765 protein entries).

Murine Ultrasound Measurements. Animals were placed in the induction chamber and anaesthetised by using 5% isoflurane mixed with 1l/min of 100% oxygen for 45 sec - 1 min. Next, mice were placed in a supine position on the heating pad to maintain body temperature with embedded ECG. 1-1.5% isoflurane mixed with 1 L/min 100% oxygen was subsequently used to maintain a steady state of sedation levels during the entire procedure. A rectal probe was gently inserted to continuously monitor the body temperature. Two-dimensional (2D) echocardiographic images of cardiovascular anatomy were obtained by a single operator. Standard and modified parasternal long axis (PLAX), suprasternal (SS), longitudinal and transverse abdominal (LA, TA) views were obtained using Visual Sonics Vevo 2100. Aortic root dimensions (aortic annulus, sinuses of Valsalva, sinotubular junction) were measured in PLAX. Ascending aortic dimensions were measured in SS where possible, and modified PLAX if SS views were considered inadequate, in systole and diastole. Abdominal aorta measurements were made in the TA view. All measurements were performed offline on (Vevo software version 1.7) by two independent investigators.

Murine Cardiovascular Magnetic Resonance Imaging (CMR). CMR imaging was performed on a 7T horizontal MR scanner (Varian, Palo Alto, CA) with mice positioned in the prone position. The gradient coil had an inner diameter of 12 cm, 1,000 mT/m (100G/cm) gradient strength, and rise-time of 120 µs. A quadrature transmit/receive coil (RAPID Biomedical). Anesthesia was maintained with 1.5% isoflurane/98.5% oxygen, and body temperature was maintained at 37 °C using a warm air fan (SA Instruments, Stony Brook, NY). The ECG was monitored via 2 metallic needles placed subcutaneously into the front paws. A pressure-transducer for respiratory gating was placed on the abdomen. To synchronize data acquisition with the ECG and to compensate for respiratory motion, simultaneous ECG triggering and respiration gating (SA Instruments) were applied. Late

gadolinium enhancement MRI was performed 20 min after intraperitoneal injection of a 30 μ l bolus of 0.5 mmol/kg gadolinium-diethylenetri-amine-pentaacetic acid (Magnevist, Schering Healthcare). Cine-MRI was used to acquire gadolinium enhanced images. Ejection fraction was obtained from cine-MR images according to a previously published method.⁹

Murine Blood Pressure Measurements. Blood pressure was measured directly via implantable radio telemetry device for collection of continuous blood pressure data. Around 200 values were acquired every 5 minutes for 18/20 hours. For each mouse the average value of these 200 points was considered.

Supplemental Table I. Sample characteristics.

Media									
Lifetime [days]	Stent/Balloon	Coronary artery	Sex	Weight [kg]	Age [months]	Size [mm]	AVD [mm]	Target overstretch [mm]	Inflation [atm]
1	BMS	LAD	M	35	3	3.5x15	3.4	4.1	22
		LCX dis	M	35	3	3.5x15	3.0	3.5	12
		RCA prox	F	38	3	3.5x15	3.0	3.6	12
	DES	LAD	F	38	3	3.0x15	3.0	3.5	23
		LCX prox	F	38	3	3.5x15	3.1	3.7	12
		RCA	M	35	3	3.0x15	3.0	3.6	24
3	BA early	LCX prox	M	35	3	3.5x15	3.0	3.5	28
		RCA dis	F	38	3	3.5x15	2.9	3.5	12
		LAD	M	45	4	3.0x15	2.7	3.2	15
	BMS	LCX	F	45	4	3.0x15	2.8	3.3	16
		RCA dis	M	45	4	3.0x15	2.7	3.2	14
		LAD	F	45	4	3.0x15	2.8	3.3	14
7	DES	LCX	M	45	4	3.0x15	2.6	3.1	11
		RCA prox	F	45	4	3.0x15	2.7	3.0	14
		RCA prox	M	45	4	3.0x15	2.8	3.4	16
	BA early	RCA dis	F	45	4	3.0x15	2.5	3.0	14
		LAD prox	M	32	3	3.5x15	3.1	3.7	14
		LCX prox	F	33.5	3	3.5x15	2.9	3.4	10
14	BMS	RCA prox	F	33.5	3	3.0x15	2.8	3.4	18
		LAD prox	F	33.5	3	3.5x15	3.0	3.5	9
		LCX prox	M	32	3	3.5x15	3.0	3.6	9
	DES	RCA prox	M	32	3	3.0x15	2.4	2.9	10
		LCX prox	M	33	3	3.0x15	2.5	2.9	14
		LAD prox	F	29	3	3.5x15	2.9	3.5	10
28	BMS	LCX prox	F	28	3	3.0x15	2.5	3.0	10
		RCA prox	F	28	3	3.0x15	2.0	2.4	10
		LCX prox	F	29	3	3.5x15	3.0	3.5	9
	DES	RCA medial	F	29	3	3.5x15	3.1	3.5	9
		RCA dis	F	28	3	3.0x15	2.0	2.4	9
		LAD	F	28	3	3.5x15	2.9	3.5	10
	BA late	RCA prox	F	29	3	3.5x15	2.9	3.5	12

Neointima									
Lifetime [days]	Stent-type	Coronary artery	Sex	Weight [kg]	Age [months]	Size [mm]	AVD [mm]	Target overstretch [mm]	Inflation [atm]
28	BMS	LAD prox	F	29	3	3.5x15	2.9	3.5	10
		LCX prox	F	28	3	3.0x15	2.5	3.0	10
		RCA prox	F	28	3	3.0x15	2.0	2.4	10
		RCA prox	M	47	3.5	3.5x8	3.0	3.6	12
		RCA dis	M	47	3.5	3.0x12	2.8	3.4	20
		RCA prox	M	48	3.5	4.0x14	3.4	4.1	12
		LCX	M	48	3.5	3.0x15	2.8	3.4	16
	DES	LCX prox	F	29	3	3.5x15	3.0	3.5	9
		RCA medial	F	29	3	3.5x15	3.1	3.5	9
		RCA dis	F	28	3	3.0x15	2.0	2.4	9
		LAD dis	M	47	3.5	3.0x15	2.6	3.1	12
		LCX med	M	47	3.5	3.5x18	3.2	3.9	18
		RCA dis	M	48	3.5	3.5x15	2.9	3.8	12
		LAD med	M	48	3.5	3.0x18	2.4	2.9	9→12

Clinical characteristics of pigs (lifetime, sex, weight, age at intervention) and PCI specific parameters are shown, including used stent type, balloon/stent size at implantation, average vessel diameter (AVD) as measured by angiography before dilatation, final size of stent/balloon after expansion (target overstretch) as well as the applied inflation pressure. Macroscopically neointima formation was detected in all arteries at 28 days, independent of stent type. Prox = proximal, dis = distal.

Supplemental Table II. Extracellular proteins identified by proteomics analysis in the neointima of stented porcine coronary arteries.

Identified Proteins	UniProt ID	MW (kDa)	BMS Av±SD	DES Av±SD	FC DES/BMS	P	FDR
Adipocyte enhancer-binding protein 1	F1SSF7_PIG	128	165.6±93.4	142.4±32.5	0.9	0.554	0.725
Aggrecan	F1SKR0_PIG	238	41.2±69.5	70.8±34.1	1.7	0.338	0.559
Agrin	I3LGD9_PIG	216	116.6±65.1	128.5±40.2	1.1	0.688	0.799
Alpha-1-antitrypsin*	A1AT_PIG	47	33.6±30.2	11.8±8.0	0.4	0.109	0.305
Alpha-2-HS-glycoprotein	FETUA_PIG	38	472.0±223.6	263.1±75.3	0.6	0.050	0.203
Annexin A1	ANXA1_PIG	39	231.1±142.4	129.4±45.3	0.6	0.113	0.305
Annexin A2	ANXA2_PIG	39	571.0±247.8	430.9±65.4	0.8	0.192	0.391
Antithrombin-III	Q7M364_PIG	49	92.2±38.7	71.2±18.1	0.8	0.228	0.433
Apolipoprotein A-I	APOA1_PIG	30	619.6±234.8	549.4±270.4	0.9	0.614	0.775
Apolipoprotein A-IV	APOA4_PIG	43	7.6±4.0	10.9±8.3	1.4	0.362	0.581
Apolipoprotein B*	Q29021_PIG	300	27.7±33.0	11.8±15.5	0.4	0.278	0.480
Apolipoprotein C-III	APOC3_PIG	11	16.2±9.2	18.8±11.9	1.2	0.658	0.799
Apolipoprotein E	APOE_PIG	37	76.6±73.2	63.8±70.2	0.8	0.745	0.840
Apolipoprotein H	I3LGN5_PIG	29	141.2±84.9	128.0±131.6	0.9	0.827	0.881
Apolipoprotein R	APOR_PIG	23	27.0±17.6	40.8±22.6	1.5	0.228	0.433
Asporin	F1SUE4_PIG	42	137.6±70.1	80.2±33.0	0.6	0.083	0.257
Biglycan	K7GP55_PIG	41	1767.1±214.9	1130.6±169.0	0.6	0.000	0.007
Bone morphogenic protein 1*	F1RMB2_PIG	114	0.0±0.0	4.9±5.6	n/a	n/a	n/a
Carboxypeptidase-like protein X2	F1SEC6_PIG	86	24.9±26.1	15.8±5.3	0.6	0.397	0.592
Cathepsin D	Q4U1U3_PIG	44	79.6±46.1	34.5±24.3	0.4	0.047	0.203
Cathepsin G	F1SGS1_PIG	29	0.4±1.0	0.0±0.0	0.0	n/a	n/a
Cathepsin Z*	A5GFX7_PIG	34	2.9±5.6	0.0±0.0	0.0	n/a	n/a
Chitinase-3-like protein 1	CH3L1_PIG	43	31.8±39.8	2.6±4.6	0.1	n/a	n/a
Chondroadherin*	CHAD_HUMAN	40	0.8±1.3	35.6±25.3	46.5	n/a	n/a
Clusterin	CLUS_PIG	52	149.6±28.5	301.7±99.0	2.0	0.006	0.083
Coatomer subunit alpha*	F1RJX8_PIG	138	16.3±14.7	14.6±7.2	0.9	0.796	0.872
Collagen alpha-1 (I)	CO1A1_PIG	100	2798.6±873.9	1842.9±504.6	0.7	0.032	0.182
Collagen alpha-1 (III)	F1RYI8_PIG	139	698.6±329.3	224.0±93.9	0.3	0.008	0.092
Collagen alpha-1 (IV)	M3V819_PIG	160	49.1±20.8	47.8±10.7	1.0	0.887	0.920
Collagen alpha-1 (V)	F1S021_PIG	182	205.5±64.2	137.6±35.9	0.7	0.036	0.188
Collagen alpha-1 (VI)	CO6A1_PIG	43	36.4±27.4	19.2±7.1	0.5	0.155	0.342
Collagen alpha-1 (VIII)	F1SKX7_PIG	73	14.1±5.2	19.8±5.7	1.4	0.075	0.252
Collagen alpha-1 (XI)	F1S571_PIG	159	19.4±20.4	10.9±12.2	0.6	0.369	0.581
Collagen alpha-1 (XII)	COCA1_PIG	229	484.1±151.0	218.6±50.9	0.5	0.003	0.063
Collagen alpha-1 (XV)	COFA1_PIG	27	68.8±36.2	137.6±20.6	2.0	0.002	0.060
Collagen alpha-1 (XVIII)	COIA1_PIG	62	216.1±61.8	248.4±36.7	1.1	0.263	0.468
Collagen alpha-1 (XX)	COKA1_PIG	192	1190.7±613.9	440.1±145.6	0.4	0.017	0.139
Collagen alpha-2 (I)	F1SFA7_PIG	129	1305.6±466.3	845.6±261.8	0.6	0.048	0.203
Collagen alpha-2 (IV)	F1RLL9_PIG	161	89.9±26.6	82.8±13.2	0.9	0.542	0.721
Collagen alpha-2 (V)	Q59IP2_PIG	145	134.8±55.5	66.7±26.4	0.5	0.018	0.139
Collagen alpha-2 (VI)	I3LQ84_PIG	106	124.7±110.6	57.2±29.7	0.5	0.163	0.350
Collagen alpha-3 (V)	Q59IP1_PIG	172	2.1±5.5	0.0±0.0	0.0	n/a	n/a
Collagen alpha-3 (VI)	I3LUR7_PIG	342	371.3±357.3	92.9±63.2	0.3	0.086	0.258
Collagen alpha-6 (VI)	CO6A6_PIG	250	8.1±12.9	0.0±0.0	0.0	n/a	n/a
Complement C3	CO3_PIG	187	805.6±730.5	687.7±404.2	0.9	0.717	0.818
Complement component C8B*	A0SEH2_PIG	69	23.1±18.9	27.3±18.4	1.2	0.682	0.799
Complement component C9	A0SEG9_PIG	62	2.4±1.5	6.9±6.4	2.9	0.115	0.305
Connective tissue growth factor	CTGF_PIG	38	1.2±3.1	6.3±7.4	5.4	n/a	n/a
Decorin	PGS2_PIG	40	185.4±59.1	104.5±81.3	0.6	0.057	0.208
Dermatopontin	DERM_PIG	22	55.8±23.6	38.1±14.2	0.7	0.121	0.314
Dystroglycan	I3LD20_PIG	95	3.3±4.4	1.7±2.5	0.5	n/a	n/a
EMILIN-1	F1SDQ5_PIG	107	64.1±34.1	62.4±12.4	1.0	0.905	0.930

EMILIN-2*	F1SBC8_PIG	106	0.5±1.2	0.0±0.0	0.0	n/a	n/a
Fibrillin-1	FBN1_PIG	313	23.8±28.1	10.4±10.8	0.4	0.274	0.480
Fibrinogen beta chain	F1RX37_PIG	56	5135.7±4558.0	4487.1±2656.8	0.9	0.752	0.840
Fibrinogen gamma chain	F1RX35_PIG	50	4287.0±3582.2	3875.7±2485.5	0.9	0.808	0.872
Fibromodulin	F1S6B5_PIG	44	549.7±94.2	350.4±115.8	0.6	0.004	0.071
Fibronectin	F1SS24_PIG	272	10317.1±3240.8	11617.1±2173.3	1.1	0.398	0.592
Fibronectin type III domain-containing protein 1	F1SB59_PIG	204	26.8±41.2	11.7±9.9	0.4	n/a	n/a
Fibulin-1	F1SM61_PIG	78	120.4±47.0	149.3±43.4	1.2	0.255	0.465
Fibulin-2	FBLN2_PIG	54	20.9±22.8	16.5±14.2	0.8	0.670	0.799
Fibulin-3	F8SIP2_PIG	54	190.2±94.1	155.0±53.8	0.8	0.412	0.602
Fibulin-4*	F1RU22_PIG	49	36.2±11.8	38.3±7.7	1.1	0.694	0.799
Fibulin-5	F1SD87_PIG	50	300.0±137.6	351.1±84.6	1.2	0.422	0.608
Filamin-C*	F1SMN5_PIG	290	310.9±151.2	387.0±102.9	1.2	0.295	0.502
Galectin-1	LEG1_PIG	15	353.4±61.5	265.0±52.4	0.7	0.014	0.131
Galectin-3	A3EX84_PIG	27	87.2±91.7	29.8±14.2	0.3	0.151	0.342
Galectin-3-binding protein	M3V7X9_PIG	61	14.3±11.8	52.4±42.3	3.7	0.056	0.208
Galectin-9*	F1RJ33_PIG	40	1.3±1.7	0.3±0.6	0.3	n/a	n/a
Gelatinase A*	Q95JA4_PIG	74	6.6±8.5	0.5±0.9	0.1	n/a	n/a
Gelsolin	GELS_PIG	85	1242.1±295.1	1123.4±194.5	0.9	0.394	0.592
Hemicentin-1*	HMCN1_PIG	180	1.3±2.2	0.7±1.8	0.5	n/a	n/a
Hyaluronan and proteoglycan link protein 1	HPLN1_PIG	40	7.7±10.8	16.2±15.4	2.1	0.257	0.465
Insulin-like growth factor-binding protein 7	C7EDN1_PIG	29	395.2±201.4	468.1±122.0	1.2	0.432	0.615
Inter-alpha-trypsin inhibitor heavy chain H1*	ITI1_PIG	100	145.1±77.4	143.1±46.0	1.0	0.955	0.964
Inter-alpha-trypsin inhibitor heavy chain H2	ITI2_PIG	105	95.1±63.8	63.5±16.7	0.7	0.247	0.462
Intercellular adhesion molecule 1*	F1S3J9_PIG	58	0.8±2.2	0.0±0.0	0.0	n/a	n/a
Kininogen-1*	KNG1_PIG	48	20.6±15.8	14.8±11.8	0.7	0.450	0.625
Lactadherin	MFGM_PIG	46	253.9±104.7	407.3±57.5	1.6	0.008	0.092
Laminin subunit alpha-4	F1RZM4_PIG	164	75.8±28.8	74.4±31.8	1.0	0.933	0.950
Laminin subunit beta-1	F1SAE9_PIG	199	246.4±69.2	265.6±65.1	1.1	0.604	0.773
Laminin subunit beta-2	F1SPT5_PIG	179	39.4±46.5	39.7±31.1	1.0	0.987	0.987
Laminin subunit gamma-1	F1S663_PIG	177	406.9±140.2	440.3±100.8	1.1	0.619	0.775
Latent TGFβ-binding protein 1	F1S405_PIG	148	28.3±9.3	19.5±6.9	0.7	0.068	0.242
Latent TGFβ-binding protein 2	F1S2T5_PIG	196	174.6±79.5	198.0±58.4	1.1	0.544	0.721
Latent TGFβ-binding protein 4	LTBP4_PIG	112	38.5±26.7	35.6±14.9	0.9	0.811	0.872
Leukocyte elastase inhibitor	ILEU_PIG	43	27.5±31.0	7.0±5.3	0.3	0.134	0.339
Lumican	F1SQ09_PIG	39	490.7±128.7	145.1±44.0	0.3	0.000	0.012
Lysyl oxidase homolog 1	F1SIC9_PIG	65	68.5±29.0	63.0±19.0	0.9	0.687	0.799
Macrophage capping protein	F1SVB0_PIG	39	109.4±87.6	62.1±38.0	0.6	0.226	0.433
Matrilin-4*	F1SDQ7_PIG	69	0.5±1.2	0.7±1.9	1.5	n/a	n/a
Matrix Gla protein	MGP_PIG	12	27.1±5.8	61.9±31.1	2.3	0.025	0.163
Matrix-remodeling-associated protein 5	F1RZ07_PIG	308	47.9±48.7	13.7±8.9	0.3	0.114	0.305
Metalloproteinase inhibitor 1*	TIMP1_PIG	23	0.4±0.9	0.0±0.0	0.0	n/a	n/a
Mimecan	I3L9T6_PIG	25	108.2±29.8	96.8±26.8	0.9	0.467	0.642
Myeloperoxidase	K7GRV6_PIG	84	4.5±8.1	0.0±0.0	0.0	n/a	n/a
Nidogen-1	NID1_PIG	50	29.1±17.4	76.6±35.8	2.6	0.012	0.127
Nidogen-2	F1SFF3_PIG	152	948.4±283.4	713.1±127.3	0.8	0.079	0.256
Osteoclast-stimulating factor 1*	OSTF1_PIG	24	13.8±11.9	6.3±5.4	0.5	0.166	0.350
Papilin	F1S3J7_PIG	141	0.1±0.2	0.7±1.8	9.3	n/a	n/a
Peptidyl-prolyl cis-trans isomerase A	PPIA_PIG	18	732.6±221.5	646.6±224.5	0.9	0.484	0.657

Periostin	F1RS37_PIG	93	2380.0±652.6	1489.0±573.9	0.6	0.019	0.139
Perlecan	PGBM_PIG	365	3168.6±652.1	3467.1±535.4	1.1	0.368	0.581
Peroxidasin homolog	I3LDA4_PIG	164	13.3±8.3	31.7±10.6	2.4	0.004	0.071
Pigment epithelium-derived factor	Q0PM28_PIG	46	264.7±46.4	314.9±70.6	1.2	0.146	0.342
Plasma glutamate carboxypeptidase*	PGCP_PIG	52	2.3±3.2	1.3±1.7	0.6	n/a	n/a
Plasminogen	PLMN_PIG	91	272.3±106.8	514.1±199.6	1.9	0.019	0.139
Podocan	I3LEB7_PIG	72	60.1±38.7	23.4±10.0	0.4	0.047	0.203
Procollagen C-endopeptidase enhancer 1	I3LEE6_PIG	50	40.2±10.6	41.9±11.6	1.0	0.778	0.861
Prolargin	F1S6B4_PIG	43	451.1±102.9	351.1±138.2	0.8	0.153	0.342
Prolow-density lipoprotein receptor-related protein 1	K9IVL7_PIG	505	30.4±26.2	20.5±7.4	0.7	0.372	0.581
Properdin	K7GQR1_PIG	51	57.9±29.3	117.1±61.8	2.0	0.049	0.203
Prophenin and tritricin precursor	PF11_PIG	24	230.0±297.6	7.5±8.9	0.0	0.095	0.279
Proteoglycan 4	I3L5Z3_PIG	149	0.9±1.5	0.0±0.0	0.0	n/a	n/a
Reticulon-3*	RTN3_PIG	105	0.0±0.0	0.6±1.5	n/a	n/a	n/a
RPE-spondin	RPESP_PIG	32	1.1±3.0	1.9±3.3	1.6	n/a	n/a
Secreted frizzled-related protein 1	I3LB66_PIG	35	12.1±6.0	9.2±6.4	0.8	0.400	0.592
Secreted frizzled-related protein 3*	F1RYL4_PIG	36	3.3±3.6	2.5±1.1	0.8	0.591	0.766
Secreted phosphoprotein 24*	SPP24_PIG	23	0.0±0.0	12.4±9.1	n/a	n/a	n/a
Serine protease HTRA1	F1SEH4_PIG	56	138.2±102.9	348.3±183.4	2.5	0.026	0.163
Serotransferrin	TRFE_PIG	77	3167.4±2227.2	1765.1±729.6	0.6	0.156	0.342
Serum amyloid P-component	SAMP_PIG	26	3.2±6.3	14.2±14.9	4.4	n/a	n/a
SPARC	SPRC_PIG	34	128.6±37.6	154.1±75.8	1.2	0.448	0.625
Spondin-1	SPON1_PIG	66	5.7±4.8	0.7±1.0	0.1	0.033	0.182
Sulfhydryl oxidase	F1S682_PIG	81	19.2±11.1	11.8±6.2	0.6	0.154	0.342
Superoxide dismutase [Cu-Zn]	Q007T6_PIG	26	236.2±133.9	155.7±49.9	0.7	0.176	0.364
T-cadherin*	A8D737_PIG	78	22.0±12.0	13.9±6.9	0.6	0.153	0.342
Tenascin	TENA_PIG	191	861.4±309.9	1192.9±318.3	1.4	0.072	0.248
Tetranectin	F1SRC8_PIG	22	156.6±34.1	171.5±75.3	1.1	0.644	0.798
TGFβ-induced protein ig-h3	BGH3_PIG	74	64.8±20.5	55.1±13.0	0.9	0.317	0.532
Thrombospondin-1	K7GPJ3_PIG	120	344.4±124.1	565.3±195.2	1.6	0.030	0.178
Thrombospondin-4*	F1RF28_PIG	104	8.9±7.9	33.3±26.4	3.7	0.051	0.203
Translationally-controlled tumor protein*	TCTP_PIG	20	50.9±23.5	49.1±19.5	1.0	0.874	0.914
Tryptase	TRYT_PIG	30	0.1±0.3	0.0±0.0	0.0	n/a	n/a
Tubulointerstitial nephritis antigen-like	F1SVA2_PIG	52	98.8±33.3	128.6±24.4	1.3	0.083	0.257
Versican	F1REZ2_PIG	369	1073.4±242.9	797.6±234.6	0.7	0.052	0.203
Vitamin D-binding protein	I3LN42_PIG	53	143.0±62.4	106.4±38.1	0.7	0.215	0.429
Vitronectin	VTNC_PIG	53	419.9±72.3	1038.1±338.7	2.5	0.003	0.063
von Willebrand factor A domain-containing protein 1	F1RJE3_PIG	44	8.3±6.4	10.0±7.6	1.2	0.660	0.799
WD repeat-containing protein 1	K9IVR7_PIG	66	288.7±36.1	297.6±112.3	1.0	0.848	0.895

P values for differential expression between neointimal DES and BMS are based on unpaired Student's *t*-tests with unequal variance (*n*=7 [BMS], *n*=7 [DES]). *T*-test was not performed if a protein was undetectable in the majority of samples from 1 of the 2 groups compared. Results in bold indicate *P* < 0.05. Values are average (Av) total ion current (TIC) × 10⁶ ± standard deviation (SD). n/a denotes not applicable, FC denotes fold change. FDR denotes false discovery rate. The FDR threshold was set at 10%. Protein changes with *P* < 0.05 and a FDR of <10% are highlighted in bold. Proteins only identified in the neointima, but not media are marked with*.

Supplemental Table III. Extracellular proteins identified by proteomics in the media of stented porcine coronary arteries.

Identified Proteins	UniProt ID	Bare-metal stent						Drug-eluting stent					
		Total ion current x 10 ⁶ Av±SD				P BMS	FDR	Total ion current x 10 ⁶ Av±SD				P DES	FDR
		BMS 1	BMS 3	BMS 7	BMS 28			DES 1	DES 3	DES 7	DES 28		
Adipocyte enhancer-binding protein 1	F1SSF7_PIG	0.3±0.5	0.2±0.3	1.6±1.3	1.1±0.5	0.136	0.326	0.1±0.2	0.0±0.0	1.0±0.9	6.2±4.8	0.046	0.140
Aggrecan	F1SKR0_PIG	6.5±2.3	2.7±0.9	18.0±11.4	28.2±9.0	0.010	0.088	5.2±2.1	10.9±9.3	18.3±7.6	52.5±11.1	0.000	0.011
Agrin	I3LGD9_PIG	5.7±2.5	5.4±2.8	8.7±1.1	9.4±1.7	0.112	0.310	5.7±3.3	5.2±3.5	8.8±1.3	6.2±1.6	0.400	0.523
Alpha-2-HS-glycoprotein	FETUA_PIG	1.4±1.4	1.6±1.5	2.6±1.9	5.2±8.5	0.717	0.751	4.0±2.1	3.7±2.4	3.7±3.7	7.8±7.5	0.623	0.679
Annexin A1	ANXA1_PIG	1.8±0.8	2.3±1.0	1.7±0.6	2.0±2.2	0.943	0.943	2.4±1.1	3.7±1.6	3.7±2.9	3.7±0.9	0.765	0.793
Annexin A2	ANXA2_PIG	10.8±1.8	14.2±4.7	24.3±4.3	37.2±31.9	0.265	0.431	9.5±1.5	12.7±7.0	20.8±4.3	28.1±7.7	0.016	0.066
Antithrombin-III	Q7M364_PIG	2.5±1.3	0.8±0.5	0.0±0.0	0.7±0.8	0.028	0.161	1.4±0.7	14.2±17.7	2.1±1.1	1.7±0.7	0.289	0.432
Apolipoprotein A-I	APOA1_PIG	18.7±4.3	11.0±8.0	21.2±12.5	25.6±16.3	0.484	0.580	17.5±2.2	26.8±13.5	19.1±13.2	24.8±10.0	0.686	0.732
Apolipoprotein A-IV	APOA4_PIG	0.1±0.1	0.0±0.0	0.1±0.1	0.4±0.6	0.394	0.536	0.0±0.1	1.7±1.1	0.4±0.5	0.5±0.3	0.053	0.142
Apolipoprotein C-III	APOC3_PIG	4.4±2.5	2.3±1.4	0.6±0.6	0.7±0.7	0.049	0.231	4.3±1.7	5.6±2.9	0.5±0.6	0.8±0.4	0.016	0.066
Apolipoprotein E	APOE_PIG	15.7±4.0	11.3±7.0	1.8±1.7	1.6±0.7	0.006	0.077	8.9±4.2	82.2±70.2	8.9±6.2	1.9±2.4	0.071	0.156
Apolipoprotein H	I3LGN5_PIG	21.7±6.2	20.3±5.4	18.7±2.7	29.4±18.3	0.603	0.657	26.7±5.1	36.6±27.2	29.3±14.7	59.5±10.6	0.139	0.260
Apolipoprotein R	APOR_PIG	1.6±1.1	1.0±0.3	0.8±0.8	0.3±0.3	0.213	0.395	2.6±1.6	6.8±2.7	0.9±0.8	0.5±0.5	0.006	0.034
Asporin	F1SUE4_PIG	78.2±16.2	62.0±11.9	86.2±17.1	150.3±37.5	0.007	0.077	77.5±16.5	81.7±37.1	90.1±30.2	157.3±43.8	0.059	0.142
Biglycan	K7GP55_PIG	796.0±130.8	648.1±186.6	952.7±42.3	1503.4±443.4	0.014	0.104	748.6±200.3	750.0±367.0	1002.9±236.7	1972.6±202.2	0.001	0.011
Carboxypeptidase-like protein X2	F1SEC6_PIG	0.0±0.0	0.0±0.0	0.0±0.0	0.0±0.0	n/a	n/a	0.0±0.0	0.0±0.0	0.0±0.0	0.4±0.2	n/a	n/a
Cathepsin D	Q4U1U3_PIG	1.6±0.5	1.9±0.3	7.2±4.8	8.8±13.1	0.523	0.604	1.1±1.5	2.3±1.6	4.1±3.6	3.7±1.8	0.412	0.523
Cathepsin G	F1SGS1_PIG	0.5±0.3	0.0±0.0	0.0±0.0	0.0±0.0	n/a	n/a	0.8±0.8	0.8±0.7	0.1±0.1	0.0±0.0	0.201	0.341
Chitinase-3-like protein 1	CH3L1_PIG	0.0±0.0	0.0±0.0	0.0±0.0	0.3±0.5	n/a	n/a	0.0±0.0	0.0±0.0	0.0±0.0	0.0±0.0	n/a	n/a
Chondroitin sulfate proteoglycan 4*	CSPG4_HUMAN	0.1±0.1	0.0±0.0	0.3±0.5	0.0±0.0	0.415	0.546	0.0±0.0	0.0±0.0	0.0±0.0	0.0±0.0	n/a	n/a
Clusterin	CLUS_PIG	98.2±51.7	59.8±17.0	45.6±16.8	16.4±10.7	0.048	0.231	59.0±19.6	273.4±202.6	61.0±24.0	21.2±10.8	0.060	0.142
Collagen alpha-1 (I)	CO1A1_PIG	2915.1±375.6	2913.2±993.1	4118.5±199.0	2622.2±1399.4	0.244	0.419	2749.1±797.9	1973.1±1213.2	3353.0±487.7	3996.0±273.1	0.062	0.142
Collagen alpha-1 (II)*	I3LSV6_PIG	108.4±22.4	127.9±54.4	149.6±3.8	68.4±34.1	0.090	0.276	100.9±39.9	77.0±38.5	122.7±62.7	116.6±15.0	0.584	0.669
Collagen alpha-1 (III)	F1RYI8_PIG	332.8±111.3	571.8±520.0	454.4±127.6	472.3±201.4	0.797	0.807	302.2±59.7	185.0±119.2	318.7±83.5	480.3±67.1	0.019	0.072
Collagen alpha-1 (IV)	M3V819_PIG	3.1±2.1	5.7±1.9	7.5±2.2	8.8±3.3	0.091	0.276	2.5±0.4	4.2±2.5	6.6±0.9	4.3±1.2	0.055	0.142
Collagen alpha-1 (V)	F1S021_PIG	81.8±19.0	108.4±42.0	181.5±36.4	174.3±88.5	0.128	0.325	82.2±11.7	109.9±66.9	126.0±20.7	251.3±25.0	0.003	0.019
Collagen alpha-1 (VI)	CO6A1_PIG	4.5±1.2	3.6±3.9	2.0±0.4	10.3±8.4	0.221	0.395	4.8±2.2	6.2±5.1	2.6±2.9	1.8±0.3	0.371	0.507
Collagen alpha-1 (VIII)	F1SKX7_PIG	0.2±0.3	0.2±0.4	1.5±0.6	0.5±0.4	0.013	0.104	0.1±0.2	0.4±0.4	1.8±0.9	3.2±1.0	0.002	0.019
Collagen alpha-1 (XI)	F1S571_PIG	48.9±9.7	50.3±22.3	111.5±27.7	103.7±54.7	0.088	0.276	45.9±2.4	62.4±36.9	60.7±17.8	190.8±17.9	0.000	0.006
Collagen alpha-1 (XII)	COCA1_PIG	7.1±0.5	3.4±2.9	17.2±16.6	46.9±52.0	0.273	0.438	5.7±0.7	3.8±1.8	14.2±10.6	53.7±15.8	0.001	0.011
Collagen alpha-1 (XV)	COFA1_PIG	3.2±1.0	2.5±0.9	9.0±2.7	9.5±4.8	0.028	0.161	2.3±1.8	2.1±1.2	10.0±2.2	14.1±3.8	0.001	0.011
Collagen alpha-1 (XVIII)	COIA1_PIG	10.5±3.5	12.3±7.3	11.4±1.1	6.7±1.3	0.420	0.546	8.5±3.5	12.9±5.7	12.2±4.8	1.6±0.3	0.035	0.115
Collagen alpha-1 (XX)	COKA1_PIG	14.6±12.5	5.7±4.3	22.3±9.2	60.8±43.8	0.081	0.276	8.2±2.6	4.0±2.6	24.8±9.2	22.2±2.9	0.003	0.019

Collagen alpha-2 (I)	F1SFA7_PIG	2540.2±281.6	2097.8±569.3	3114.0±344.6	2616.7±1337.8	0.482	0.580	2441.6±563.3	1949.6±1173.6	2966.9±215.8	4329.5±613.6	0.019	0.072
Collagen alpha-2 (IV)	F1RLL9_PIG	3.1±1.8	6.9±2.4	7.2±4.2	7.8±0.2	0.184	0.365	1.9±0.6	4.1±3.7	8.4±3.2	2.1±0.4	0.038	0.120
Collagen alpha-2 (V)	Q59IP2_PIG	84.2±45.2	108.2±40.4	172.3±73.6	173.7±84.4	0.281	0.444	87.0±14.8	91.2±57.0	156.5±6.4	200.7±119.1	0.188	0.328
Collagen alpha-2 (VI)	I3LQ84_PIG	13.4±3.9	15.3±15.9	7.1±1.6	41.7±41.5	0.309	0.461	14.8±5.6	23.3±24.5	10.3±4.8	8.5±3.2	0.534	0.630
Collagen alpha-2 (XI)*	A5D9K7_PIG	23.6±4.3	36.2±12.2	49.2±10.5	37.8±22.7	0.250	0.420	22.2±5.9	32.8±16.0	30.3±10.1	52.3±10.3	0.055	0.142
Collagen alpha-3 (V)	Q59IP1_PIG	1.1±0.7	1.6±1.2	1.9±0.8	5.8±5.3	0.220	0.395	1.2±0.7	1.9±2.1	2.1±1.0	3.2±1.3	0.402	0.523
Collagen alpha-3 (VI)	I3LUR7_PIG	42.7±11.3	38.2±40.2	16.2±6.8	92.4±98.5	0.411	0.546	32.6±15.3	41.5±39.4	21.3±16.8	18.4±11.3	0.624	0.679
Collagen alpha-6 (VI)	CO6A6_PIG	0.0±0.0	0.0±0.0	0.0±0.0	14.1±24.5	n/a	n/a	0.0±0.0	0.0±0.0	0.0±0.0	0.0±0.0	n/a	n/a
Complement C3	CO3_PIG	4.3±1.1	0.1±0.2	0.6±0.3	1.8±3.1	0.063	0.249	3.3±1.4	14.2±20.9	1.4±1.6	0.4±0.6	0.405	0.523
Complement component C9	A0SEG9_PIG	0.0±0.0	0.0±0.0	0.0±0.0	0.0±0.0	n/a	n/a	0.0±0.0	1.0±1.7	0.0±0.0	0.0±0.0	n/a	n/a
Connective tissue growth factor	CTGF_PIG	0.4±0.3	0.3±0.5	0.7±0.6	0.0±0.0	0.308	0.461	0.8±0.4	0.4±0.3	0.7±0.4	0.1±0.2	0.212	0.345
Decorin	PGS2_PIG	581.1±67.5	418.8±208.1	411.1±91.6	1166.4±602.8	0.064	0.249	610.5±85.3	554.8±357.0	441.8±67.1	1145.6±50.6	0.008	0.039
Dermatopontin	DERM_PIG	52.5±13.7	43.6±33.0	45.1±3.3	126.2±69.7	0.090	0.276	64.5±12.2	59.9±38.4	80.7±23.7	150.5±20.2	0.008	0.039
Dystroglycan	I3LD20_PIG	1.2±1.1	0.6±0.5	0.7±0.2	0.7±0.6	0.729	0.756	0.9±0.6	0.8±1.1	0.6±0.2	0.8±0.5	0.945	0.953
EMILIN-1	F1SDQ5_PIG	6.1±3.2	8.3±2.1	7.9±2.5	10.7±2.4	0.261	0.431	5.6±1.8	6.4±2.8	9.1±1.0	8.8±3.8	0.316	0.461
Fibrillin-1	FBN1_PIG	0.2±0.4	0.8±1.4	0.0±0.0	0.0±0.0	0.519	0.604	0.2±0.3	0.0±0.0	0.0±0.0	0.0±0.0	n/a	n/a
Fibrinogen beta chain	F1RX37_PIG	1240.6±374.6	268.9±219.0	49.0±38.0	3.3±0.7	0.000	0.025	1240.6±892.3	2814.7±3732.6	77.6±53.1	53.8±46.6	0.317	0.461
Fibrinogen gamma chain	F1RX35_PIG	1124.9±400.8	267.0±197.3	43.8±31.0	8.0±0.7	0.001	0.025	994.9±674.2	2014.6±2519.2	69.7±42.6	39.7±31.3	0.277	0.431
Fibromodulin	F1S6B5_PIG	144.8±77.4	73.5±29.1	200.7±36.9	299.2±28.4	0.002	0.046	135.1±50.9	62.4±47.7	185.0±36.5	598.9±175.3	0.001	0.011
Fibronectin	F1SS24_PIG	557.8±157.1	983.5±206.3	1109.9±420.0	503.9±198.9	0.055	0.241	527.0±248.9	1237.2±357.0	870.3±360.6	925.0±188.5	0.104	0.205
Fibronectin type III domain-containing protein 1	F1SB59_PIG	0.0±0.0	0.0±0.0	0.0±0.0	0.2±0.2	n/a	n/a	0.0±0.0	0.0±0.0	0.0±0.0	1.0±1.5	n/a	n/a
Fibulin-1	F1SM61_PIG	0.3±0.1	0.0±0.1	0.4±0.3	0.4±0.5	0.438	0.562	0.1±0.2	0.3±0.6	0.4±0.2	2.0±1.5	0.077	0.160
Fibulin-2	FBLN2_PIG	0.0±0.0	0.2±0.3	0.3±0.3	0.3±0.4	0.634	0.677	0.0±0.0	0.0±0.0	1.5±1.4	4.0±2.0	0.011	0.052
Fibulin-3	F8SIP2_PIG	0.0±0.0	0.0±0.0	0.0±0.0	0.2±0.3	n/a	n/a	0.0±0.0	0.0±0.0	0.0±0.0	0.0±0.0	n/a	n/a
Fibulin-5	F1SD87_PIG	11.3±1.8	4.4±1.7	7.6±1.1	17.7±13.6	0.185	0.365	9.5±2.7	7.4±3.1	7.3±3.9	7.8±1.5	0.772	0.793
Galectin-1	LEG1_PIG	16.2±4.0	23.5±12.5	40.8±10.8	30.3±8.2	0.062	0.249	23.7±5.0	14.6±10.3	34.3±3.1	25.7±8.6	0.062	0.142
Galectin-3	A3EX84_PIG	0.1±0.1	0.2±0.3	1.0±0.2	3.9±6.0	0.421	0.546	0.2±0.2	0.1±0.1	0.5±0.4	1.1±0.2	0.002	0.017
Galectin-3-binding protein	M3V7X9_PIG	0.4±0.8	2.4±3.2	4.1±1.5	0.7±0.6	0.127	0.325	0.0±0.0	1.3±2.0	1.8±1.5	1.3±0.9	0.475	0.579
Gelsolin	GELS_PIG	217.8±17.2	129.6±51.0	160.6±18.1	179.7±80.3	0.246	0.419	227.7±68.3	150.1±78.2	194.7±35.8	155.4±18.4	0.345	0.495
Hyaluronan and proteoglycan link protein 1	HPLN1_PIG	2.6±2.2	3.5±2.7	7.1±2.5	3.4±0.7	0.128	0.325	4.4±2.5	9.6±2.5	10.9±6.5	0.9±0.8	0.036	0.116
Hyaluronan and proteoglycan link protein 3*	HPLN3_HUMAN	0.2±0.3	0.4±0.8	0.6±0.7	0.0±0.0	0.552	0.613	0.7±0.6	0.6±1.0	1.0±1.1	0.1±0.2	0.604	0.677
Hyaluronan and proteoglycan link protein 4*	HPLN4_HUMAN	0.0±0.0	0.0±0.0	0.2±0.3	0.0±0.0	n/a	n/a	0.0±0.0	0.6±0.6	0.0±0.0	0.0±0.0	n/a	n/a
Insulin-like growth factor-binding protein 7	C7EDN1_PIG	2.0±1.2	4.3±3.8	22.3±2.8	11.1±9.9	0.008	0.080	2.1±2.3	1.5±1.7	21.0±7.4	8.8±0.8	0.001	0.011
Inter-alpha-trypsin inhibitor heavy chain H2	ITI2_PIG	8.4±3.7	4.5±2.1	3.6±2.2	4.1±1.6	0.163	0.356	6.8±1.5	6.4±3.9	5.7±1.8	6.1±5.2	0.985	0.985
Lactadherin	MFGM_PIG	7.9±4.8	11.7±5.7	17.8±9.7	19.1±15.3	0.499	0.591	4.8±3.8	9.3±7.2	19.7±5.5	6.1±0.6	0.022	0.081
Laminin subunit alpha-4	F1RZM4_PIG	6.2±1.5	2.1±1.5	3.5±1.5	11.2±3.5	0.004	0.065	6.7±4.6	3.9±2.2	3.6±3.9	3.9±1.5	0.655	0.705
Laminin subunit beta-1	F1SAE9_PIG	2.8±1.3	1.4±1.2	6.2±4.7	9.4±1.0	0.020	0.127	1.6±1.9	1.4±1.0	4.6±2.7	2.0±1.2	0.188	0.328

Laminin subunit beta-2	F1SPT5_PIG	8.8±2.3	8.1±0.2	7.1±0.9	8.7±1.3	0.462	0.577	6.2±3.7	11.0±2.8	8.3±5.3	4.3±1.9	0.205	0.343
Laminin subunit gamma-1	F1S663_PIG	41.7±11.2	35.9±1.9	38.7±5.3	47.8±8.8	0.330	0.477	36.6±21.7	39.7±6.9	42.7±18.6	16.7±4.9	0.213	0.345
Latent-TGFβ-binding protein 1	F1S405_PIG	0.7±0.7	0.4±0.1	0.3±0.2	0.2±0.2	0.526	0.604	0.3±0.1	0.5±0.5	0.6±0.5	0.0±0.0	0.285	0.432
Latent-TGFβ-binding protein 2	F1S2T5_PIG	2.5±1.3	2.9±2.0	5.5±1.0	2.7±2.4	0.213	0.395	2.4±1.1	2.4±1.8	10.2±0.8	9.1±1.6	0.000	0.006
Latent-TGFβ-binding protein 4	LTBP4_PIG	3.7±1.9	0.1±0.1	0.0±0.0	4.9±5.6	0.177	0.365	5.5±1.7	1.1±1.7	1.4±0.6	2.8±2.9	0.074	0.156
Leukocyte elastase inhibitor	ILEU_PIG	0.0±0.0	0.0±0.0	0.0±0.0	0.1±0.2	n/a	n/a	1.0±0.4	1.6±2.8	0.0±0.0	0.0±0.0	0.463	0.577
Lipoprotein lipase*	LIPL_PIG	1.8±0.4	1.2±2.0	0.0±0.0	0.0±0.0	0.150	0.335	1.4±0.6	6.1±2.7	3.3±2.1	0.0±0.0	0.012	0.052
Lumican	F1SQ09_PIG	288.9±36.6	204.3±53.9	312.6±49.2	431.5±212.7	0.188	0.365	257.0±73.7	277.8±152.9	282.2±61.7	405.1±59.0	0.286	0.432
Lysyl oxidase homolog 1	F1SIC9_PIG	5.7±5.2	0.7±0.6	3.9±1.2	7.8±3.3	0.110	0.310	6.2±7.8	2.0±1.7	6.6±4.9	11.3±1.1	0.195	0.336
Macrophage-capping protein	F1SVB0_PIG	0.0±0.0	0.0±0.0	0.1±0.1	0.6±1.0	n/a	n/a	0.1±0.1	0.0±0.0	0.2±0.2	0.4±0.2	0.060	0.142
Matrix Gla protein	MGP_PIG	1.2±0.4	1.7±0.1	2.5±1.1	1.3±0.8	0.149	0.335	1.3±0.7	1.3±0.7	2.8±0.3	1.4±0.5	0.035	0.115
Matrix-remodeling-associated protein 5	F1RZ07_PIG	0.3±0.4	6.3±5.4	6.5±9.2	7.4±9.7	0.631	0.677	0.1±0.2	3.9±1.9	7.3±9.9	11.5±5.5	0.175	0.321
Mimecan	I3L9T6_PIG	426.0±40.0	220.5±139.0	255.7±34.2	495.6±304.8	0.220	0.395	389.9±27.1	292.7±193.6	283.7±7.3	581.3±152.7	0.061	0.142
Myeloperoxidase	K7GRV6_PIG	1.1±1.1	0.3±0.5	0.0±0.0	0.7±1.2	0.479	0.580	2.6±2.9	4.4±7.5	0.0±0.0	0.0±0.0	0.494	0.589
Nidogen-1	NID1_PIG	1.5±0.8	2.2±2.2	4.3±1.7	6.1±2.5	0.070	0.255	2.0±0.7	3.8±2.2	5.3±2.6	8.1±2.7	0.049	0.142
Nidogen-2	F1SFF3_PIG	109.6±14.8	137.7±31.0	155.9±5.2	173.2±56.0	0.187	0.365	104.0±32.6	157.8±56.4	161.3±12.5	96.8±25.8	0.109	0.211
Papilin	F1S3J7_PIG	0.6±1.0	0.3±0.6	0.2±0.2	0.1±0.2	0.800	0.807	0.6±0.5	0.7±0.5	0.3±0.3	0.0±0.0	0.218	0.349
Pentraxin-related protein PTX3*	F1SJM0_PIG	0.9±0.8	1.2±1.1	0.0±0.0	0.1±0.1	0.138	0.326	0.8±0.3	0.5±0.9	1.4±1.1	0.0±0.0	0.234	0.369
Peptidyl-prolyl cis-trans isomerase A	PPIA_PIG	2.2±1.0	1.5±0.7	4.3±1.5	6.2±8.1	0.536	0.604	3.8±1.8	3.6±2.5	5.8±4.0	7.3±2.8	0.385	0.519
Periostin	F1RS37_PIG	2.5±2.3	22.6±19.5	100.3±69.3	148.3±199.7	0.361	0.505	0.5±0.5	6.8±7.0	86.6±62.7	287.5±33.2	0.000	0.003
Perlecan	PGBM_PIG	210.9±42.8	188.9±59.9	245.7±21.6	384.9±98.0	0.019	0.127	215.7±38.4	237.8±121.6	321.6±78.5	336.2±111.9	0.359	0.506
Peroxidasin homolog	I3LDA4_PIG	0.0±0.0	0.3±0.3	0.2±0.1	0.2±0.4	0.565	0.622	0.0±0.0	0.0±0.0	0.1±0.2	0.0±0.0	n/a	n/a
Pigment epithelium-derived factor	Q0PM28_PIG	0.4±0.5	0.5±0.9	2.2±0.9	0.9±1.2	0.134	0.326	0.3±0.5	0.2±0.3	3.3±2.7	1.9±1.3	0.101	0.203
Plasminogen	PLMN_PIG	57.8±54.2	79.7±55.9	10.7±5.6	2.1±1.8	0.114	0.310	34.6±16.9	146.3±54.8	11.2±6.5	2.6±1.8	0.001	0.011
Podocan	I3LEB7_PIG	0.8±0.4	0.1±0.2	1.1±0.8	2.8±1.6	0.030	0.163	0.6±0.7	0.5±0.3	0.9±1.1	1.0±0.8	0.888	0.905
Procollagen C-endopeptidase enhancer 1	I3LEE6_PIG	0.2±0.1	0.1±0.1	0.8±0.5	0.7±0.3	0.069	0.255	0.2±0.2	0.1±0.1	2.7±3.8	1.1±0.5	0.366	0.506
Prolargin	F1S6B4_PIG	269.7±21.2	200.2±42.2	300.6±54.5	608.6±187.3	0.005	0.065	263.7±49.7	255.3±109.7	341.3±134.5	995.5±337.7	0.004	0.024
Prolow-density lipoprotein receptor-related protein 1	K9IVL7_PIG	1.1±0.3	1.4±1.6	3.5±3.5	4.2±2.1	0.295	0.454	1.4±1.2	0.7±0.5	3.6±2.8	4.5±1.2	0.066	0.147
Properdin	K7GQR1_PIG	0.7±0.6	0.3±0.3	0.0±0.0	0.3±0.3	0.228	0.401	0.6±0.7	0.6±0.7	0.3±0.5	0.2±0.1	0.749	0.783
Prophenin and tritrtpticin precursor	PF11_PIG	63.9±15.1	16.9±10.5	2.1±1.0	8.0±13.4	0.001	0.025	94.1±47.6	186.5±155.5	9.8±2.0	1.1±1.6	0.074	0.156
Proteoglycan 4	I3L5Z3_PIG	0.5±0.2	0.0±0.0	0.0±0.0	0.0±0.0	n/a	n/a	0.0±0.1	0.1±0.2	0.0±0.0	0.0±0.0	0.554	0.646
RPE-spondin	RPESP_PIG	4.8±2.1	7.9±7.7	5.8±3.3	1.5±1.3	0.393	0.536	9.0±9.3	4.7±2.9	9.3±5.6	2.4±0.4	0.415	0.523
Secreted frizzled-related protein 1	I3LB66_PIG	0.0±0.0	0.0±0.0	0.4±0.6	0.9±0.9	0.183	0.365	0.0±0.0	0.0±0.0	0.2±0.3	0.7±0.0	0.001	0.011
Serine protease HTRA1	F1SEH4_PIG	7.0±1.7	10.8±4.9	46.7±13.0	45.6±41.4	0.100	0.296	5.5±2.7	6.5±3.8	37.4±17.4	37.2±21.0	0.029	0.101
Serotransferrin	TRFE_PIG	0.4±0.4	2.3±0.7	1.7±1.8	3.2±5.6	0.710	0.751	3.0±2.3	6.0±2.7	1.6±2.0	6.6±9.7	0.624	0.679

Serum amyloid P-component	SAMP_PIG	0.1±0.1	0.0±0.0	0.0±0.0	0.0±0.0	n/a	n/a	0.1±0.1	0.0±0.0	0.0±0.0	0.0±0.1	0.713	0.753
SPARC	SPRC_PIG	0.3±0.6	3.6±1.3	3.5±1.4	0.8±1.0	0.010	0.088	0.4±0.7	0.5±0.7	3.2±1.9	4.7±1.2	0.008	0.039
Spondin-1	SPON1_PIG	0.0±0.0	0.1±0.1	0.5±0.5	0.4±0.7	0.449	0.569	0.1±0.1	0.1±0.2	0.5±0.3	0.9±0.8	0.187	0.328
Sulfhydryl oxidase	F1S682_PIG	0.0±0.0	0.0±0.0	0.0±0.0	0.0±0.0	n/a	n/a	0.0±0.0	0.1±0.2	0.0±0.0	0.0±0.0	n/a	n/a
Superoxide dismutase [Cu-Zn]	Q007T6_PIG	1.1±0.4	0.2±0.2	1.6±0.6	1.3±0.7	0.042	0.215	1.8±1.5	0.2±0.2	1.3±0.3	2.1±0.6	0.098	0.200
Target of Nesh-SH3*	F1SL03_PIG	3.1±1.9	0.9±1.5	1.3±2.0	4.1±4.5	0.466	0.577	4.3±2.0	0.8±0.8	3.3±1.0	13.5±5.4	0.004	0.024
Tenascin	TENA_PIG	64.2±20.0	52.4±13.9	257.6±39.4	168.2±84.9	0.003	0.046	44.9±12.4	82.6±47.7	168.9±41.0	106.5±33.4	0.017	0.070
Tenascin XB*	A5A8W4_PIG	5.5±2.3	4.4±7.1	3.4±4.8	9.4±11.0	0.747	0.769	5.7±4.1	5.9±5.4	1.8±1.4	6.1±5.3	0.586	0.669
Tetranectin	F1SRC8_PIG	1.6±0.5	0.9±0.8	2.5±2.0	2.3±0.4	0.324	0.477	1.7±0.8	2.2±2.0	3.5±2.6	6.7±2.1	0.059	0.142
TGFβ-1*	TGFB1_PIG	0.0±0.0	0.0±0.0	0.0±0.0	0.0±0.0	n/a	n/a	0.0±0.0	0.2±0.3	0.0±0.0	0.0±0.0	n/a	n/a
TGFβ-3*	K7GSJ9_PIG	0.0±0.0	0.0±0.0	0.0±0.0	0.0±0.0	n/a	n/a	0.0±0.0	0.0±0.0	0.0±0.0	0.6±0.9	n/a	n/a
TGFβ-induced protein ig-h3	BGH3_PIG	19.5±5.0	15.1±11.9	9.5±4.3	27.0±17.6	0.333	0.477	9.0±3.3	15.7±8.3	22.6±19.7	8.6±4.8	0.415	0.523
Thrombospondin-1	K7GPJ3_PIG	5.8±2.3	4.2±1.7	7.2±2.1	2.7±0.9	0.073	0.257	4.3±0.9	6.3±2.1	7.1±1.8	6.1±3.2	0.491	0.589
Tryptase	TRYT_PIG	0.0±0.0	0.0±0.0	0.0±0.0	3.8±6.6	n/a	n/a	0.0±0.0	0.0±0.1	0.0±0.0	0.4±0.7	0.475	0.579
Tubulointerstitial nephritis antigen-like	F1SVA2_PIG	83.0±10.1	56.6±25.4	53.2±6.7	65.1±9.5	0.142	0.329	71.7±13.9	67.8±36.6	69.5±11.8	43.5±5.7	0.364	0.506
Versican	F1REZ2_PIG	70.2±5.8	103.0±18.5	153.5±7.9	148.5±26.1	0.001	0.025	112.2±54.7	81.1±31.6	231.4±38.8	398.1±137.4	0.004	0.025
Vitamin D-binding protein	I3LN42_PIG	8.7±5.6	1.3±1.0	2.7±1.1	1.4±1.8	0.051	0.231	5.3±1.1	9.0±5.5	2.8±1.9	1.4±1.0	0.062	0.142
Vitronectin	VTNC_PIG	298.1±250.1	239.7±90.3	148.2±65.3	87.3±94.7	0.352	0.498	202.6±40.6	694.9±156.0	235.4±154.0	82.8±48.1	0.001	0.011
von Willebrand factor A domain-containing protein 1	F1RJE3_PIG	17.6±8.1	8.6±3.6	10.6±3.4	14.5±6.4	0.294	0.454	18.7±5.6	11.7±6.0	14.6±4.6	7.3±4.4	0.129	0.245
WD repeat-containing protein 1	K9IVR7_PIG	0.0±0.0	0.1±0.2	0.1±0.1	0.1±0.2	0.537	0.604	0.0±0.0	0.0±0.0	0.0±0.1	0.0±0.1	0.595	0.673

P values for changes in BM or DES at different time-points were identified by one-way ANOVA (BMS: n=3 [BMS1/3/7/28], 1-way ANOVA; DES: n=3 [DES 1/3/7/28], 1-way ANOVA). ANOVA was not applied if a protein was detected at only a single time point. Results in bold indicate *P* < 0.05. Values are average (Av) total ion current (TIC) × 10⁶ ± standard deviation (SD). n/a denotes not applicable. FDR denotes false discovery rate. The FDR threshold was set at 10%. Protein changes with *P* < 0.05 and a FDR of <10% are highlighted in bold. Proteins only identified in the media, but not neointima are marked with*.

Supplemental Table IV. Extracellular proteins identified by proteomics in the media of balloon dilated porcine coronary arteries.

Identified Proteins	UniProt ID	Balloon angioplasty Total ion current x 10 ⁶ Av±SD				
		BA early	BA late	FC late/early	P BA	FDR
Adipocyte enhancer-binding protein 1	F1SSF7_PIG	0.9±0.6	2.0±1.2	2.1	0.258	0.519
Aggrecan	F1SKR0_PIG	5.3±3.0	17.3±10.7	3.3	0.187	0.431
Agrin	I3LGD9_PIG	5.6±4.0	9.9±1.1	1.8	0.118	0.403
Alpha-2-HS-glycoprotein	FETUA_PIG	3.7±2.2	1.9±1.4	0.5	0.232	0.492
Annexin A1	ANXA1_PIG	3.1±0.8	0.5±0.2	0.2	0.005	0.217
Annexin A2	ANXA2_PIG	14.2±10.5	14.9±2.9	1.1	0.898	0.951
Antithrombin-III	Q7M364_PIG	2.5±1.8	0.3±0.5	0.1	n/a	n/a
Apolipoprotein A-I	APOA1_PIG	19.5±7.7	12.7±5.6	0.7	0.231	0.492
Apolipoprotein A-IV	APOA4_PIG	0.0±0.0	0.1±0.1	n/a	n/a	n/a
Apolipoprotein C-III	APOC3_PIG	6.5±3.9	0.2±0.4	0.0	0.048	0.301
Apolipoprotein E	APOE_PIG	26.2±20.3	1.2±0.3	0.0	n/a	n/a
Apolipoprotein H	I3LGN5_PIG	23.1±4.4	19.5±8.5	0.8	0.551	0.720
Apolipoprotein R	APOR_PIG	1.9±2.3	0.0±0.0	0.0	n/a	n/a
Asporin	F1SUE4_PIG	61.0±14.8	87.4±40.2	1.4	0.375	0.565
Biglycan	K7GP55_PIG	659.9±210.4	971.4±110.9	1.5	0.056	0.301
Carboxypeptidase-like protein X2	F1SEC6_PIG	0.0±0.0	0.0±0.0	n/a	n/a	n/a
Cathepsin D	Q4U1U3_PIG	3.6±3.7	3.2±1.8	0.9	0.852	0.925
Cathepsin G	F1SGS1_PIG	0.7±0.9	0.0±0.0	0.0	n/a	n/a
Chitinase-3-like protein 1	CH3L1_PIG	0.0±0.0	0.0±0.0	n/a	n/a	n/a
Chondroitin sulfate proteoglycan 4*	CSPG4_HUMAN	0.1±0.2	0.0±0.0	0.0	n/a	n/a
Clusterin	CLUS_PIG	95.9±46.7	19.7±8.5	0.2	0.044	0.301
Collagen alpha-1 (I)	CO1A1_PIG	2055.2±391.6	2088.2±468.7	1.0	0.926	0.958
Collagen alpha-1 (II)*	I3LSV6_PIG	82.5±12.5	67.2±16.1	0.8	0.248	0.514
Collagen alpha-1 (III)	F1RYI8_PIG	252.0±85.1	431.9±112.0	1.7	0.087	0.384
Collagen alpha-1 (IV)	M3V819_PIG	4.3±2.7	5.2±1.7	1.2	0.628	0.778
Collagen alpha-1 (V)	F1S021_PIG	75.2±29.8	96.9±37.1	1.3	0.453	0.640
Collagen alpha-1 (VI)	CO6A1_PIG	6.2±4.7	7.9±6.9	1.3	0.746	0.851
Collagen alpha-1 (VIII)	F1SKX7_PIG	0.2±0.4	0.2±0.3	1.1	n/a	n/a
Collagen alpha-1 (XI)	F1S571_PIG	42.1±14.8	56.5±23.0	1.3	0.408	0.595
Collagen alpha-1 (XII)	COCA1_PIG	6.1±2.5	3.4±3.6	0.6	0.338	0.548
Collagen alpha-1 (XV)	COFA1_PIG	4.4±3.8	6.8±4.6	1.6	0.491	0.672
Collagen alpha-1 (XVIII)	COIA1_PIG	10.6±4.7	10.5±1.4	1.0	0.990	0.990
Collagen alpha-1 (XX)	COKA1_PIG	12.5±4.4	21.3±4.4	1.7	0.053	0.301
Collagen alpha-2 (I)	F1SFA7_PIG	1819.5±446.0	2184.2±434.5	1.2	0.332	0.548
Collagen alpha-2 (IV)	F1RLL9_PIG	5.4±6.5	5.6±2.6	1.0	0.961	0.972
Collagen alpha-2 (V)	Q59IP2_PIG	75.8±40.3	84.1±59.3	1.1	0.846	0.925
Collagen alpha-2 (VI)	I3LQ84_PIG	24.5±16.6	31.7±22.6	1.3	0.669	0.804
Collagen alpha-2 (XI)*	A5D9K7_PIG	24.6±9.4	25.0±7.5	1.0	0.951	0.972
Collagen alpha-3 (V)	Q59IP1_PIG	0.6±0.4	1.2±0.9	2.0	0.338	0.548
Collagen alpha-3 (VI)	I3LUR7_PIG	58.0±38.7	63.2±66.2	1.1	0.911	0.953
Collagen alpha-6 (VI)	CO6A6_PIG	0.2±0.3	0.0±0.0	0.0	n/a	n/a
Complement C3	CO3_PIG	12.3±8.9	1.8±2.1	0.1	0.097	0.384
Complement component C9	A0SEG9_PIG	0.0±0.0	0.0±0.0	n/a	n/a	n/a
Connective tissue growth factor	CTGF_PIG	0.2±0.2	0.0±0.0	0.0	n/a	n/a
Decorin	PGS2_PIG	369.9±68.6	569.0±248.3	1.5	0.298	0.548
Dermatopontin	DERM_PIG	36.2±8.6	74.7±13.9	2.1	0.022	0.288
Dystroglycan	I3LD20_PIG	0.5±0.3	2.2±0.6	4.5	0.026	0.288
EMILIN-1	F1SDQ5_PIG	9.4±4.2	14.5±3.6	1.5	0.148	0.420
Fibrillin-1	FBN1_PIG	0.0±0.0	0.0±0.0	n/a	n/a	n/a
Fibrinogen beta chain	F1RX37_PIG	1514.5±1633.6	17.6±25.7	0.0	0.164	0.429
Fibrinogen gamma chain	F1RX35_PIG	1214.6±1333.0	16.2±19.1	0.0	0.170	0.429

Fibromodulin	F1S6B5_PIG	76.2±40.4	273.4±67.2	3.6	0.019	0.288
Fibronectin	F1SS24_PIG	996.9±285.9	314.4±116.2	0.3	0.011	0.253
Fibronectin type III domain-containing protein 1	F1SB59_PIG	0.0±0.0	0.0±0.1	n/a	n/a	n/a
Fibulin-1	F1SM61_PIG	0.6±0.4	0.3±0.3	0.4	0.269	0.519
Fibulin-2	FBLN2_PIG	0.2±0.3	0.2±0.4	1.1	n/a	n/a
Fibulin-3	F8SIP2_PIG	0.0±0.0	0.0±0.0	n/a	n/a	n/a
Fibulin-5	F1SD87_PIG	10.0±5.2	14.0±8.2	1.4	0.511	0.689
Galectin-1	LEG1_PIG	22.8±13.4	44.5±6.0	2.0	0.041	0.301
Galectin-3	A3EX84_PIG	0.1±0.2	0.2±0.1	2.0	n/a	n/a
Galectin-3-binding protein	M3V7X9_PIG	4.7±7.0	0.0±0.0	0.0	n/a	n/a
Gelsolin	GELS_PIG	164.9±7.5	250.3±39.5	1.5	0.061	0.301
Hyaluronan and proteoglycan link protein 1	HPLN1_PIG	6.1±3.8	9.8±4.3	1.6	0.302	0.548
Hyaluronan and proteoglycan link protein 3*	HPLN3_HUMAN	1.6±0.7	0.8±1.1	0.5	0.367	0.565
Hyaluronan and proteoglycan link protein 4*	HPLN4_HUMAN	0.3±0.6	0.0±0.0	0.0	n/a	n/a
Insulin-like growth factor-binding protein 7	C7EDN1_PIG	2.7±1.7	6.4±5.0	2.4	0.329	0.548
Inter-alpha-trypsin inhibitor heavy chain H2	ITI2_PIG	7.2±1.4	2.1±1.6	0.3	0.011	0.253
Lactadherin	MFGM_PIG	13.5±7.6	11.8±2.5	0.9	0.686	0.815
Laminin subunit alpha-4	F1RZM4_PIG	6.5±4.6	9.1±5.2	1.4	0.522	0.694
Laminin subunit beta-1	F1SAE9_PIG	3.6±2.6	7.6±1.7	2.1	0.060	0.301
Laminin subunit beta-2	F1SPT5_PIG	9.4±2.0	10.5±3.3	1.1	0.630	0.778
Laminin subunit gamma-1	F1S663_PIG	41.1±7.8	51.6±4.7	1.3	0.080	0.374
Latent-TGFβ-binding protein 1	F1S405_PIG	0.5±0.5	0.2±0.3	0.3	0.272	0.519
Latent-TGFβ-binding protein 2	F1S2T5_PIG	3.3±2.5	2.3±1.5	0.7	0.558	0.720
Latent-TGFβ-binding protein 4	LTBP4_PIG	1.0±1.9	2.9±0.9	3.1	n/a	n/a
Leukocyte elastase inhibitor	ILEU_PIG	1.3±1.7	0.0±0.0	0.0	n/a	n/a
Lipoprotein lipase*	LIPL_PIG	1.4±1.0	0.0±0.0	0.0	n/a	n/a
Lumican	F1SQ09_PIG	201.5±83.1	274.7±84.1	1.4	0.310	0.548
Lysyl oxidase homolog 1	F1SIC9_PIG	2.3±2.5	8.9±5.1	3.9	0.140	0.417
Macrophage-capping protein	F1SVB0_PIG	0.0±0.0	0.1±0.1	n/a	n/a	n/a
Matrix Gla protein	MGP_PIG	1.1±0.6	1.3±0.7	1.2	0.726	0.840
Matrix-remodeling-associated protein5	F1RZ07_PIG	5.8±7.9	2.3±3.1	0.4	0.467	0.649
Mimecan	I3L9T6_PIG	222.1±65.9	359.4±47.8	1.6	0.024	0.288
Myeloperoxidase	K7GRV6_PIG	5.0±5.4	0.0±0.0	0.0	n/a	n/a
Nidogen-1	NID1_PIG	1.3±0.3	2.2±0.6	1.7	0.095	0.384
Nidogen-2	F1SFF3_PIG	107.0±40.5	191.0±42.9	1.8	0.055	0.301
Papilin	F1S3J7_PIG	1.5±2.1	0.6±0.5	0.4	0.428	0.614
Pentraxin-related protein PTX3*	F1SJM0_PIG	1.6±0.5	0.0±0.0	0.0	n/a	n/a
Peptidyl-prolyl cis-trans isomerase A	PPIA_PIG	3.5±2.1	3.2±0.8	0.9	0.780	0.879
Periostin	F1RS37_PIG	18.4±18.6	24.1±13.7	1.3	0.660	0.804
Perlecan	PGBM_PIG	223.6±75.7	314.7±59.1	1.4	0.134	0.413
Peroxidasin homolog	I3LDA4_PIG	0.3±0.3	0.1±0.2	0.4	n/a	n/a
Pigment epithelium-derived factor	Q0PM28_PIG	0.8±1.1	0.7±0.5	0.9	0.876	0.939
Plasminogen	PLMN_PIG	28.7±24.0	0.4±0.6	0.0	0.099	0.384
Podocan	I3LEB7_PIG	0.9±0.8	3.7±1.3	4.3	0.045	0.301
Procollagen C-endopeptidase enhancer 1	I3LEE6_PIG	0.4±0.5	0.9±0.7	2.3	0.373	0.565
Prolargin	F1S6B4_PIG	203.8±44.9	319.0±81.4	1.6	0.117	0.403
Prolow-density lipoprotein receptor-related protein 1	K9IVL7_PIG	3.7±1.9	1.8±1.4	0.5	0.189	0.431
Properdin	K7GQR1_PIG	0.7±0.6	0.1±0.1	0.2	0.152	0.420
Propenin and tritrypticin precursor	PF11_PIG	116.0±100.2	0.3±0.5	0.0	n/a	n/a
Proteoglycan 4	I3L5Z3_PIG	0.0±0.0	0.0±0.0	n/a	n/a	n/a
RPE-spondin	RPESP_PIG	6.6±1.5	7.6±0.6	1.2	0.274	0.519

Secreted frizzled-related protein 1	I3LB66_PIG	0.0±0.0	0.8±0.4	n/a	n/a	n/a
Serine protease HTRA1	F1SEH4_PIG	5.9±3.4	24.5±17.8	4.2	0.208	0.463
Serotransferrin	TRFE_PIG	3.3±3.0	0.2±0.3	0.1	n/a	n/a
Serum amyloid P-component	SAMP_PIG	0.2±0.3	0.0±0.0	0.0	n/a	n/a
SPARC	SPRC_PIG	1.4±1.6	3.1±0.6	2.2	0.122	0.403
Spondin-1	SPON1_PIG	0.2±0.4	0.5±0.4	2.8	n/a	n/a
Sulfhydryl oxidase	F1S682_PIG	0.1±0.2	0.0±0.0	0.0	n/a	n/a
Superoxide dismutase [Cu-Zn]	Q007T6_PIG	0.9±1.0	3.2±1.9	3.4	0.156	0.420
Target of Nesh-SH3*	F1SL03_PIG	1.0±1.7	2.7±2.2	2.7	0.339	0.548
Tenascin	TENA_PIG	81.9±36.9	36.0±30.0	0.4	0.131	0.413
Tenascin XB*	A5A8W4_PIG	2.8±4.7	3.4±2.3	1.2	0.831	0.924
Tetranectin	F1SRC8_PIG	1.1±1.0	1.4±0.7	1.2	0.698	0.818
TGFβ-1*	TGFB1_PIG	0.0±0.0	0.0±0.0	n/a	n/a	n/a
TGFβ-3*	K7GSJ9_PIG	0.0±0.0	0.0±0.0	n/a	n/a	n/a
TGFβ-induced protein ig-h3	BGH3_PIG	34.6±17.0	16.1±8.1	0.5	0.121	0.403
Thrombospondin-1	K7GPJ3_PIG	5.7±0.9	0.4±0.4	0.1	0.000	0.024
Tryptase	TRYT_PIG	0.0±0.0	0.0±0.0	n/a	n/a	n/a
Tubulointerstitial nephritis antigen-like	F1SVA2_PIG	58.3±3.7	67.8±14.1	1.2	0.362	0.565
Versican	F1REZ2_PIG	106.1±58.1	142.6±42.5	1.3	0.381	0.566
Vitamin D-binding protein	I3LN42_PIG	7.3±7.7	0.5±0.5	0.1	0.173	0.429
Vitronectin	VTNC_PIG	149.0±66.3	43.5±29.8	0.3	0.043	0.301
von Willebrand factor A domain-containing protein 1	F1RJE3_PIG	11.1±2.7	16.8±5.1	1.5	0.183	0.431
WD repeat-containing protein 1	K9IVR7_PIG	0.0±0.1	0.1±0.0	1.4	0.598	0.760

P values for differential expression between BA early and BA late are based on unpaired Student's *t*-tests with unequal variance (early: n=4 [day 1 + 3], late: n=3 [day 14 + 28]). *T*-test was not performed if a protein was undetectable in the majority of samples from 1 of the 2 groups compared. Results in bold indicate *P* < 0.05. Values are average (Av) total ion current (TIC) × 10⁶ ± standard deviation (SD). n/a denotes not applicable, FC denotes fold change. FDR denotes false discovery rate. The FDR threshold was set at 10%. Protein changes with *P* < 0.05 and a FDR of <10% are highlighted in bold. Proteins only identified in the media, but not neointima are marked with*.

Supplemental Table V. Significant extracellular protein changes between BMS or DES day 28 vs. BA late.

Identified Proteins	UniProt ID	MW (kDa)	BMS/BA			DES/BA		
			FC	<i>P</i>	FDR	FC	<i>P</i>	FDR
RPE-spondin	RPESP_PIG	32	0.2	0.006	0.172	0.3	0.001	0.012
Laminin subunit gamma-1	F1S663_PIG	177	0.9	0.562	0.697	0.3	0.001	0.012
Galectin-3	A3EX84_PIG	27	23.4	0.395	0.612	6.8	0.002	0.012
Collagen alpha-1 (XI)	F1S571_PIG	159	1.8	0.272	0.584	3.4	0.002	0.012
Periostin	F1RS37_PIG	93	6.1	0.394	0.612	11.9	0.002	0.012
Biglycan	K7GP55_PIG	41	1.5	0.167	0.584	2.0	0.004	0.021
Collagen alpha-1 (V)	F1S021_PIG	182	1.8	0.267	0.584	2.6	0.006	0.021
Latent-TGFβ-binding protein 2	F1S2T5_PIG	196	1.2	0.833	0.860	3.9	0.006	0.021
Collagen alpha-1 (XVIII)	COIA1_PIG	62	0.6	0.027	0.256	0.2	0.007	0.021
Collagen alpha-1 (I)	CO1A1_PIG	100	1.3	0.584	0.697	1.9	0.007	0.021
Apolipoprotein H	I3LGN5_PIG	29	1.5	0.463	0.648	3.1	0.008	0.021
Dermatopontin	DERM_PIG	22	1.7	0.328	0.599	2.0	0.008	0.021
Collagen alpha-2 (I)	F1SFA7_PIG	129	1.2	0.639	0.734	2.0	0.010	0.024
Laminin subunit beta-1	F1SAE9_PIG	199	1.2	0.197	0.584	0.3	0.013	0.028
Fibronectin	F1SS24_PIG	272	1.6	0.243	0.584	2.9	0.014	0.028
Aggrecan	F1SKR0_PIG	238	1.6	0.250	0.584	3.0	0.017	0.032
Collagen alpha-1 (II)	I3LSV6_PIG	130	1.0	0.961	0.961	1.7	0.018	0.032
Annexin A1	ANXA1_PIG	39	4.0	0.364	0.612	7.4	0.022	0.038
Collagen alpha-2 (XI)	A5D9K7_PIG	162	1.5	0.436	0.643	2.1	0.024	0.040
Collagen alpha-1 (XII)	COCA1_PIG	229	13.7	0.284	0.584	15.7	0.026	0.041
Collagen alpha-1 (VIII)	F1SKX7_PIG	73	2.6	0.301	0.584	15.3	0.028	0.041
Tetranectin	F1SRC8_PIG	22	1.7	0.118	0.523	4.9	0.036	0.049
Gelsolin	GELS_PIG	85	0.7	0.267	0.584	0.6	0.036	0.049
Agrin	I3LGD9_PIG	216	0.9	0.693	0.740	0.6	0.040	0.050
Nidogen-2	F1SFF3_PIG	152	0.9	0.687	0.740	0.5	0.042	0.050
Galectin-1	LEG1_PIG	15	0.7	0.080	0.411	0.6	0.042	0.050
Dystroglycan	I3LD20_PIG	95	0.3	0.046	0.285	0.4	0.043	0.050
Podocan	I3LEB7_PIG	72	0.8	0.502	0.648	0.3	0.049	0.053
Lactadherin	MFGM_PIG	46	1.6	0.498	0.648	0.5	0.050	0.053
Thrombospondin-1	K7GPJ3_PIG	120	6.5	0.031	0.256	14.8	0.090	0.093
SPARC	SPRC_PIG	34	0.3	0.033	0.256	1.5	0.144	0.144

P value and fold change (FC) for changes between BMS or DES day 28 and BA late are shown. *P* values are based on unpaired Student's *t*-tests with unequal variance (n=3 [BMS day 28] or n=3 [DES day 28], n=3 [BA late]). *T*-test was not performed if a protein was undetectable in the majority of samples from 1 of the 2 groups compared. Results in bold indicate *P* < 0.05. FDR denotes false discovery rate. The FDR threshold was set at 10%.

Supplemental Table VI. Differentially expressed proteins between DES and BMS at different time points.

Identified Proteins	UniProt ID	MW (kDa)	Day 1			Day 3			Day 7			Day 28		
			FC	P	FDR	FC	P	FDR	FC	P	FDR	FC	P	FDR
Collagen alpha-2 (IV)	F1RLL9_PIG	161	0.6	0.362	0.683	0.6	0.338	0.676	1.2	0.707	0.868	0.3	<0.001	0.008
Laminin subunit beta-1	F1SAE9_PIG	199	0.6	0.432	0.683	1.0	0.975	0.975	0.7	0.639	0.868	0.2	0.001	0.008
Laminin subunit gamma-1	F1S663_PIG	177	0.9	0.741	0.803	1.1	0.440	0.770	1.1	0.753	0.868	0.3	0.011	0.050
SPARC	SPRC_PIG	34	1.3	n/a	n/a	0.1	0.036	0.201	0.9	0.802	0.868	5.6	0.014	0.050
Hyaluronan and proteoglycan link protein 1	HPLN1_PIG	40	1.7	0.427	0.683	2.8	0.043	0.201	1.5	0.419	0.868	0.3	0.019	0.050
Collagen alpha-1 (XVIII)	COIA1_PIG	62	0.8	0.540	0.683	1.0	0.921	0.975	1.1	0.788	0.868	0.2	0.020	0.050
Latent-TGFβ-binding protein 2	F1S2T5_PIG	196	1.0	0.952	0.952	0.8	0.753	0.975	1.9	0.003	0.045	3.3	0.026	0.054
Collagen alpha-1 (VIII)	F1SKX7_PIG	73	0.6	n/a	n/a	2.0	n/a	n/a	1.2	0.645	0.868	5.9	0.029	0.054
Laminin subunit beta-2	F1SPT5_PIG	179	0.7	0.364	0.683	1.4	0.201	0.563	1.2	0.728	0.868	0.5	0.038	0.057
Tubulointerstitial nephritis antigen-like	F1SVA2_PIG	52	0.9	0.326	0.683	1.2	0.686	0.975	1.3	0.125	0.625	0.7	0.038	0.057
Aggrecan	F1SKR0_PIG	238	0.8	0.523	0.683	4.1	0.263	0.614	1.0	0.971	0.971	1.9	0.044	0.060
TGFβ-induced protein ig-h3	BGH3_PIG	74	0.5	0.045	0.293	1.0	0.950	0.975	2.4	0.368	0.868	0.3	0.206	0.258
Prophenin and tritrypticin precursor	PF11_PIG	24	1.5	0.388	0.683	11.1	0.199	0.563	4.6	0.010	0.075	0.1	0.467	0.539
Collagen alpha-1 (XII)	COCA1_PIG	229	0.8	0.045	0.293	1.1	0.849	0.975	0.8	0.810	0.868	1.1	0.846	0.906
Vitronectin	VTNC_PIG	53	0.7	0.578	0.683	2.9	0.019	0.201	1.6	0.440	0.868	0.9	0.947	0.947

P values between DES and BMS at each time point are based on unpaired *t*-tests with unequal variance (n=3 [BMS day 1/3/7/28], n=3 [DES 1/3/7/28]). *T*-test was not performed if a protein was undetectable in the majority of samples from 1 of the 2 groups compared. Only proteins with at least one significant result at any time point are shown. Results in bold indicate *P* < 0.05. n/a denotes not applicable, FC denotes fold change (DES/BMS). FDR denotes false discovery rate. The FDR threshold was set at 10%.

Supplemental Table VII. Transitions for targeted proteomics in human vessels.

Protein	Proteotypic peptide + position	Average RT (min)	Precursor m/z	Precursor z	Fragment ion	Fragment ion m/z
Aggrecan	C[+57]GGNLLGVR C318 - R326	45.0	473.2504	2	y3	331.21
					y4	444.29
					y5	557.38
					y6	671.42
					y7	728.44
					y8	785.46
Versican	LATVGELQAAWR L277 - R288	124.6	657.8619	2	y4	503.27
					y5	631.33
					y6	744.42
					y7	873.46
					y8	930.48
					y9	1029.55
					y10	1130.60
Decorin	NLHALILVNNK N106 - K116	67.6	416.9189	3	y11	1201.63
					y3	375.20
					y4	474.27
					y5	587.35
					y6	700.44

Supplemental Table VIII. Aortic extracellular proteins identified by proteomics analysis in mice lacking the catalytic domain of *Adamts5* (*Adamts5* Δ cat) compared to controls.

Identified Proteins	UniProt ID	MW (kDa)	Adamts5		P	FC (Δcat /WT)
			WT	Δcat		
			Total ion current x 10 ⁶ Av±SD			
Adipocyte enhancer-binding protein 1	AEBP1_MOUSE	128	64.1±31.6	58.4±25.3	0.746	0.9
Adiponectin	ADIPO_MOUSE	27	40.9±9.0	33.2±20.2	0.465	0.8
Aggrecan	PGCA_MOUSE	222	176.9±30.6	255.3±56.3	0.032	1.4
Agrin	AGRIN_MOUSE	208	34.0±16.3	33.0±13.1	0.914	1.0
Alpha-2-HS-glycoprotein	FETUA_MOUSE	37	11.8±14.4	15.4±14.3	0.689	1.3
Amyloid beta A4 protein	A4_MOUSE	87	18.1±15.0	11.1±10.9	0.397	0.6
Annexin A2	ANXA2_MOUSE	39	41.3±26.3	58.4±46.5	0.492	1.4
Apolipoprotein A-I	APOA1_MOUSE	31	43.3±21.6	53.3±32.3	0.573	1.2
Apolipoprotein A-IV	APOA4_MOUSE	45	21.6±13.2	26.7±7.4	0.450	1.2
Apolipoprotein E	APOE_MOUSE	36	0.0±0.0	4.7±10.6	n/a	n/a
Asporin	ASPN_MOUSE	43	235.9±42.9	236.6±39.4	0.976	1.0
Basal cell adhesion molecule	BCAM_MOUSE	68	180.7±43.3	185.7±33.6	0.835	1.0
Basement membrane-specific heparan sulfate proteoglycan core protein	PGBM_MOUSE	398	2277.5±241.7	2497.0±107.5	0.085	1.1
Beta-2-glycoprotein 1	APOH_MOUSE	39	54.3±19.6	64.0±16.8	0.400	1.2
Biglycan	PGS1_MOUSE	42	2026.4±473.1	1924.8±417.8	0.714	0.9
Cadherin-13	CAD13_MOUSE	78	24.6±12.0	30.7±10.3	0.388	1.2
Cathepsin D	CATD_MOUSE	45	21.1±5.4	15.8±11.7	0.394	0.7
Cell surface glycoprotein MUC18	MUC18_MOUSE	72	16.7±14.0	19.7±12.4	0.719	1.2
Chondroitin sulfate proteoglycan 4	CSPG4_MOUSE	252	14.8±12.7	6.1±8.3	n/a	0.4
Chymase	CMA1_MOUSE	28	76.0±27.3	79.1±27.5	0.854	1.0
Clusterin	CLUS_MOUSE	52	80.6±14.8	93.2±31.9	0.450	1.2
Collagen alpha-1 (I)	CO1A1_MOUSE	138	17254.0±2798.8	21811.8±4876.9	0.113	1.3
Collagen alpha-1 (II)	CO2A1_MOUSE	142	645.2±292.1	562.5±183.9	0.583	0.9
Collagen alpha-1 (III)	CO3A1_MOUSE	139	2265.9±1681.1	1177.9±635.7	0.189	0.5
Collagen alpha-1 (IV)	CO4A1_MOUSE	161	91.4±30.3	61.6±16.9	0.074	0.7
Collagen alpha-1 (V)	CO5A1_MOUSE	184	281.7±52.1	290.4±66.5	0.817	1.0
Collagen alpha-1 (VI)	CO6A1_MOUSE	108	213.0±64.7	209.5±106.6	0.951	1.0
Collagen alpha-1 (XI)	COBA1_MOUSE	181	62.6±54.8	0.0±0.0	n/a	0.0
Collagen alpha-1 (XIV)	COEA1_MOUSE	193	14.5±17.3	5.7±12.8	n/a	0.4
Collagen alpha-1 (XV)	COFA1_MOUSE	140	137.4±35.4	151.9±42.4	0.560	1.1
Collagen alpha-1 (XVIII)	COIA1_MOUSE	182	295.6±66.3	277.6±64.0	0.660	0.9
Collagen alpha-2 (I)	CO1A2_MOUSE	130	11217.6±3451.6	11447.8±2260.1	0.897	1.0
Collagen alpha-2 (IV)	CO4A2_MOUSE	167	36.9±26.3	53.8±31.3	0.367	1.5
Collagen alpha-2 (V)	CO5A2_MOUSE	145	408.7±94.8	442.8±135.1	0.649	1.1
Collagen alpha-2 (VI)	CO6A2_MOUSE	110	122.8±66.3	81.2±54.4	0.282	0.7
Collagen alpha-2 (XI)	COBA2_MOUSE	172	7.5±18.3	0.0±0.0	n/a	0.0
Collagen alpha-5 (VI)	CO6A5_MOUSE	290	5.7±13.8	0.0±0.0	n/a	0.0
Collagen alpha-6 (VI)	CO6A6_MOUSE	246	81.1±50.5	91.9±86.1	0.812	1.1
Connective tissue growth factor	CTGF_MOUSE	38	2.6±6.4	11.2±15.7	n/a	4.3
Decorin	PGS2_MOUSE	40	1366.3±105.8	1401.5±270.2	0.795	1.0
Dermatopontin	DERM_MOUSE	24	151.7±30.2	136.3±39.5	0.495	0.9
Destrin	DEST_MOUSE	19	277.8±70.8	326.5±62.5	0.257	1.2
Dystroglycan	DAG1_MOUSE	97	31.3±15.6	57.0±30.4	0.140	1.8
Elastin	ELN_MOUSE	72	44.4±19.8	44.0±19.3	0.978	1.0
EMILIN-1	EMIL1_MOUSE	108	4.2±10.3	0.0±0.0	n/a	0.0
Extracellular superoxide dismutase [Cu-Zn]	SODE_MOUSE	27	430.7±126.7	416.8±106.0	0.847	1.0
Fibrillin-1	FBN1_MOUSE	312	25.2±25.4	0.0±0.0	n/a	0.0
Fibrinogen alpha chain	FIBA_MOUSE	87	38.7±26.0	23.2±27.0	0.360	0.6

Fibrinogen beta chain	FIBB_MOUSE	55	33.8±29.5	30.0±41.8	0.868	0.9
Fibrinogen gamma chain	FIBG_MOUSE	49	60.0±56.4	40.0±34.1	0.487	0.7
Fibromodulin	FMOD_MOUSE	43	9.6±7.6	6.9±7.4	0.578	0.7
Fibronectin	FINC_MOUSE	273	1061.0±222.9	951.9±142.2	0.353	0.9
Fibulin-5	FBLN5_MOUSE	50	62.2±27.6	73.3±23.2	0.487	1.2
Galectin-1	LEG1_MOUSE	15	224.4±39.5	265.8±56.3	0.209	1.2
Galectin-3	LEG3_MOUSE	28	14.3±7.3	30.5±29.9	0.297	2.1
Hyaluronan and proteoglycan link protein 1	HPLN1_MOUSE	40	8.5±8.1	11.2±15.7	n/a	1.3
Insulin-like growth factor-binding protein 7	IBP7_MOUSE	29	154.1±49.6	129.6±35.5	0.367	0.8
Inter-alpha-trypsin inhibitor heavy chain H1	ITIH1_MOUSE	101	5.7±11.2	4.6±6.4	n/a	0.8
Lactadherin	MFGM_MOUSE	51	384.5±33.4	387.7±63.6	0.923	1.0
Laminin subunit alpha-2	LAMA2_MOUSE	344	1.8±4.4	0.0±0.0	n/a	0.0
Laminin subunit alpha-4	LAMA4_MOUSE	202	43.6±8.6	37.0±25.6	0.611	0.9
Laminin subunit alpha-5	LAMA5_MOUSE	404	48.3±13.5	35.5±20.4	0.272	0.7
Laminin subunit beta-2	LAMB2_MOUSE	197	113.1±57.2	96.3±58.5	0.644	0.9
Laminin subunit gamma-1	LAMC1_MOUSE	177	113.4±28.6	91.6±15.7	0.148	0.8
Latent-TGFβ-binding protein 1	LTBP1_MOUSE	187	47.3±15.7	50.1±13.6	0.756	1.1
Latent-TGFβ-binding protein 4	LTBP4_MOUSE	179	456.7±66.7	429.5±95.6	0.608	0.9
Lumican	LUM_MOUSE	38	1799.7±751.8	1778.6±220.8	0.950	1.0
Lysyl oxidase homolog 1	LOXL1_MOUSE	67	368.2±63.6	376.3±39.2	0.802	1.0
Matrin-3	MATR3_MOUSE	95	1.4±3.4	0.0±0.0	n/a	0.0
Microfibril-associated glycoprotein 4	MFAP4_MOUSE	29	101.6±32.5	127.7±31.3	0.210	1.3
Microfibrillar-associated protein 5	MFAP5_MOUSE	19	66.0±70.8	88.8±90.0	0.658	1.3
Mimecan	MIME_MOUSE	34	1299.0±180.9	1605.9±194.2	0.026	1.2
Nidogen-1	NID1_MOUSE	137	193.9±65.0	192.4±24.6	0.959	1.0
Nidogen-2	NID2_MOUSE	154	123.2±35.4	109.1±36.4	0.533	0.9
Periostin	POSTN_MOUSE	93	182.1±59.7	193.5±156.6	0.884	1.1
Prolargin	PRELP_MOUSE	43	578.3±87.4	622.8±159.5	0.597	1.1
Prosaposin	SAP_MOUSE	61	31.9±24.8	15.2±21.6	n/a	0.5
Protein S100-A10	S10AA_MOUSE	11	15.8±24.4	0.0±0.0	n/a	0.0
Protein S100-A11	S10AB_MOUSE	11	0.0±0.0	7.4±10.1	n/a	n/a
Secreted frizzled-related protein 1	SFRP1_MOUSE	35	1.0±2.5	0.0±0.0	n/a	0.0
Serine protease HTRA1	HTRA1_MOUSE	51	169.9±40.2	197.7±38.0	0.270	1.2
SPARC	SPRC_MOUSE	34	2.9±4.6	3.2±7.2	n/a	1.1
Tenascin	TENA_MOUSE	232	6.2±9.7	1.8±4.0	n/a	0.3
Tetranectin	TETN_MOUSE	22	0.0±0.0	2.4±5.3	n/a	n/a
TGFβ-induced protein ig-h3	BGH3_MOUSE	75	24.2±16.2	9.8±17.5	n/a	0.4
Thrombospondin type-1 domain-containing protein 4	THSD4_MOUSE	113	44.1±26.6	64.0±21.0	0.198	1.5
Versican	CSPG2_MOUSE	367	254.8±25.0	240.0±36.3	0.467	0.9
Vitamin D-binding protein	VTDB_MOUSE	54	0.0±0.0	3.5±7.8	n/a	n/a
Vitronectin	VTNC_MOUSE	55	71.5±22.0	115.2±31.8	0.036	1.6

P values for differential expression between aortas of wild type controls (WT) and mice lacking the catalytic domain of *Adamts5* (*Adamts5* Δcat) are based on unpaired Student's *t*-tests with unequal variance (n=6 [WT] and n=5 [*Adamts5* Δcat]). *T*-test was not performed if a protein was undetectable in the majority of samples from 1 of the 2 groups compared. Results in bold indicate *P* < 0.05. Values are average (Av) total ion current (TIC) × 10⁶ ± standard deviation (SD). n/a denotes not applicable; FC denotes fold change.

Supplemental Table IX. Transitions for targeted proteomics in murine vessels.

Protein	Proteotypic peptide	Amino acid position	Collision energy	Retention time (min)	m/z light	m/z heavy	charge state
Aggrecan	GDPETSVSGVGDDFSGLPSPGK	G1172 – K1192	37.1	n/a	1004.4607	1007.4708	2
	TVYLYPN[+3]QTGLPDPLSK	T661 – K677	35.3	163.22	954.9956	958.0057	2
Versican	VSVPTHPDDVGDAALTMVK	V101 – K119	36.4	92.82	984.4908	987.5008	2
	VSVPTHPDDVGDAALTMVK	V101 – K119	27.8	92.82	656.6629	658.6697	3
Decorin	DLHTLILVNNK	D101 – K111	24	84.52	640.3721	643.3821	2
	DLHTLILVNNK	D101 – K111	19.3	84.52	427.2505	429.2572	3
	NSGIENGAFQGLK	N183 – K195	25	n/a	667.8386	670.8487	2
	VVQC[+57]SDLGLDK	V59 – K69	23.2	37.16	617.3108	620.3209	2

SUPPLEMENTAL FIGURES

Supplemental Figure I. Overview of proteomics comparisons. The following proteomics comparisons were conducted in porcine tissue: a) Stent dependent changes in the neointima. b) Changes in BMS/DES/BA at different time points. c) Comparison stent vs. BA at late stage. d) BMS/DES dependent changes at each time point.

Supplemental Figure II. Reproducibility of LC-MS/MS. The neointima samples were run in duplicates by LC-MS/MS. The total spectral counts ($R=0.998$) and the sequence coverage ($R=0.969$) for each ECM protein correlated well between technical replicates. $n=140$ proteins x 14 samples (Pearson correlation). The Venn diagram displays the unique peptides identified either in both or only in the 1st and only in the 2nd analysis.

Supplemental Figure III. Database search. The publically available porcine databases do not cover the entire sequence of each protein. In addition, not all proteins are well annotated in porcine databases. Thus, a custom-made database containing porcine sequences of previously published ECM proteins was generated. This figure shows the identification of total spectral counts for selected proteins using different databases: The application of a hybrid database, which is the combination of a pig and human database, is superior to a pig or human database alone for identifying and quantifying proteins analysed by LC-MS/MS due to a higher sequence match. For many ECM proteins, such as fibronectin and decorin, which are well annotated and fully sequenced, the custom-made database does not offer a major improvement. However, for other proteins, such as collagen alpha-1 (I) and perlecan, which are not well annotated or fully sequenced, the custom-made database has a remarkable impact on the sequence coverage and protein quantification.

Supplemental Figure IV. Total identified proteins. Overall in the media and neointima a total of 151 unique ECM proteins were identified with a minimum of 2 high-confidence peptides. The Venn diagram depicts the findings in the media and neointima (114 common proteins, 11 only in the media, 26 only in the neointima).

Supplemental Figure V. Densitometry DES at different time points. Aggrecan NITEGE and versican DPEAAE neoepitopes generated by aggrecanase activity in DES at different time points. n=3 per time point. * $P<0.05$, ** $P<0.01$, *** $P<0.001$ (1-way ANOVA [$P<0.001$] with Dunnett post hoc test to day 1).

Supplemental Figure VI. Densitometry BMS vs DES day 28. Differences between BMS and DES at day 28. n=4 per group. ** $P<0.01$ (t -test with unequal variance).

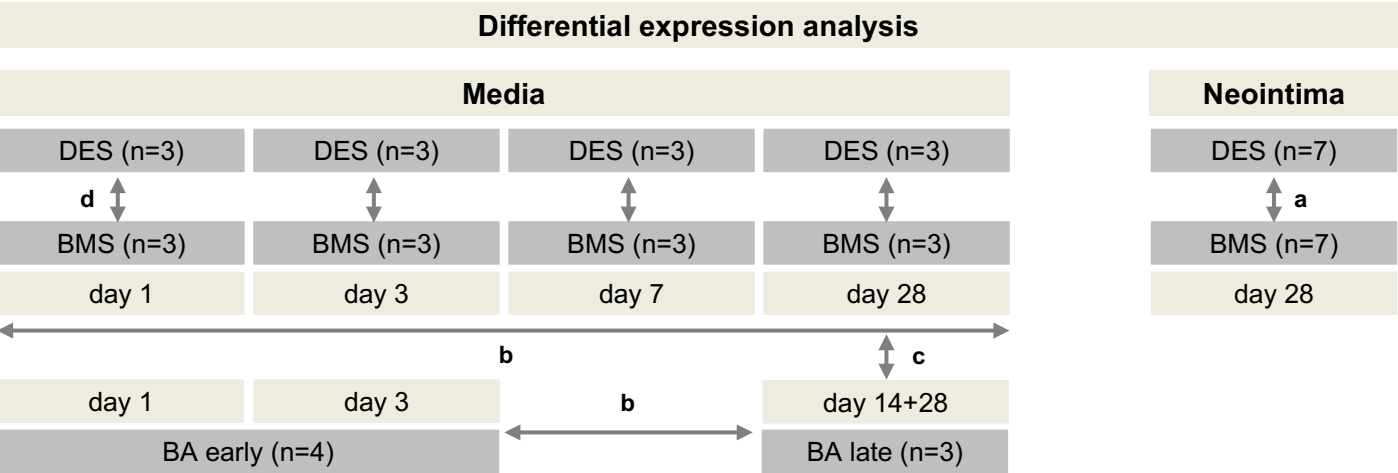
Supplemental Figure VII. Aggrecan in human stented coronary artery. Co-localization of aggrecan (Alexa 633, displayed in green) and aggrecan NITEGE neoepitope (Alexa 568, displayed in red) in human stented coronary artery visualized by immunofluorescence. Overview image 20x, scale bar=500 μm ; Zoomed-in areas 60x, scale bar=25 μm .

Supplemental Figure VIII. Densitometry aggrecan in human vasculature. Protein abundance quantified by densitometry of immunoblots for the aggrecan NITEGE neoepitope, versican and decorin in human thoracic aortas and saphenous veins. n=4 per group. * $P<0.05$ (t test with unequal variance).

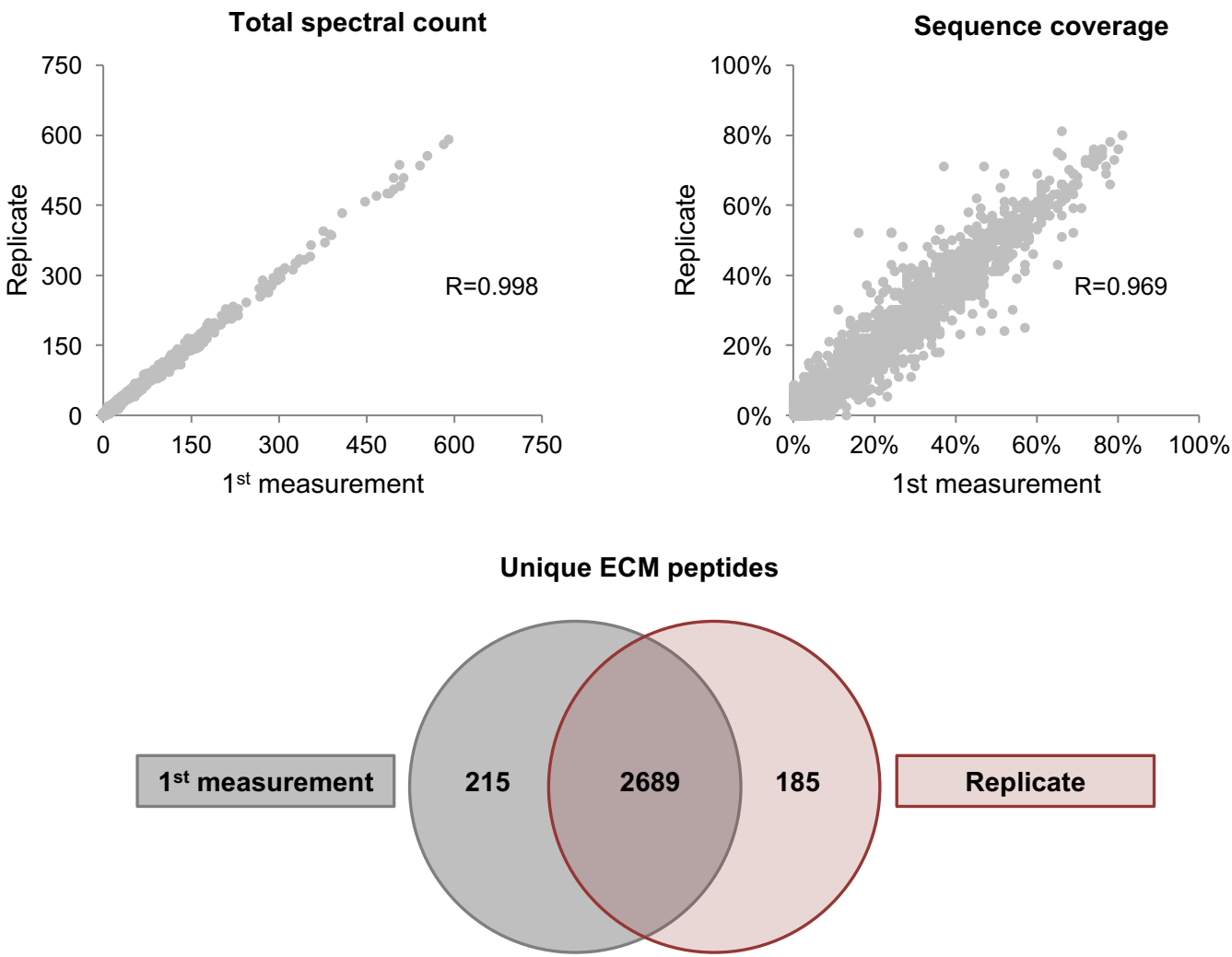
Supplemental Figure IX. Blood pressure measurements in mice. Systolic and diastolic blood pressure measurements. n=7 (WT), n=5 (*Adamts5* Δcat), t -test with unequal variance.

Supplemental Figure X. Cardiac output measurements in mice. Left ventricular ejection fraction (LVEF) as measured by CMR. n=5 (WT), n=7 (*Adamts5* Δcat), t -test with unequal variance.

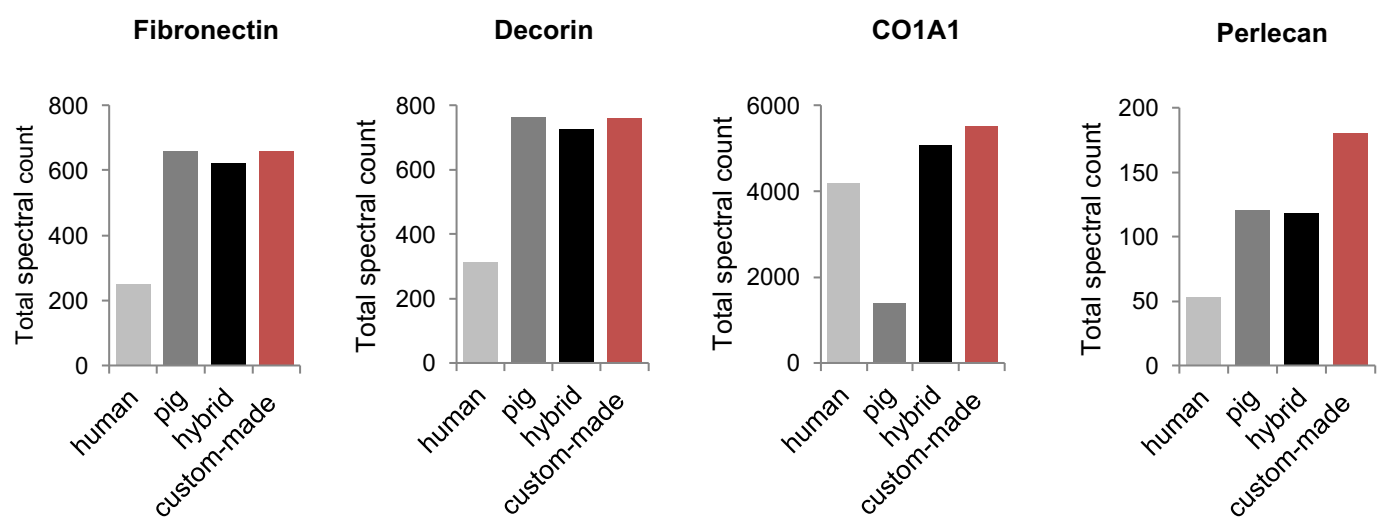
Supplemental Figure I



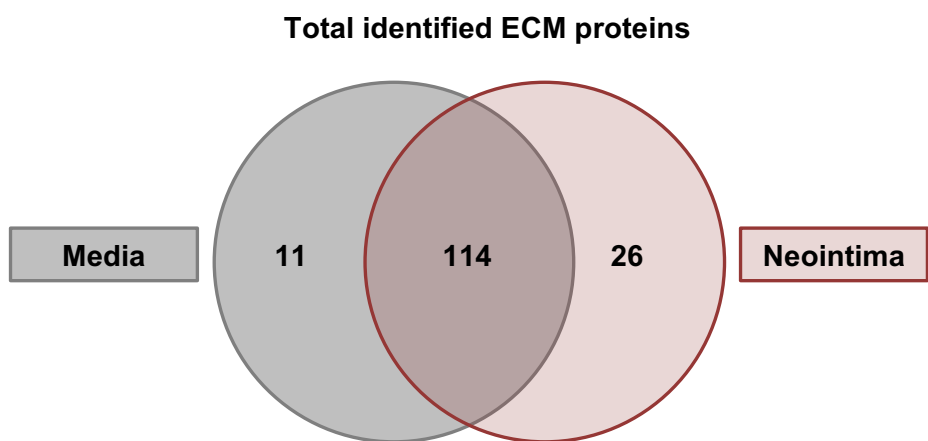
Supplemental Figure II



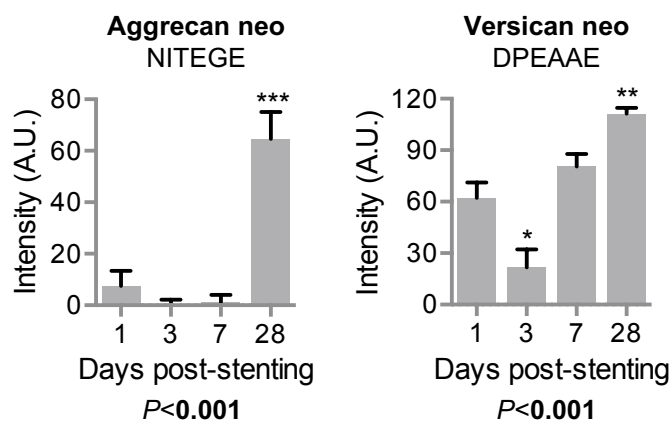
Supplemental Figure III



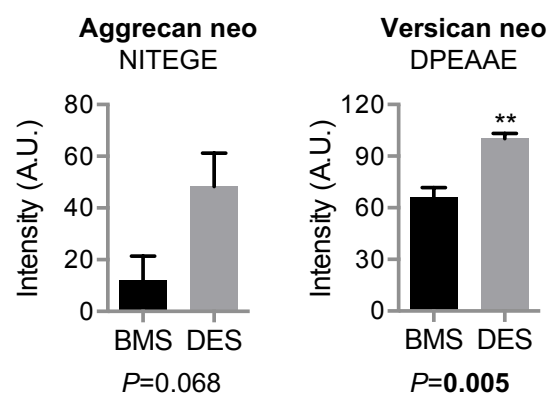
Supplemental Figure IV



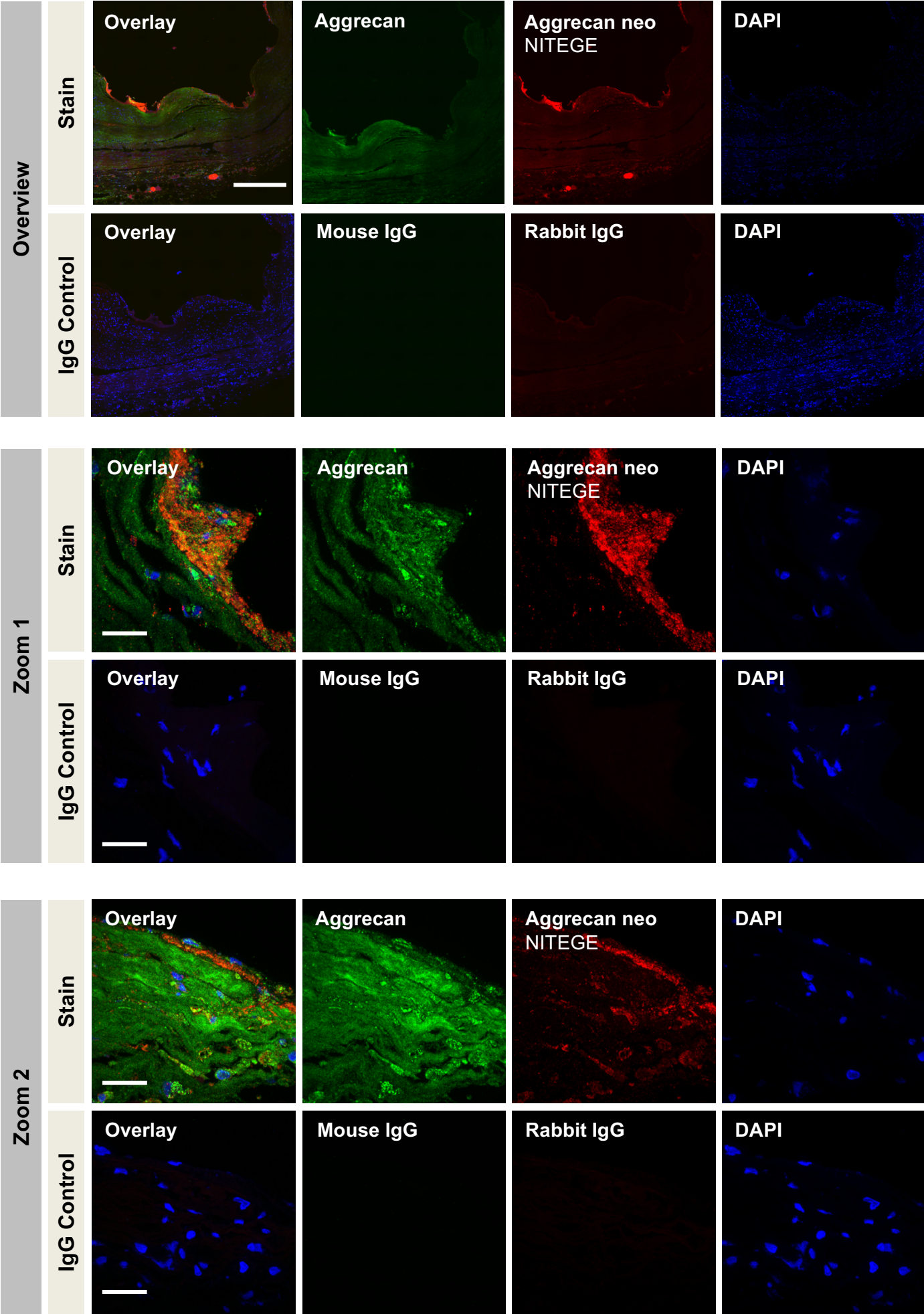
Supplemental Figure V



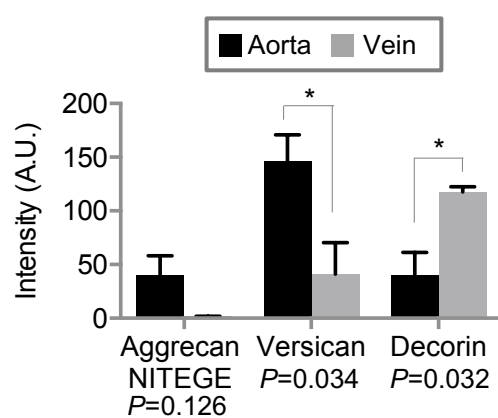
Supplemental Figure VI



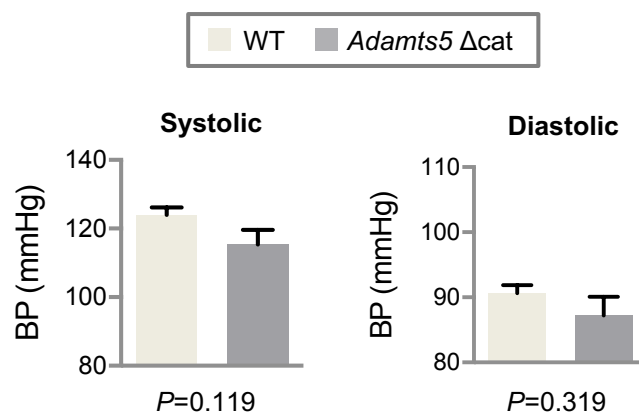
Supplemental Figure VII



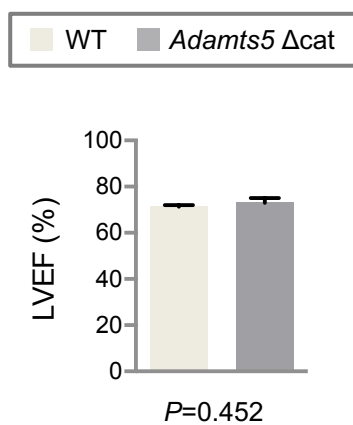
Supplemental Figure VIII



Supplemental Figure IX



Supplemental Figure X



SUPPLEMENTAL REFERENCES

1. Gonzalo N, Serruys PW, Okamura T, van Beusekom HM, Garcia-Garcia HM, van Soest G, van der Giessen W, Regar E. Optical coherence tomography patterns of stent restenosis. *Am Heart J*. 2009;158:284-93. doi:10.1016/j.ahj.2009.06.004.
2. Barallobre-Barreiro J, Didangelos A, Schoendube FA, Drozdov I, Yin X, Fernandez-Caggiano M, Willeit P, Puntmann VO, Aldama-Lopez G, Shah AM, Domenech N, Mayr M. Proteomics analysis of cardiac extracellular matrix remodeling in a porcine model of ischemia/reperfusion injury. *Circulation*. 2012;125:789-802. doi:10.1161/CIRCULATIONAHA.111.056952.
3. Cuello F, Shankar-Hari M, Mayr U, Yin X, Marshall M, Suna G, Willeit P, Langley SR, Jayawardhana T, Zeller T, Terblanche M, Shah AM, Mayr M. Redox state of pentraxin 3 as a novel biomarker for resolution of inflammation and survival in sepsis. *Mol Cell Proteomics*. 2014;13:2545-57. doi:10.1074/mcp.M114.039446.
4. Didangelos A, Yin X, Mandal K, Baumert M, Jahangiri M, Mayr M. Proteomics characterization of extracellular space components in the human aorta. *Mol Cell Proteomics*. 2010;9:2048-62. doi:10.1074/mcp.M110.001693.
5. Kapustin AN, Chatrou ML, Drozdov I, Zheng Y, Davidson SM, Soong D, Furmanik M, Sanchis P, De Rosales RT, Alvarez-Hernandez D, Shroff R, Yin X, Muller K, Skepper JN, Mayr M, Reutelingsperger CP, Chester A, Bertazzo S, Schurgers LJ, Shanahan CM. Vascular smooth muscle cell calcification is mediated by regulated exosome secretion. *Circ Res*. 2015;116:1312-23. doi:10.1161/CIRCRESAHA.
6. Livak KJ and Schmittgen TD. Analysis of relative gene expression data using real-time quantitative PCR and the 2^{(-Delta Delta C(T))} Method. *Methods*. 2001;25:402-8. doi:10.1006/meth.2001.1262.
7. Zou Y, Dietrich H, Hu Y, Metzler B, Wick G, Xu Q. Mouse model of venous bypass graft arteriosclerosis. *Am J Pathol*. 1998;153:1301-10. doi: 10.1016/S0002-9440(10)65675-1.

8. Stanton H, Rogerson FM, East CJ, Golub SB, Lawlor KE, Meeker CT, Little CB, Last K, Farmer PJ, Campbell IK, Fourie AM, Fosang AJ. ADAMTS5 is the major aggrecanase in mouse cartilage in vivo and in vitro. *Nature*. 2005; 434:648-652. doi:10.1038/nature03417.
9. Schneider JE, Wiesmann F, Lygate CA, Neubauer S. How to perform an accurate assessment of cardiac function in mice using high-resolution magnetic resonance imaging. *J Cardiovasc Magn Reson*. 2006; 8:893-701. doi: 10.1080/10976640600723664.